# STUDYING STATISTICAL PHYSICS OF SOME COMPLEX SYSTEMS

Thesis submitted for

the degree of Doctor of Philosophy (Science)

of the University of Jadavpur

**Kunal Bhattacharya**

S. N. Bose National Centre for Basic Sciences

Block - JD, Sector-III, Salt Lake

Kolkata - 700 098, India

March 2009

# CERTIFICATE FROM THE SUPERVISOR

This is to certify that the thesis entitled "Studying Statistical Physics of some Complex Systems" submitted by Sri Kunal Bhattacharya, who got his name registered on November 11, 2006 for the award of Ph.D. (Science) degree of Jadavpur University, is absolutely based upon his own work under the supervision of Dr. Subhrangshu Sekhar Manna and that neither this thesis nor any part of it has been submitted for any degree / diploma or any other academic award anywhere before.

Date:

**Subhrangshu Sekhar Manna**
Professor
Department of Theoretical Sciences
Satyendra Nath Bose National Centre for Basic Sciences
Block-JD, Sector-III, Salt Lake, Kolkata - 700098, India.

# Acknowledgments

The present Thesis is based on the research work that I performed at the S. N. Bose National Centre for Basic Sciences, Kolkata starting from the August of 2004. Here I express my gratitude to those who had provided help and support during the past few years.

First, I would like to thank my supervisor Prof. Subhrangshu Sekhar Manna for his constant support and friendly guidance during my Ph.D tenure. We had innumerable fruitful discussions during the last few years. He always insisted on working hard and staying focused. It was a unforgettable experience working with him.

I would like thank Gautam Mukherjee who was a part of our group. It was a pleasure collaborating with him. His deep perception of the problems we dealt with always surprised me. As for other members of our group I would like to thank Anjan Nandi who was my also friend. Although our problems did not overlap but I always made it sure to discuss whatever came up in my mind. I was very happy to collaborate with him on a project during the last year. I also acknowledge the constant support and motivation from Arnab Chatterjee of Saha Institute of Nuclear Physics, Kolkata.

I also thank all my senior and junior colleagues from SNBNCBS for their support and companionship. In this regard I would like to specially mention the names of Abhishek Chaudhuri, Monodeep Chakraborti, Asish Bakshi, Debashish Chaudhri, Ankush Sengupta, Dipanjan Chakraborty, Saurav Samanta, Arya Paul, Tamoghna K. Das, Arnab Saha, Bipul Das and Sagar Chakraborty. I would always relish the memories of interactions that I had with them during my Ph.D tenure. I also appreciate the help that I received from the staff of the Computer Centre at the SNBNCBS.

I also take this opportunity to acknowledge the inspiration that I received as a student of the subject of Statistical Mechanics from Prof. J. K. Bhattacharjee, Prof. Abhijeet Mookerjee, and Prof. Surajit Sengupta of SNBNCBS and Prof. Debashish Chowdhury of IITK.

Finally, I end this acknowledgment by mentioning the unconditional support and encouragement that I received from my wife, my mother and the rest of my family.

**Kunal Bhattacharya**

Research Fellow

Satyendra Nath Bose National Centre for Basic Sciences

Block-JD, Sector-III, Salt Lake, Kolkata - 700098, India

# List of Publications

[1] K. Bhattacharya, G. Mukherjee, J. Saramäki, K. Kaski and S. S. Manna, *The International Trade Network: weighted network analysis and modeling*, J. Stat. Mech. P02002 (2008).

[2] K. Bhattacharya and S. S. Manna, *Self-organized critical models of earthquakes*, Physica A **384**, 15 (2007).

[3] K. Bhattacharya, G.Mukherjee and S. S. Manna, *The International Trade Network* in Econophysics of Markets and Business Networks, (Springer, 2007).

[4] S. S. Manna and K. Bhattacharya, *Self-organized critical earthquake models with moving boundary*, Eur. Phys. J. B **54** 493 (2006).

[5] K. Bhattacharya, G. Mukherjee and S. S. Manna, *Detailed Simulation Results for Some Wealth Distribution Models in Econophysics* in Econophysics of Wealth Distributions, (Spinger, 2005).

# Synopsis of the Thesis

Criticality in the sense of power-law decay of distributions of fluctuations and correlations is ubiquitous in systems we call complex. These systems are essentially composed of many interacting units and are in general in out of equilibrium states. There are other properties, like formation of self similar structures over all length scales, which are found to emerge in such systems. Equilibrium systems like liquid-gas or magnets show similar behavior near phase transitions achieved by fine tuning of temperature. However, in general, in complex systems any external control is absent. During past few years we have investigated the nature of complexity and hence criticality in systems whose study became popular in the last couple of decades using different methods and models in non-equilibrium statistical mechanics. In this thesis we report the kind of progress that we have made in studying the properties of some of such systems which fall under the following three broad topics:

1. *Complex Networks: International Trade Network.*

    We analyzed the world economy as a complex weighted network where concepts of critical phenomena, namely scaling and universality are argued to be applicable. Using a detailed analysis of the real data of the International Trade Network (ITN) we argued that the scaled link weight distribution has an approximate log-normal distribution which remains robust over a period of 53 years (from the year 1948 to the year 2000). Another universal feature was observed in the power-law growth of the total trade with gross domestic product, the exponent being similar for all countries.

    We also developed a prescription to quantify the rich-club effect in *weighted* networks by building the proper random ensemble. Although, using the rich-club coefficient, it is difficult to extract non-trivial correlations due to the high link density, we probed the ITN with other measures relevant to weighted networks which showed that the size of the rich-club, whose members trade among themselves half of the world's trade, is actually shrinking with time. While the Gravity law is known to describe well the social interactions in the static networks of population migration, international trade, etc, here for the first time we studied a non-conservative dynamical model based on the Gravity law which excellently reproduced many empirical features of the ITN.

    Further we investigated the properties related to the largest communities (in our definition this is the largest clique that a node belongs to) in the ITN as it has evolved over the years. Identification of these largest cliques is NP-hard, but we developed an algorithm which worked

well for the ITNs for the 53 years. In fact the use of Bootstrap Percolation enhanced the speed of our searching method. We obtained several results showing the heterogeneity and a scale-free hierarchy in the structure of the ITN. However we found that the nature of overlap (in terms of trade) between communities changed drastically from a scale-free nature to a modal one in the period between 1960 and 1970.

2. *Self-organized Criticality: Modeling of earthquakes.*

The modeling of emergence of criticality from complexity is believed to be possible by the general approach of self-organized criticality. We chose to study a globally driven self-organized critical model of earthquakes with conservative dynamics. We introduced an open but moving boundary condition so that the origin (epicenter) of every avalanche (earthquake) is at the center of the system.

This moving boundary removed the heterogeneity that is introduced by working with a open but fixed boundary. As a result, all avalanches grew in equivalent conditions and the avalanche size distribution obeyed finite size scaling in an excellent fashion. The recurrence time distribution of the time series of avalanche sizes from our model obeyed well both the scaling forms, by Bak et al. and Corral, observed in analysis of the real data of earthquakes. However, we found that the scaling function in our model decays only exponentially in contrast to the generalized gamma distribution observed in the real data analysis. The non-conservative version of the model showed periodicity even with a open boundary.

3. *Econophysics: Wealth distribution in societies.*

It is well known that the distributions of wealth and income of individuals in societies follow a definite pattern. The nature of distribution in the high income regime is a power-law decay. This behavior is known as the Pareto law. The distribution in the low and middle-income range is, however, found to be described by distributions like log-normal or exponential. There are several *asset exchange models* which try to simulate the above behavior. The distribution of wealth in such a model evolves through pairwise interactions between agents.

We obtained detailed and large scale simulation results on the wealth distribution model with quenched saving propensities which unearthed a number of crucial features of this model which were not known before. Unlike other wealth distribution models where the saving propensities are either zero or constant, this model was *not* found to be ergodic and self-averaging. The wealth distribution statistics with a single realization of quenched disorder was observed to be significantly different in nature from that of the statistics averaged over a large number of independent quenched configurations. The peculiarities in the single realization statistics refused to vanish irrespective of whatever large sample size was used. We concluded that previously observed Pareto law is essentially a convolution of the single member distributions.

# Contents

# 1 Introduction to Complex Systems

The subject of physics as it has evolved since the days of Newton has necessarily been reductionist. That is to say that one observes nature and then tries to isolate laws regarding matter separated from the environment as well as the initial conditions. And to say the least, physics has been successful in doing so in very many different areas. To start with, the emphasis of physics was in studying motion of bodies. The study of dynamics of bodies inspires division of matter itself into smaller and smaller entities; from atoms to nucleons to quarks and so forth. From the time when Galileo was able to discover the local law of gravity bypassing the air resistance to the era of contemporary high-energy physics with much more sophisticated experiments, the hope is to provide a better description of nature. However, guided mostly by experiments physicists started describing and studying properties of matter which is constituted not by few but $10^{23}$ or more number of atoms, i.e., bulk matter. Superconductivity and Superfluidity [1], to name only two, are phenomena which is only to be seen in matter in bulk and totally absent on an atomistic scale. These type of phenomena are called emergent. Laws have been framed describing such emergent phenomena by experiments to be verified by theory and vice-versa.

During the 1960's the framework of renormalization group [2] was greatly successful in describing another type of emergent phenomena in physics called equilibrium critical phenomena. For example when the temperature $T$ of a magnet is raised beyond a critical value $T_c$, its magnetization vanishes completely. Near $T_c$ large fluctuations are observed in the magnetization and other thermodynamic variables describing the state of the magnet. In fact fluctuations of all sizes are seen and the different variables like susceptibility and specific heat are found to diverge as power-laws as temperature approaches $T_c$. Below but near $T_c$, magnetization itself varies as a power-law in $T_c - T$. Another feature near the critical point is self-similarity or *scale invariance*. Near the critical point the magnet is found to be statistically similar on all scales. The arrangement of magnetized zones is such that roughness, irregularities and holes are to be found on all length scales. This sort of pattern in ubiquitous in nature and are called *fractals* [3]. Now, systems other than magnets like a liquid-gas coexistence systems also have critical points characterized by power-laws divergences for different thermodynamic variables. However, strikingly all the exponents of these power-laws for the liquid-gas systems agree (within limits of experimental accuracy) with the corresponding exponents for the magnets. The behavior near a critical point is found to be independent of the microscopic details of the system. This similarity in behavior

is called *universality* such that the magnets and the liquid-gas systems are said to belong to the same universality class.

Criticality, in the sense of fluctuations at all length scales and other scale invariant behavior like fractality, however, is not unique to systems of magnets or liquid-gases. These sort of phenomena is found to develop in systems outside the realm of equilibrium critical phenomena; and not only in physics but ubiquitous in different other fields like geophysics [4], biology [5], social sciences [6], linguistics [7], and finance [8]. Firstly, let us consider geophysics. The magnitude of an earthquake is measured as the logarithm of the energy released. Very small earthquakes are taking place almost continuously due to the motion and friction between the tectonic plates in continental drift. But at times the energy released is huge and such earthquakes (with magnitude seven or more) cause serious damage and are catastrophic. Concentrated study is done on specific large earthquakes and their fault zones to theorize their behavior. However, a more holistic description of earthquakes is the Gutenberg-Richter law. Sampling over energies of earthquakes in a given region and time period reveals that number of earthquakes of energy at least $E$ follows the power-law $\sim E^{-b}$ where $b$ is a constant. The values of $b$ obtained from observations in different parts of the world are found to be near unity.

Phenomena which scale with volume($V$) or mass($M$) in three dimensional Euclidean space have exponents which are multiples of $1/3$, e.g., linear dimensions scale as $V^{1/3}$ and surface areas scale as $V^{2/3}$. However, different biological traits are found to scale with body mass $M^{1/4}$ [9]. For example, diameter of tree trunks and aortas scale as $M^{3/8}$ and rates of cellular metabolism and heartbeat scale as $M^{-1/4}$. The assumption of the $1/3$ scaling exponent does not hold good in biology because the metabolic processes of different organisms rely on the hierarchical fractal-like nature of resource distribution networks. Examples include the macroscopic branching vascular networks of plants and animals and the complicated structure within cells. Although these networks may give rise to the quarter-power scaling but then the occurrence of these networks poses the question that how the fundamental processes conspire to produce such patterns among widely diverse forms of life.

Power-laws are also observed to emerge in different aspects of human behavior. For example distribution of population of cities. George Kingsley Zipf made an in depth study of such situations. These type of distributions are commonly known as Zipf's laws [6, 10]. For example distribution of population of cities is found to be a power-law. Historically it is seen that old cities grow in size, new cities built up and people migrate from one city to the other and from villages to cities. However why this type of dynamics gives rise to a power-law i.e., scale-free, population distribution and not a distribution where there is a characteristic scale for population about which the population of cities fluctuate, is not yet known. Such an holistic law has also emerged in the study of different languages. The Internet [11], which is the network of computers all over the world shows a power-law in the number of connections of a computer (with other computers). In

the end of 19th century Italian economist Vilfredo Pareto [12] made the observation of inequality of the income distribution. His study revealed that the wealth and income ($w$) of individuals follow a power-law $P(w) \sim w^{-(1+\nu)}$ where $\nu$ is close to $1.5$. Later, however, it was found that only the distribution for the high income group was a power-law where the value of $\nu$ was between $2$ and $3$. The income distribution for the USA revealed $\nu$ to be $1.8$ whereas for Japan it was found to vary between $1.8 - 2.2$. This type of behavior is known as *Pareto law.*

Such diverse natural and artificial systems, composed of many different components, which interact among themselves and with the environment, are called *complex systems* [13]. We are interested mostly in those systems where we find empirical statistical regularities, like criticality; and we intend to employ statistical physics [14] to understand and describe some of such systems, mostly because of it's success in equilibrium systems. However, before attempting to explain their behavior of complex systems using physics several questions need to be answered. But first, we try to figure out what are the common features of complex systems other than the emergent properties. Firstly, we find they are all way out of equilibrium. For example finance markets where signatures of power-laws and scale invariance have been found. These markets drive other markets and influence regional and global economic systems. Finance markets evolve under the action of trading agents. Such agents participating in trading activities constantly learn and acquire knowledge from their past successes and failures; and influence the market through different actions at different points of time. Therefore such systems evolve continuously. These are reflected in the nature of fluctuations in the time series for the markets' indices. Such time series show signatures of non-stationarity. And in fact a time series for the energy releases by earthquakes in a given region shows very similar behavior. System like the earth's crust which causes earthquakes changes with time. The Internet grows every minute as does the biological networks embedded in different living organisms which evolve and grow during their life spans. Another common feature of these systems is the absence of any tuning parameter responsible for their criticality as compared to a parameter like temperature or pressure in equilibrium critical phenomena.

The motivation for studying complex systems, in the sense of mathematical modeling was historically rooted in conventional goals of physics. In physics when we observe and analyze a phenomena we ideally try to frame a dynamical equation, essentially a law like Newton's law of gravity or an equation for the probability (of some dynamical variable) like the diffusion equation, and try to solve them either exactly or numerically to understand how the system evolves in time. More clearly we are interested to know the exact future state of the system or at least, in the probabilistic picture, make predictions about the future. However, is this approach relevant in case of complex systems? This question is crucial because laws of physics can be seen to hold good at any place on the earth by performing experiments and in general at any place in the universe from astronomical observations. However, not all countries [15] have power-law income

distributions and therefore Pareto law is not universal as Newton's laws are. Here we must keep this in mind that Pareto law is a holistic description unlike the microscopic description in Newton's formalism. However, when we aim to model a complex system using statistical physics we also need guidance regarding the microscopic behavior of the system, for example how the components interact between themselves. In a gas at 300K (say) the molecules continuously collide with each other and with the walls of the container and at a microscopic level governing principle is Newton's laws of motion. Therefore, we encounter the question that whether in principle such laws can exist in such complex systems and even if they do, can we extract them when the system is constantly interacting with the environment.

The questions raised above become more relevant when we have socio-economic systems in mind. For example the traders mentioned above. These traders are in fact influenced by other political and economic affairs around the globe. They are rational in the sense they make willful decisions. In the real-world, assigning any model behavior to such a rational agent is difficult because he or she is potentially capable of violating it any moment if he chooses to. Certain approaches in the modeling of complex systems allow us to tackle such problems. For example the assumption of "bounded rationality" [16, 20] and the careful identification of important factors can shrink the set of options of each agent in the model. With such assumptions in mind we try to study and model complex systems. The models are considered successful if they are able to reproduce the macroscopic features of the real system especially statistical distributions.

In this thesis we investigate three problems which belong to three broad areas in complex systems *viz.* complex networks [18, 19], self-organized criticality [20, 21] and econophysics [8, 17]. In the following we provide a brief introduction to these topics and try to explain how tools of statistical physics are employed within this areas to tackle the problems in complex systems.

## 1.1 Complex Networks

To analyze the structure and function of some complex systems mentioned above it has been found to be useful to model them as networks. While networks form a very natural way of understanding structures like electric power grids [22], the Internet [23] or river basins [26] it can be used to study other systems like acquaintances between individuals in the society, the interdependence of living organisms on each other, namely food webs [24, 25] or the trade relations [27] between different countries. Traditionally the study of networks has been a branch of mathematics called *graph theory*. In the jargon of graph theory a graph(network) consists of a set of entities called vertices (also called nodes) and a set of connections between them called edges (also called links). It is believed that graph theory started with the study [28] of a network of bridges around the city of Königsberg by Leonhard Euler in early 17th century. In addition to these, study of networks
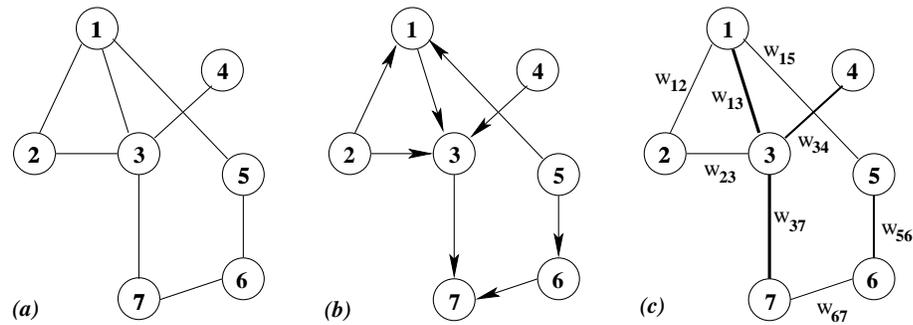
FIGURE 1.1: The representation of (a) an undirected, (b) a directed and (c) a weighted graph with $N = 7$ nodes and $L = 8$ links. The arrow-heads in (b) indicate the direction of the links. The thicknesses of the links in (c) represent the values of the weights associated with the links.

was also carried out by *social network analysts* since early the 20th century.

About a decade ago, graph theory mainly focused on properties of individual nodes and links in small networks consisting of few hundred nodes; it is only recently the approach has changed. This has been triggered by scientists looking at networks of millions of nodes. Presently the focus is on studying statistical properties in these huge networks. In fact, after two seminal papers, one by Watts and Strogatz [22] and the other by Barabási and Albert [29], successfully modeled different emergent properties of large real-world networks, there has been a flurry of activity in this field.

A graph or a network $G(\mathcal{V}, \mathcal{E})$ consists of two sets of elements, $\mathcal{V} = \{v_1, v_2, v_3, ..., v_N\}$ and $\mathcal{E} = \{e_1, e_2, e_3, ..., e_L\}$ such that each element $e_k$ in the set $\mathcal{E}$ corresponds to a unique pair of elements $(v_i, v_j)$ of the set $\mathcal{V}$ [30–32]. The elements of the set $\mathcal{V}$ are called nodes or vertices ($N$ in number) and the elements of the set $\mathcal{E}$ are called links or edges ($L$ in number). More precisely this is the definition of an undirected graph. Graphs can also be *directed*. In case of directed graphs, each element $e_k$ in $\mathcal{E}$ corresponds to a unique *ordered* pair of elements $(v_i, v_j)$ of $\mathcal{V}$. However, in this thesis, and to be particular in Chapter 2, we deal with only undirected graphs. The Fig. 1.1(a) and Fig. 1.1(b) shows the examples an undirected graph and a directed graph, respectively.

A graph can be represented accurately using some matrices. For example a graph can be completely enumerated by defining its *adjacency* matrix. For a network with $N$ nodes, its adjacency matrix $\mathcal{A}$ is a $N \times N$ square matrix whose element $a_{i,j} = 1$ $(i, j = 1, ..., N)$ if there is an edge between the vertices $v_i$ and $v_j$, otherwise $a_{ij} = 0$. If the network is undirected, $\mathcal{A}$ is a symmetric matrix. In the following, we list some properties of networks as measurables in terms of the adjacency matrix.

### 1.1.1 Nodal Degree

The *degree* of a node is the total number of links that meet at this node. Therefore the degree $k_i$ of a node $i$ is given by:

$$k_i = \sum_{j \in \mathcal{V}} a_{ij}. \tag{1.1}$$

For a node in a directed network the *in-degree* $k_i^{in}$ i.e., the number of incoming links, and the *out-degree* $k_i^{out}$ i.e., the number of outgoing links, may be defined separately so that total degree is $k_i = k_i^{in} + k_i^{out}$.

### 1.1.2 Degree Distribution

In all real-world networks and in associated graphs [19, 29, 33] the *degree distribution* has turned out to be a primary quantity for characterization of networks. The degree distribution $P(k)$ is the probability that a randomly selected node has degree $k$. For a given network it is calculated as:

$$P(k) = \frac{N(k)}{N}, \tag{1.2}$$

where $N(k)$ is the number of nodes with degree $k$.

### 1.1.3 Clustering Coefficient

This quantity is one measure of local correlations [22, 33] in a network. From the perspective of social networks it quantifies the likelihood that if A and B are friends, as are B and C then A and C are also likely to be friends of each other. The *clustering coefficient $c_i$* at a particular node $i$ is thus the ratio of actual number of triangles $e_i$ connected to the vertex $i$ to the maximum number of such triangles possible. If $i$ has the degree $k_i$ and $e_i$ is the number of links actually that exists among the $k_i$ neighbours where the maximum number possible being $k_i(k_i - 1)/2$, then

$$c_i = \frac{2e_i}{k_i(k_i - 1)} = \frac{\sum_{jm} a_{ij} a_{im} a_{jm}}{k_i(k_i - 1)}. \tag{1.3}$$

For a node which has only one or no neighbour $c_i$ is set to zero. The clustering coefficient for the whole network is given by averaging $c_i$ over all nodes:

$$C = \frac{1}{N} \sum_{i \in \mathcal{V}} c_i. \tag{1.4}$$

From the definitions it follows $0 \leq c_i, C \leq 1$. Often a quantity which can be calculated for individual nodes in a network is also expressed as a function of the degree. Thus in addition to $c_i$ we can determine $c(k)$ which is the average clustering coefficient of all nodes having degree $k$:

$$c(k) = \frac{\sum_{i \in \mathcal{V}} c_i \delta_{k_i, k}}{N(k)}. \tag{1.5}$$

This forms a useful tool in exploring the hierarchical structure present in many real-world networks [34].

## 1.1.4 Shortest Paths and Diameter

These concepts are important for studying transport processes of any form taking place on the network. Examples are flow of data packets in the Internet [11] and the passenger traffic through railways connecting cities [35] or the traffic within cities themselves [36]. The concept of traversal along a network is as follows. To travel from one node $i$ to another node $j$ we need to hop along the network from one node to an adjacent node and likewise, starting at $i$ until we reach the destination $j$. The sequence of nodes that we traverse in the process (excluding $i$ and $j$) constitute a particular *path* from $i$ to $j$. If the number of nodes in this sequence be $n_{ij}$ then $n_{ij} + 1$ will be the *length* of the path. There can be in principle many different paths between any two nodes $i$ and $j$. The path for which $n_{ij}$ is the smallest (in general there can be more than one) is called the *shortest* path. Thus if $i$ and $j$ are adjacent nodes then the shortest path is just a hop from $i$ to $j$ with the path length being unity ($n_{ij}$ is zero).

The *diameter* of a network is defined as the largest of all possible shortest paths on the network i.e.,

$$D = \max_{i,j \in \mathcal{V}} \{n_{ij}\} + 1. \tag{1.6}$$

In case there are disjoint clusters in the network, the diameter of the network may be taken to be diameter of the largest cluster.

## 1.1.5 Betweenness Centrality

*Betweenness Centrality* is a quantity which highlights the importance of a node with respect to the global topology of the network. It is the number of shortest paths that pass through a particular node. Historically, the concept of betweenness was in fact introduced in the field of sociology [38, 39] . From the viewpoint of social networks [40, 41], the higher betweenness centrality of an individual the more 'important' the person is. Also in the study of network traffic, betweenness centrality becomes relevant. In a network where either information or physical objects (like vehicles) are traveling [42, 43] from a source node to a destination node via shortest paths there is high probability of congestion at the nodes with high betweenness centrality.

Mathematically, betweenness centrality $b_i$ of a node $i$ is calculated as:

$$b_i = \sum_{j,m \in \mathcal{V}, j \neq m} \frac{\sigma_{jm}(i)}{\sigma_{jm}}, \tag{1.7}$$

where $\sigma_{jm}$ is the number of shortest paths that exist between node $j$ and node $m$, out of which $\sigma_{jm}(i)$ such paths pass through node $i$. The determination of betweenness centrality by a

brute-force approach is computationally very expensive and takes up $\mathcal{O}(n^3)$ CPU-time and $\mathcal{O}(n^2)$ storage space. However, the calculation in linear time and with linear space is possible by a 'fast' algorithm by Brandes [44]. The concept of edge-betweennness where the the number of shortest paths passing through an edge is counted, has also been studied [45].

## 1.1.6 Degree Correlations

When high degree nodes are found to be preferentially attached to high degree nodes or preferentially attach to low degree nodes, the network is said to have degree correlations. One way of quantifying these correlations is by the means of the conditional probability [23] $P(k'|k)$ that a vertex of degree $k$ is connected to a vertex of degree $k'$.

Now average degree $k_{nn,i}$ of the nearest neighbour nodes of a node $i$ is given by:

$$k_{nn,i} = \frac{1}{k_i} \sum_{j \in \mathcal{V}} a_{ij} k_j. \tag{1.8}$$

This quantity when expressed as the function of degree, i.e., $k_{nn}(k)$ can be expressed as:

$$k_{nn}(k) = \sum_{k'} k' P(k'|k). \tag{1.9}$$

For real-world networks, where due to effects of finite size, measuring the correlation function $P(k'|k)$ becomes difficult, one resorts [23] to $k_{nn}(k)$. In case of uncorrelated network, $k_{nn}(k)$ is independent of $k$. When $k_{nn}(k)$ rises with $k$ it implies high degree nodes are preferentially attached to high degree nodes. Such networks are called assortative. When $k_{nn}(k)$ decreases with $k$ it implies nodes with vastly different degree values are preferentially linked. Such networks are called disassortative. It is a general observation [33, 46, 47] that almost all social networks, for example the Physics co-authorship network[48], appear to be assortative while other type of networks like biological networks like the protein-protein interaction network in the yeast $S.$ $Cerevisiae$ [49]; or technological and information networks like the network of hyperlinks between pages in the World Wide Web domain [50] appear to be disassortative. More examples of such real-world networks can found in reference [47].

### Weighted Networks

Till now we have investigated networks in terms of their structure which is enumerated in terms of presence and absence of links amongst the nodes. However, a finer description is possible which is the *weighted networks* [51] picture. Neither all the ties between individuals in a social network are of same strength [52–56] nor is the passenger traffic in a airlines network homogeneous [34, 57–59]. There are many similar examples of networks where there is strong heterogeneity in

the strengths of the links. The *weight* of a link is a measure of the strength of that link. For example, in a airlines network a link between two airports (nodes) is assigned a weight equal to the number of passengers commuting [34] along the link. The larger the weight along a link, the more important is its control on the properties of the network.

Most of the measures that are available for unweighted networks can be generalized to weighted networks. The natural generalization of the adjacency matrix $\mathcal{A}$ is the *weights matrix* $\mathcal{W}$ whose entry $w_{ij}$ is the weight of the link between node $i$ and node $j$. The Fig. 1.1(c) shows a representation of a weighted graph. We list below few quantities [60] pertinent to weighted networks in general and to the analysis done in Chapter 2, in particular. These are generalizations of the measurables defined above with respect to unweighted networks.

### 1.1.7  Nodal Strength

This quantity [34, 61] is the generalization of degree $k_i$ of a node $i$ for weighted networks. The *node strength* $s_i$ is given by:

$$s_i = \sum_{j \in \mathcal{V}} w_{ij}. \tag{1.10}$$

The strength when expressed as a function of the degree i.e., the function $s(k)$ gives a measure of *weight-topology* correlation in the network. If the weights are distributed on the network independent of the topology then on the average, $s(k) \simeq \langle w \rangle k$. However, in the presence of non-trivial correlations one obtains $s(k) \sim k^{\beta}$ with $\beta \neq 1$. For example, in the world-wide airport network (WAN) [34] $\beta$ is found to be $1.5$.

### 1.1.8  Weighted Clustering Coefficient

The *weighted clustering coefficient* $c_i^w$ of a node $i$ is given by:

$$c_i^w = \frac{1}{s_i(k_i - 1)} \sum_{j,m \in \mathcal{V}} \frac{w_{ij} + w_{im}}{2} a_{ij} a_{im} a_{jm}. \tag{1.11}$$

This quantity [34] is designed so as to give relatively more importance to those triangles which are incident on the node $i$ with larger weights and $c_i^w$ reduces to $c_i$ in case all the weights are equal. The normalization factor $s_i(k_i - 1)$ ensures that $0 \leq c_i^w \leq 1$.

### 1.1.9  Weighted Average Nearest Neighbour Degree

The assortative or disassortative nature of weighted networks is examined by means of the *weighted average nearest neighbour degree* $k_{nn}^w(i)$ of a node $i$. It is defined [34] as:

$$k_{nn}^w(i) = \frac{1}{s_i} \sum_{j \in \mathcal{V}} a_{ij} a_{im} w_{ij} k_j. \tag{1.12}$$

The variation of $k_{nn}^w(k)$ with degree $k$ points to the nature of correlations in a weighted network.

## 1.2 Self-organized Criticality

Beginning in the sixties with the investigations by Benoit Mandelbrot, the presence of fractal patterns in nature started becoming evident. Mandelbrot made the general observation that in most geological structures like mountain ranges, coastlines, river networks, fjords, etc, a part is statistically similar (this fact is also evident from the visual appearance) to the whole pattern. He made the proper characterization of such objects by the means of non-trivial, non-integral *fractal dimensions* [3, 62]. For example when the mass $M(R)$ of an object of physical size $R$ varies as $M(R) \sim R^{d_f}$, $d_f$ is known as the fractal dimension of the object.

However, it is not always the case that the fractal behavior is in the spatial structure itself but is manifested by the power-law relationship between two physical observables. An example is the Gutenberg-Richter law which we have already discussed above. Similar behavior is observed in the phenomenon of rainfall where a power-law dependence of the frequency of rainfall on the intensity has been found [63]. There are many other phenomena which show irregular bursts of large activity and we discuss some such systems in the section 1.3 The time series corresponding to such systems have power-law tails in their power spectra i.e., $S(f) \sim f^{-\beta}$, where the exponent $\beta$ has been found to be near unity at low frequencies. Examples [64, 65] include electrical noise, intensity variation of light from stellar objects, stock market price variations etc.

Bak, Tang and Wiesenfeld (BTW) first argued in favour of a unified framework for the different phenomena mentioned in the above paragraphs. They suggested that there is a self-organization built in the dynamics of such systems, which are all in non-equilibrium steady states. This gives rise to the scale invariance of the spatial and temporal correlation functions similar to that observed in equilibrium critical phenomena. However, here it is without the fine tuning of a control parameter. They called this sort of phenomena *self-organized criticality* (SOC). BTW suggested that a sandpile should be the simplest possible system exhibiting SOC.

### 1.2.1 The Bak, Tang and Wiesenfeld sandpile model

In their original paper [66] Bak, Tang and Wiesenfeld described this cellular automaton model of a sandpile. In a simple possible version the BTW model is defined on finite square lattice of size $L \times L$. This lattice represents a flat surface on which sand is dropped very slowly and sandpile growth takes place. A non-negative integer $z_{ij}$ is associated with every lattice site $(i, j)$, representing the height of sand column at that site measured by the number of sand grains. The rules for evolution of this model sandpile are as follows. Starting with an arbitrary initial configuration, specified by the heights of sand at every lattice site, sand grains are added at
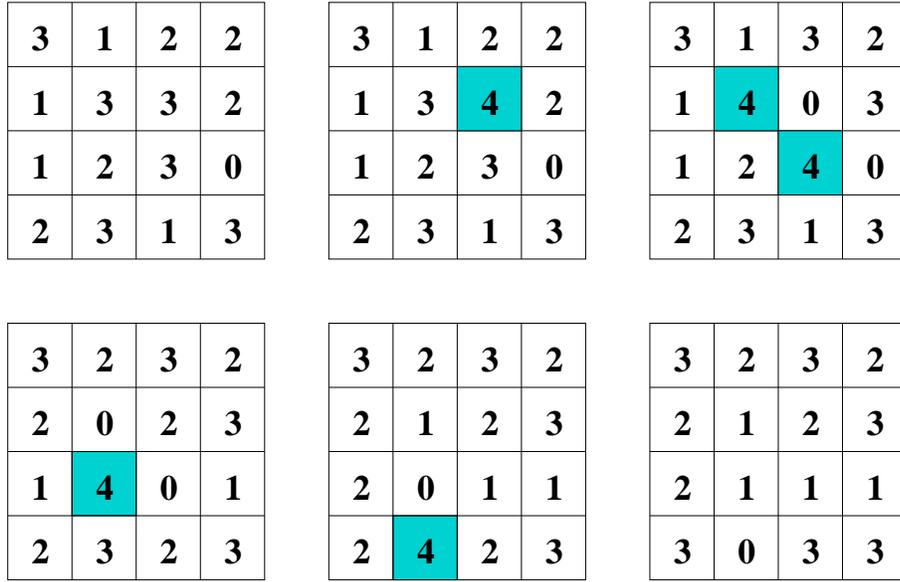
| 3 | 1 | 2 | 2 |
|---|---|---|---|
| 1 | 3 | 3 | 2 |
| 1 | 2 | 3 | 0 |
| 2 | 3 | 1 | 3 |

| 3 | 1 | 2 | 2 |
|---|---|---|---|
| 1 | 3 | 4 | 2 |
| 1 | 2 | 3 | 0 |
| 2 | 3 | 1 | 3 |

| 3 | 1 | 3 | 2 |
|---|---|---|---|
| 1 | 4 | 0 | 3 |
| 1 | 2 | 4 | 0 |
| 2 | 3 | 1 | 3 |

| 3 | 2 | 3 | 2 |
|---|---|---|---|
| 2 | 0 | 2 | 3 |
| 1 | 4 | 0 | 1 |
| 2 | 3 | 2 | 3 |

| 3 | 2 | 3 | 2 |
|---|---|---|---|
| 2 | 1 | 2 | 3 |
| 2 | 0 | 1 | 1 |
| 2 | 4 | 2 | 3 |

| 3 | 2 | 3 | 2 |
|---|---|---|---|
| 2 | 1 | 2 | 3 |
| 2 | 1 | 1 | 1 |
| 3 | 0 | 3 | 3 |

FIGURE 1.2: Illustration of an *avalanche* in the BTW sandpile model. The addition of a grain at a site with height $z = 3$ leads to an avalanche of size $s = 5$ and time duration $T = 4$.

randomly selected sites thus increasing the heights of sand columns at those sites. Thus when one unit of sand is added to a site $(i, j)$, the height of the column $z_{i,j}$ at $(i, j)$ increases by unity:

$$z_{i,j} \rightarrow z_{i,j} + 1. \tag{1.13}$$

However, when the height of the column at a site $(i, j)$ increases beyond a critical height $z_c = 3$ (the numerical value of $z_c$ assigned here is without the loss of generality) the column becomes unstable. As a result toppling occurs and the site $(i, j)$ relaxes by losing $z_c + 1 = 4$ grains of sand:

$$z_{i,j} \rightarrow z_{i,j} - 4, \tag{1.14}$$

whereby each of the four neighbours of $(i, j)$ gains one unit of sand:

$$z_{i\pm1,j} \rightarrow z_{i\pm1,j} + 1, z_{i,j\pm1} \rightarrow z_{i,j\pm1} + 1. \tag{1.15}$$

In many situations it happens that some of the neighbouring sites have sand column heights equal to $z_c$ before they receive the sand grains due to toppling of the site $(i, j)$. In such a case, these sites become unstable and they themselves topple. The toppling of all unstable sites in the neighbourhood are carried out in parallel. Eventually these topplings may lead to other topplings. Thus the system relaxes through a cascade of topplings of sand columns when the addition of a single sand grain to the system makes a column unstable. A cascade terminates when all sites on the lattice are stable. Such a relaxation process in termed as an *avalanche*. Now, the toppling at

a lattice site which is at the boundary of the system causes the loss of a sand grain because the grain falling outside the lattice is removed from the system. Thus constant inflow of sand grains into the system and the simultaneous dissipation at the boundaries ensures that all avalanches have finite life time and that the system passes through non-equilibrium stationary states.

One of the ways of quantifying the size of an avalanche is by counting the total number $s$ of topplings in the avalanche. The life time $T$ of an avalanche is the duration over which unstable sites are found in the system. These facts are illustrated in Fig. 1.2 where a $4 \times 4$ lattice is shown, on which the addition of a sand grain causes an avalanche of size $s = 5$ and duration $T = 4$. The probability distribution of avalanche sizes is characterized by a power-law tail. This is the signature of the long-range spatio-temporal correlations and hence criticality in the system. If $D(s)$ be the probability of occurrence of an avalanche of size $s$, then:

$$D(s) \sim s^{-\tau}. \tag{1.16}$$

When one probes the motion of a sand grain that leaves the system after its entry it is found to be diffusive in the sense that a toppling at a site results in its distribution to all the four neighbours of that site with equal probability. Since on the average a grain requires to traverse a distance $L$ on the $L \times L$ lattice to reach the boundary it accomplishes it in order $L^2$ steps. Therefore during the steady state when for every grain added one grain has to leave through the boundary, the system accomplishes it by $L^2$ topplings on average. This provides an estimate for $\langle s \rangle$:

$$\langle s(L) \rangle \sim L^2. \tag{1.17}$$

## 1.2.2 Finite size scaling of avalanche size distributions

The power-law for the avalanche size distribution $D(s)$ given in Eq. (1.16) has a cut-off at a value $s = s_c$ after which the decay is much faster. The cut-off is governed by the system size $L$ as:

$$s_c(L) \sim L^{\nu}. \tag{1.18}$$

It is generally assumed that the avalanche size distribution in a system of dimensions $L$ obeys standard finite size scaling ansatz [67–69]:

$$D(s, L) \sim s^{-\tau} \mathcal{D}(s/L^{\nu}) \tag{1.19}$$

where the scaling function $\mathcal{D}(y) \sim constant$ for $y \to 0$ and $\mathcal{D}(y)$ approaches zero very fast for $y \gg 1$. However, the values of the different exponents like $\tau$ and $\nu$ have still not been ascertained [70].

The BTW sandpile model is a prototype model of a system exhibiting the phenomenon of SOC. The sand grains can also be identified with energy, pressure, force, etc. as we will find out

in the Chapter 3. There are also many other models of SOC which are different from the BTW sandpile model. References to these models can be found in [70].

## 1.3  Econophysics

We borrow the definition of econophysics from the *Encyclopedia of Quantitative Finance* where [71] it has been proposed to be the "multidisciplinary study of complex large-scale financial and economic systems". However, in essence it has been the application of concepts from physics to investigate correlations and statistical regularities in distributions of different quantities which are relevant from the point of view of economics and finance. Such quantities include fluctuations in stock prices, foreign exchange quotes and gross domestic product of countries.

The quantities mentioned above are measurables belonging to very complex socio-economic systems. We have already discussed the case of finance markets in the previous paragraphs. It is arguable to an extent that whether physics, which is successful in modeling of inanimate matter, can be effective in probing such systems. In fact from the viewpoint of statistical physics it is also interesting to search for evidences of universal behavior.

The studies in econophysics are also greatly enhanced and facilitated by the huge amount of data that has become available presently. Essentially, the type of data that is obtained from the financial markets are time series data. The data contains the logarithm of price of some commodity, varying with time. Historically, the modeling of such time series was one of the pioneering contributions from the field of physics to finance. In 1959, M.F.M. Osborne modeled the time series for stock prices as a geometric Brownian motion [72]. This model predicted that the distribution of logarithmic price changes to be a log-normal. However, Mandelbrot in 1963 [73] showed that the distribution of price changes decays as a power-law with an exponent close to $2.7$. From then on investigations by different groups into time series' have demonstrated evidence of *scaling* and *data collapse* of distributions of different market related quantities [8, 74]. The subtlety in the nature of correlations in such time series and the non-stationarity of increments has also been explored [75].

The evidence of power-laws and scaling have prompted the research in econophysics to draw parallels between systems of market agents with systems like magnets and fluids which show such behavior at the critical point during phase transitions [76]. From a different point of view the absence of any control parameter, like temperature, in economic systems have encouraged modeling in the paradigm of self-organized criticality [77]. We have already introduced this general approach of self-organized criticality in section 1.2.

The models of statistical physics that are successful in simulating the behavior materials at criticality have been applied to model markets. In a very simplified picture consisting of trading agents where the trading volume is not considered and only the options of a trader *i.e.*, to buy

or sell or to stay out of market are considered, modeling has been possible on the lines of Ising and Potts spin sytems [14]. Such models are in general called agent-based models. In Chapter 4 of this thesis we consider some such models. The aim is to simulate the wealth distribution in societies which is the Pareto law, mentioned earlier. Here, however, the parallel is drawn between the members in a society with a system of gas molecules which interact with each other and exchange energy.

## 1.4  Plan of the Thesis

In the previous sections we have defined and described the various methods and tools as briefly as possible, in three broad areas which deal with complex systems. In the next three chapters we analyze the particular problems. In Chapter 2 we analyze international trade in the framework of complex networks, in Chapter 3 we examine how earthquakes can be modeled in the paradigm of self-organized criticality and in Chapter 4 we study about the modeling of wealth distributions in societies which is a problem that eonophysics deals with.

# 2 The International Trade Network: weighted analysis and modeling

## 2.1 Introduction

In Chapter 1 we have seen how the inequality in the distribution of wealth of individuals in a particular society or within a country gives rise to a Pareto tail for the distribution function. We will look into the detail of this problem in Chapter 4. Here however, we try to observe this scenario at a different scale. Individuals make up a society, societies constitute a country and countries make up the global society or world economy. Buying of goods or services by agencies (government and non-government) within one country from similar agencies in another country constitute a trade link between the two countries. Such bilateral trade ties, according to modern economic theory [78], are considered mutually advantageous and give rise to an international market. While a country which produces and sells different commodities and services, i.e., exports to other countries, has a purpose of making profit in this market to strengthen its own economy, a country may buy i.e., import such commodities with the purpose of meeting it's internal demands or for production of other salable commodities. These trading activities give rise to cooperation as well as competition between countries. Countries become dependent on each other as well as engage in conflict. Since every country participates in trade and due to the fact that each country is strongly interrelated with other countries via trade, the economy and politics of one country affects the economy and politics of others and vice-versa. One way to probe into such a complex organization of countries is to describe the system as a complex network where the countries are the nodes and trade channels between them are edges. This is what we call the International Trade Network (ITN).

In the last century the political scenario of the world has gone through revolutionary changes. These changes have influenced and shaped world trade and commerce. Major influential events include the World War I (1914-1918), the World War II (1930-1945), the Cold War (1947-1989) and the eventual dissolution of the Soviet Union (1991). Wars and war like situations have given rise to competition for market shares in world trade whereas allies in wars have become partners in trade. Several regional blocs have also emerged in the course of time where the promotion of trade between member states has been an important issue. Examples of active regional blocs
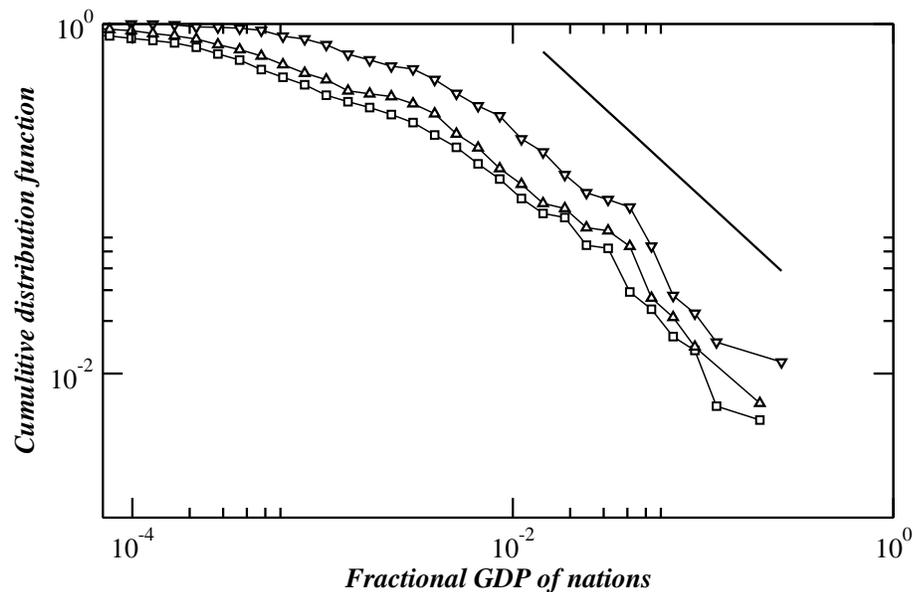
FIGURE 2.1: (a) Cumulative distributions of gross domestic products of nations (as fraction of the total annual GDP) averaged over the ten year periods during 1951-60, 1971-80 and 1991-2000 (from left to right). The solid line is a guide to the eye and is a power-law with slope -1.

include the NAFTA (1994), consisting of the United States of America, Canada and Mexico, and the ASEAN (1967) consisting of countries in south-east Asia. However, increasingly, cooperation in trade is not being confined to regions and this aspect of economic *globalization* has been an important factor in the evolution of the ITN.

The ITN, over the years, has grown in size, by the emergence and international recognition of new nations, as well as become more densely connected by the formation of trade links between existing countries and *strengthening* of existing links i.e., increase in amounts of trade in a link. To quantify strength or weakness of a link, we use the amount of trade measured in US dollars, which we define below as the weight of the link. Another aspect of the ITN that we investigate below in detail is the level of heterogeneity. There has always been few key players in the world trade. These are the countries with high economic strengths. Economic strengths being measured by the income of nations i.e., the *gross domestic product* (GDP). The GDP of a country is defined as the total market value of all final goods and services produced within the country, generally in a calender year. Broadly, countries are classified into three different categories. According to the World Bank classification of different countries in July 2005 based on GDP per capita as mentioned in the human development reports of 2003 [86], high income countries have GDP/capita at least $9,386, middle income countries have GDP/capita in between $9,386 and $766 where as low income countries have GDP/capita less than $766.
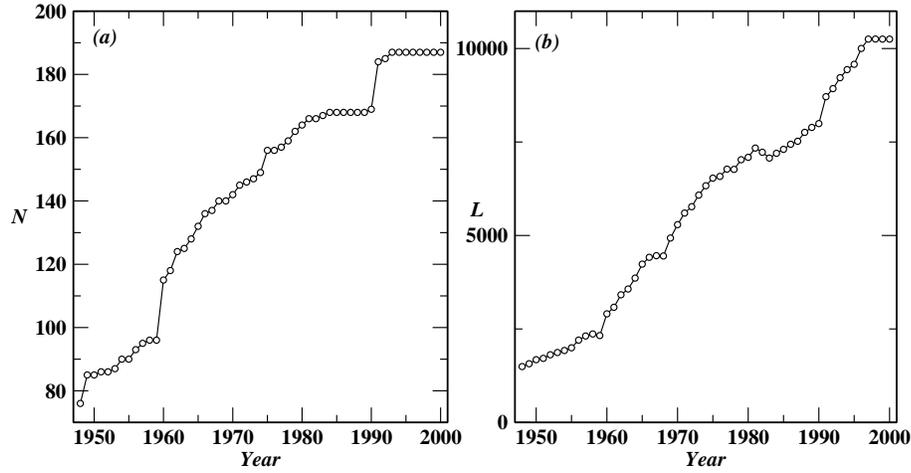
FIGURE 2.2: Variations of (a) the total number of nodes $N$ and (b) the total number of links of the annual ITN over a period of 53 years from 1948 to 2000.

International trade has been first considered from the network modeling framework in [27]. Here the topological characterization of the ITN for the year 2000 was done. A scale-free degree distribution and small world property for the network was found. In [81] the fractional GDP's of different countries have been looked upon as the 'fitness' for the international trade. In this model links are placed between a pair of nodes according to a probability distribution function of their fitnesses. In Fig. 2.1 the cumulative distribution function for the GDP of different nations (as fractions of the total world GDP) has been plotted. The figure suggests that distribution of GDP has a Pareto tail with exponent $-2$. Also the trade imbalances between different pairs of countries, measuring the excess of export of one country to another over its import from the same country have been studied [82, 83]. This method could define the backbone of the ITN [82].

## 2.2  Scheme of Analysis

This chapter is based on our publications [87] and [88]. Here we analyze the ITN as it has evolved in the time span of $53$ years from 1948 to 2000 . In the data [89] annual trade is expressed in terms of millions of US dollars ($M\$$) of imports and exports between countries $i$ and $j$ using four different quantities $\exp_{ij}$, $\exp_{ji}$, $\mathrm{imp}_{ij}$ and $\mathrm{imp}_{ji}$. In general the value of export from country $i$ to country $j$, $\exp_{ij}$ and the value of import of $j$ from $i$, $\mathrm{imp}_{ji}$ should be the same yet they have been quoted differently since exports from $i$ to $j$ and import of $j$ from $i$ are reported as different flows in the IMF (International Monetary Fund, Department of Trade) data. Although magnitudes of these quantities are approximately same in most cases, they do differ in many
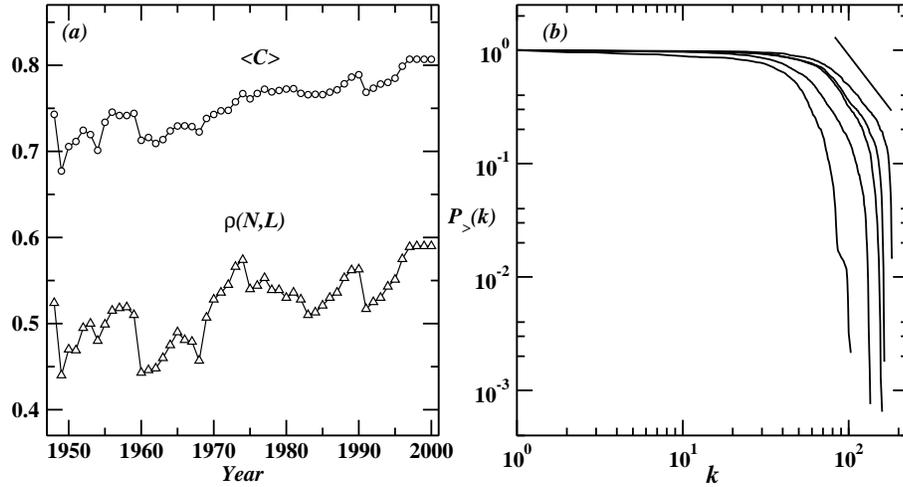
FIGURE 2.3: A subnetwork of the ITN for the year 2000, where only links with the highest 4 % of weights and the associated nodes (countries) are included [90], yielding in total 80 nodes and 411 links. The node size is proportional to its strength and link color to its weight. Link weights are defined as the volume of annual trade between two countries in $M\$$.

FIGURE 2.4: (a) Variations of the link density $\rho(N, L)$ and the average clustering coefficient $\langle C \rangle$ of the annual ITN over a period of 53 years from 1948 to 2000. (b)Cumulative degree distributions $P_{>}(k)$ versus degree $k$ averaged over ten year periods during 1951-60, 1961-70, 1971-80, 1981,1990 and 1991-2000 (from left to right). No power-law variation is observed for the 1951-60 plot. For the next decades, however, power-laws over small regions are observed whose slopes gradually decrease to $-1.74$ (indicated by the solid line) for the 1991-2000 plot.

instances due to different reporting procedures followed and different rates of duties applicable in different countries etc. [91].

Between two countries $i$ and $j$ we denote the amount of export from $i$ to $j$ by $w_{ij}^{exp}$, the amount of import from $j$ to $i$ by $w_{ij}^{imp}$ and the total trade by $w_{ij}$ and define them as:

$$w_{ij}^{exp} = \frac{1}{2}(\exp_{ij} + \text{imp}_{ji}), w_{ij}^{imp} = \frac{1}{2}(\exp_{ji} + \text{imp}_{ij}), w_{ij} = w_{ij}^{exp} + w_{ij}^{imp}. \tag{2.1}$$

Using these data we construct the International Trade Network for every calender year. Evidently nodes of the ITN represent different countries in the world. There is a link between a pair of nodes if there is non-zero amount of annual trade between them. This information is sufficient when we study the bare topological properties of the ITN for different years. However, here we move on to the weighted network description. The export $w_{ij}^{exp}$ is the outward flow from $i$ to $j$ and the import $w_{ij}^{imp}$ is the inward flow from $j$ with respect to $i$. Therefore the ITN is inherently a directed graph with two opposite flows along a link except cases of few links which have flows only in one direction. In our study we ignore the direction and define an undirected link between an arbitrary pair of nodes with a weight equal to the total trade $w_{ij}$ between the corresponding countries.
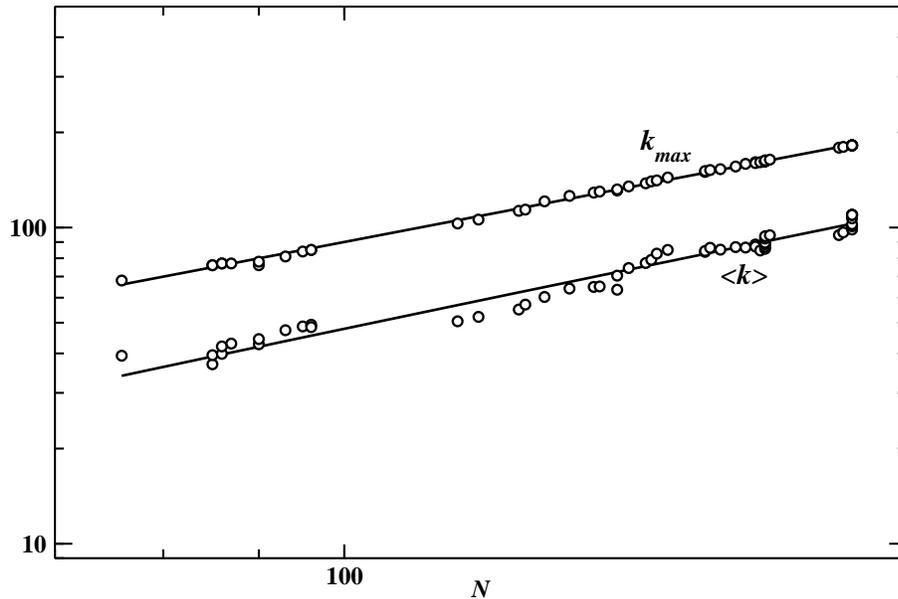
FIGURE 2.5: The variation of average nodal degree $\langle k \rangle$ and the largest degree $k_{max}$ with the size $N$ of the ITN. The solid lines are power-law fits to the data.

## 2.3 Topology

We first investigate the evolution of the ITN with respect to the the topological characteristics. Both the number of nodes $N$ as well as the number of links $L$ in the annual ITN varied from one year to the other. In fact they had grown almost systematically over the years. For example, the number of nodes have increased from $N = 76$ in 1948 to 187 in 2000 (Fig. 2.2(a)), the number of links have increased from $L = 1494$ in 1948 to 10252 in the year 2000 (Fig. 2.2(b)) where as the link density $\rho(N, L) = L/[(N(N-1))/2]$ fluctuated widely but with a slow increasing trend around a mean value of 0.52 over this period (Fig. 2.4(a)).

### 2.3.1 Degree Distribution

The degree $k$ of a node is the number of other countries with which this country has trade relationships. This can be further classified by the number of countries to which this country exports and is denoted by $k_{exp}$ where as $k_{imp}$ is the number of countries from which this country imports. In general $k_{exp} \neq k_{imp}$ but for some nodes they may be the same. To a great extent the structure of the ITN is reflected in its degree distribution. For the year 2000 this has been already studied in [27] and [81] in which a power-law for the cumulative distribution $P_>(k) \sim k^{1-\gamma}$ has been observed over a small range of $k$ values with $\gamma \approx 2.6$. We have studied the degree
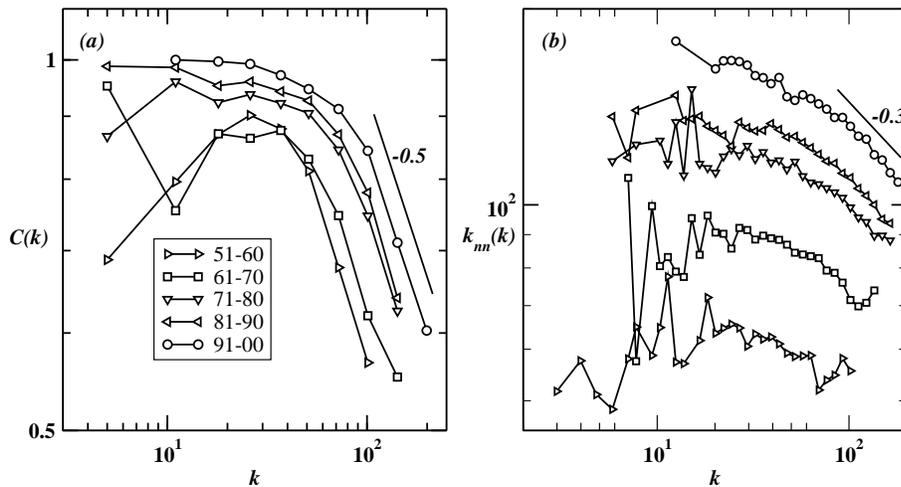
FIGURE 2.6: Plot of different topological quantities averaged over the ten year periods during 1951-60, 1961-70, 1971-80, 1981-90 and 1991-2000: (a) Clustering coefficient as function of degree, and (b) Nearest-neighbor degree as a function of degree. The solid lines are power-laws with slopes (a) $-0.5$ and (b) $-0.3$, plotted as references.

distributions, each averaged over ten successive ITNs, namely, 1951-60, 1961-70, 1971-80, 1981-90 and 1991-2000. The plots are given in Fig. 2.4(b). We see that indeed a small power-law region appears for the period 1991-2000 with a value of $\gamma \approx 2.74$. Such a region is completely absent in the decade 1951-1960. In the intermediate decades similar short power-law regions are observed with larger values of $\gamma$.

We have also studied the average degree of a node $\langle k \rangle$ and the maximal degree of a node $k_{max}$ for all the 53 years where the size $N$ of the ITN varied. We plot these quantities in Fig. 2.5 using double-log scale and observe the following power law growths as: $\langle k \rangle \sim N^{1.19}$ and $k_{max} \sim N^{1.14}$. Obviously these exponents have the upper bound equal to unity yet they are found out to be larger than one since both $\langle k \rangle/N$ and $k_{max}/N$ ratios have grown slowly with time as time progresses. This implies that as years have passed not only more countries have taken part in the ITN but in general individual countries have very rapidly established trade relationships with increasing number of other countries, a reflection of the economic global liberalization.

## 2.3.2 Clustering and Nearest-neighbor Degree

The Fig. 2.6(a) shows the plot of clustering coefficient averaged over ten year periods within the total span of 1951-2000. Here the clustering coefficient is plotted as a function of degree. The finding is similar to that originally presented in [27]. However, in [27] the clustering coefficient was only calculated for the year 2000. The power-law decay $c(k) \sim k^{-\omega}$ with $\omega$ around $0.5$
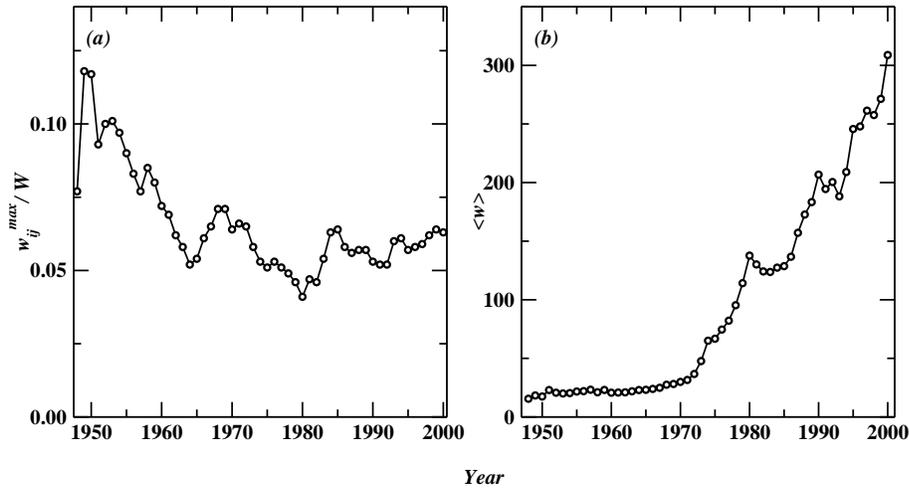
FIGURE 2.7: Plots of (a) the ratio of maximal trade $w_{max}$ along a link to the total volume of trade $W$ and (b) the average trade per link $\langle w \rangle$ of the ITN, over the period from 1948 to 2000.

signifies a hierarchical structure present in the system. The variation of the average clustering coefficient over the period of investigation can be seen in Fig. 2.4(a). The average clustering coefficient $\langle C \rangle$ is sum of the clustering coefficients $C_i$ for all nodes $i$ of the network divided by the total number of nodes. If the structure of the ITN was random then $\langle C \rangle$ would be equal to the value of the link density $\rho(N, L)$. However, as seen from the figure, $\langle C \rangle$ is about $1.3$ times larger than $\rho(N, L)$. Fig. 2.6(b) shows the plot of average degree of nearest neighbors $k_{nn}$ as a function of degree. The quantity $k_{nn}(k)$ is a measure of degree-degree correlations present in the system. The decaying form of $k_{nn}(k)$ also suggests hierarchy where richly connected countries or hubs provide connectivity to nations with low degrees and also have connections in between them.

## 2.4  Weighted Analysis

A huge variation of the volume of the bilateral trade is observed starting from a fraction of a million dollar to million million dollars. There are large number of links with very small weights and this number gradually decreases to a few links with very large weights (Fig. 2.3). The tail of the distribution consists of links with very large weights corresponding to mutual trades among very few high income countries [86]. The variation of the ratio of maximal trade $w_{max}$ in a year to the total world trade $W$ in that year is shown in Fig. 2.7(a). The average weight per link $\langle w \rangle$ had also grown almost systematically from 15.54 $M\$$ in 1948 to 308.8 $M\$$ in 2000 (Fig. 2.7(b)). Again $W$ had grown with years from $2.3 \times 10^{10}$ dollars in 1948 to $3.2 \times 10^{12}$ dollars in
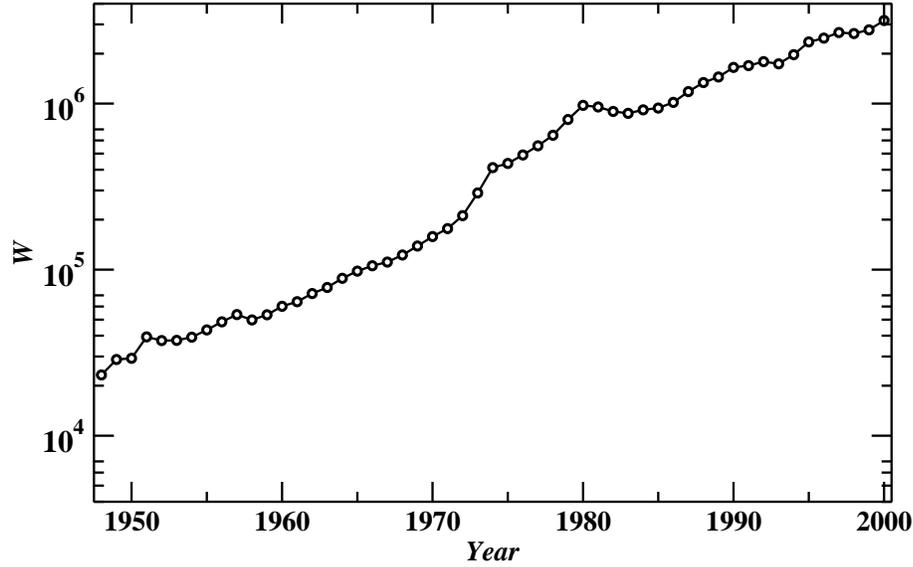
FIGURE 2.8: Plot of the total volume of annual world trade $W$ over the period from 1948 to 2000.

2000 (Fig. 2.8).

## 2.4.1 Weight Distribution

We have studied the distribution of the total trade $w_{ij}$ along a link in detail, without distinguishing between the exports and the imports. We denote $\mathrm{Prob}(w)dw$ as the probability to find a randomly selected link whose weight lies between $w$ and $w+dw$. In general in a typical ITN, the link weights vary over a wide range. There are many many links with small weights whose number gradually decreases to a few links with large weights. In the first attempt we plot the distribution on a double logarithmic scale as shown in Fig. 2.9(a). Data for the six different years from 1950 to 2000 at the interval of ten years have been plotted with different colored symbols. Each plot has considerable noise which is more prominent at the tail of the distribution. Yet one can identify an intermediate region spanning little more than two decades of $w_{ij}$ where the individual plots look rather straight. This indicates the existence of a power-law dependence of the distribution: $\mathrm{Prob}(w) \sim w^{-\tau_w}$ in the intermediate regime. Therefore we measured the slopes of these plots in the intermediate region for every annual ITN for 53 years from 1948 to 2000. These values have fluctuations around their means and our final estimate for the exponent is: $\tau_w = 1.22 \pm 0.15$.

We re-analyzed the same data by trying to fit a log-normal distribution as:

$$\mathrm{Prob}(w) = \frac{1}{\sqrt{2\pi\sigma^2}} \frac{1}{w} \exp\left(-\frac{\ln^2(w/w_0)}{2\sigma^2}\right), \tag{2.2}$$

where the characteristic constants constants of the distribution are defined as $w_0 = \exp(\langle \ln(w) \rangle)$
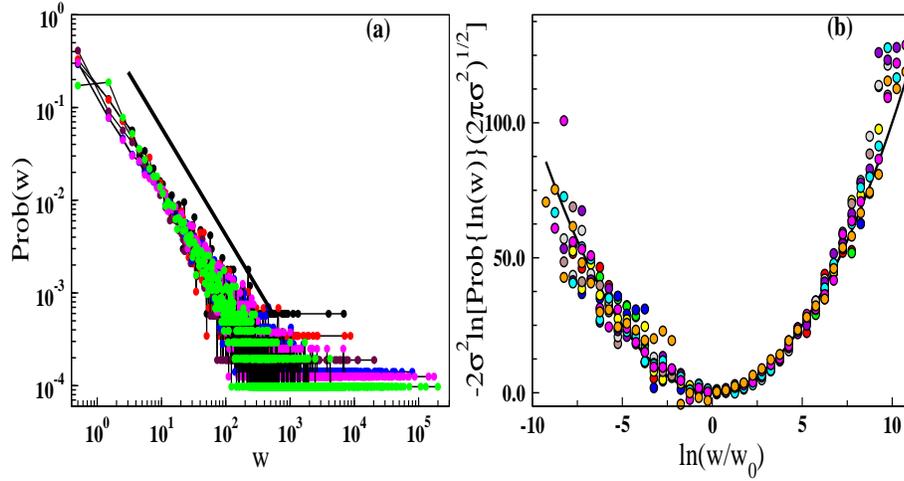
FIGURE 2.9: Trial of power-law and log-normal fits: (a) A double logarithmic plot of the probability distribution $\mathrm{Prob}(w)$ of the link weights for the six different years at the ten years interval from 1950 to 2000. The straight line shows average slope of the intermediate regime of all distributions giving an average estimate for the exponent $\tau_w = 1.22 \pm 0.15$. (b) Scaled plot of the probability distribution of the link weights $-2\sigma^2 \ln[\mathrm{Prob}\{\ln(w)\}\sqrt{2\pi\sigma^2}]$ as a function of $\ln(w/w_0)$. The five year averaged data have been plotted for ten different periods from 1951 to 2000. Points scatter around the scaled form of the log-normal distribution $y = x^2$ evenly except at the ends.

and $\sigma = \{\langle(\ln(w))^2\rangle - \langle\ln(w)\rangle^2\}^{1/2}$. It is found that different annual ITNs have different values for $w_0$ and $\sigma$. However we observed that one can make a plot independent of these constants. Given the $w_{ij}$ values of an ITN one calculates first $w_0$ and $\sigma$. Then calculating the $\mathrm{Prob}\{ln(w)\}$ one plots $-2\sigma^2 \ln[\mathrm{Prob}\{\ln(w)\}\sqrt{2\pi\sigma^2}]$ as a function of $\ln(w/w_0)$ which should be consistent with a simple parabola $y = x^2$ for all years (Note that $\mathrm{Prob}\{\ln(w)\}d\{\ln(w)\} = \mathrm{Prob}(w)dw$ implies $\mathrm{Prob}\{\ln(w)\} = w\mathrm{Prob}(w)$). This analysis has been done for fifty years for the period 1951-2000 but the data for every successive five years period have been averaged to reduce noise and ten plots for the intervals 1951-55, 1956-60, ... , 1996-2000 have been plotted in Fig. 2.9(b) with different colored symbols. We observe that the data points are evenly distributed around the $y = x^2$ parabola in most of the intermediate region with slight deviations at the two extremes, i.e., at the lowest and highest values of $\ln(w/w_0)$. We conclude that the probability distribution of link weights of the annual ITNs is well approximated by the log-normal distribution and is a better candidate to represent the actual functional form of the $\mathrm{Prob}(w)$ than a power-law. We mention here that the trade imbalances have also been claimed to follow the log-normal distribution [82].
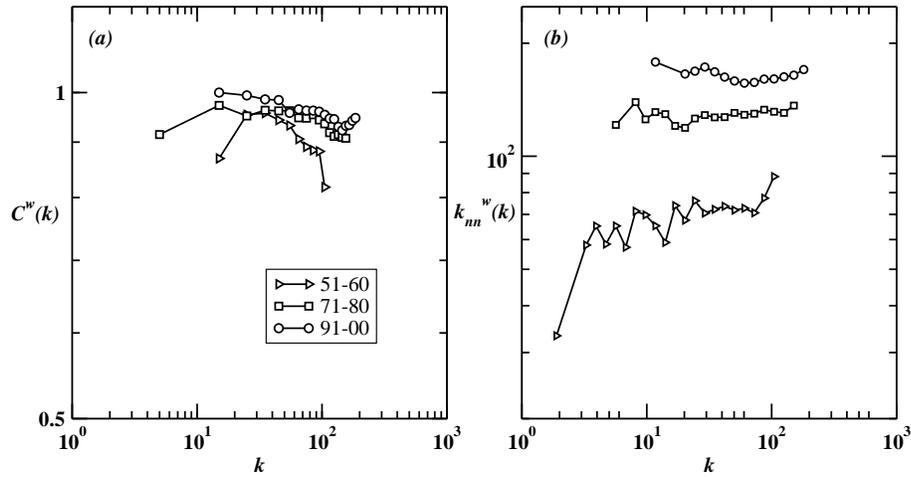
FIGURE 2.10: Plot of different weighted topological quantities averaged over the ten year periods during 1951-60, 1971-80, and 1991-2000: (a) Weighted clustering coefficient as function of degree, and (b) Weighted nearest-neighbor degree as a function of degree.

## 2.4.2 Weight-topology Correlations

In Fig. 2.10 we plot the weighted clustering coefficient $C_k^w$ and the weighted average degree of nearest neighbors $k_{nn}^w$ as functions of degree $k$. We compare these plots to Fig. 2.6 where the bare topological correlations are plotted. Interestingly, we observe few regularities [36]. It is found that $C^w > C$ and $k_{nn}^w > k_{nn}$ for the entire range of degree values. In addition it is found that $C_k^w$ is flat unlike $C_k$ which is decreasing, and $k_{nn}^w$ is slightly increasing form. These facts indicate the presence of very large amounts of trade between high degree nations which in fact balances the lack of topological correlations.

## 2.4.3 Giant Component

The ITNs for all the years within our period of investigation are single component graphs. However, we probe more closely into this aspect of structural organization of the ITN. We investigate the robustness of the structure from a viewpoint similar to percolation theory [92]. We consider a process which starts from $N$ nodes but with no links. Links are then inserted between pairs of nodes with a probability proportional to the weight of the link since a large weight link is more likely to be occupied than a small weight link. To do this, at first the link weights in the ITN have been ordered in an increasing sequence. Then the links are dropped in the descending order of the link weights starting from the maximum weight $w_{max}$. We have also studied the reverse procedure when links are dropped in the increasing sequence of the link weights starting from the weakest link. In the Fig. 2.11(a) we show the growth of the fractional size of the giant
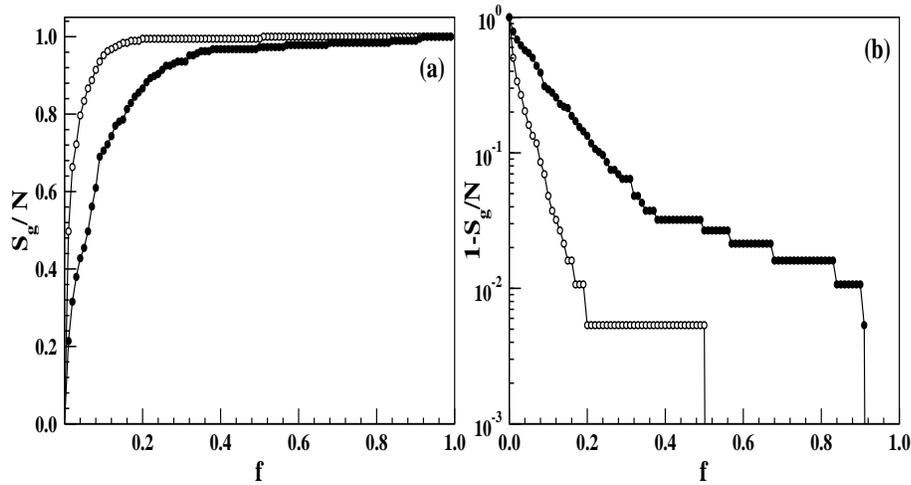
FIGURE 2.11: (a) Fractional size $S_g/N$ of the giant component of the ITN is plotted with the fraction $f$ of the links that are dropped in the descending (filled circles) sequence from the strongest and in the ascending (unfilled circles) sequence from the weakest weight of the links. (b) The difference $1 - S_g/N$ has been plotted on a semi-log scale which indicates an exponential approach to the fully connected network.

component $S_g/N$ with the fraction $f$ of links dropped. The plot shows that the growth rate is slower in the first case and the giant component spans the whole ITN faster than when links are dropped in the ascending order of strengths. Moreover, how the single connected component is attained has been quantitatively studied by plotting $1 - S_g/N$ and $f$ on a semi-log scale in Fig. 2.11(b). The intermediate straight portions in both plots indicate exponential growths of the size of the giant component.

## 2.4.4 Nodal Strength

The strength $s_i$ of a node $i$, $s_i = \Sigma_j a_{ij} w_{ij}$, in the case of ITN corresponds to the total volume of annual trade associated with the node. Intuitively, one can expect that in general the strengths of high-GDP countries are higher than those of the low-GDP countries. To see this in a quantitative fashion, we have utilized an elastic constant $\gamma$ to measure how changes in strength($s$) respond to changes in GDP($G$). Formally, we define:

$$\gamma = \frac{ds/s}{dG/G}, \tag{2.3}$$

where both $s$ and $G$ are measured in US dollars.

In Fig. 2.12 we plot the strengths $s_i$ vs. GDP $G_i$ (in units of millions of US dollars) for 22 different countries, representing a mix of economic strengths, i.e., 12 high, 7 middle and 3 low
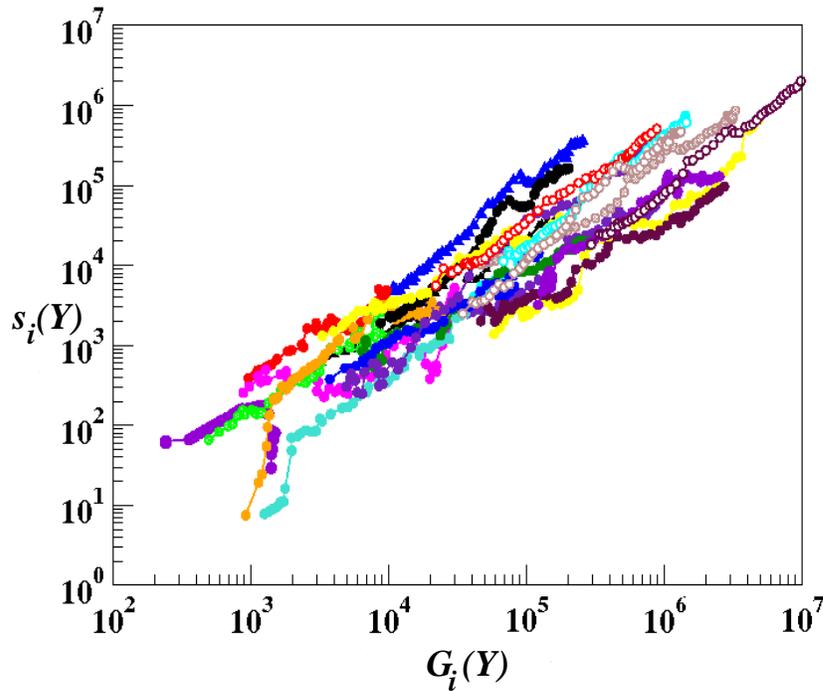
FIGURE 2.12: The dependence of the strength $s_i(Y)$ of a country $i$ on its GDP $G_i(Y)$ in year $Y$, plotted for each country (with a different color) over the 53 year span from 1948 to 2000. The strength and GDP being measured in millions of US dollars. General trend corresponds to a non-linear growth with an average exponent of around 1.2.

income countries. It is observed that the strength of each country grows non-linearly with its GDP with approximately the same slope $\gamma$. To take into account inflation we scale the strengths by the GDP deflation factor as it can be easily calculated from the data [89]. The deflation factor $f(Y)$, for a particular year $Y$, is calculated by dividing the GDP current to the year by the real GDP. In Fig. 2.13(a) we plot the scaled strengths $s_i(Y)/f(Y)$ vs. real GDP $G_i^R(Y)$ for different countries. Here we make an observation that due to the small magnitude of variation of the GDP deflation factor (this quantity is plotted in Fig. 2.13(b)) compared to the large magnitude of changes in the values of strength and GDP, the value of $\gamma$ does not change appreciably.

In Fig. 2.13(c) we show the probability distribution of $\gamma$ values for 168 different countries. The distribution has a long tail and the $\gamma$ values of 12 countries are found to be larger than 2. A detailed inspection reveals that majority of these 12 countries are those originated after Soviet Union, Yugoslavia and Czechoslovakia were fragmented. An overall average of the growth exponents has been estimated to be $\gamma = 1.26$ which comes down to 1.06 if these 12 countries are not considered for the averaging. The peak value of the distribution occurs very close to $\gamma = 1$. Interestingly, Irwin [93] has observed earlier that the total world export volume varies as a
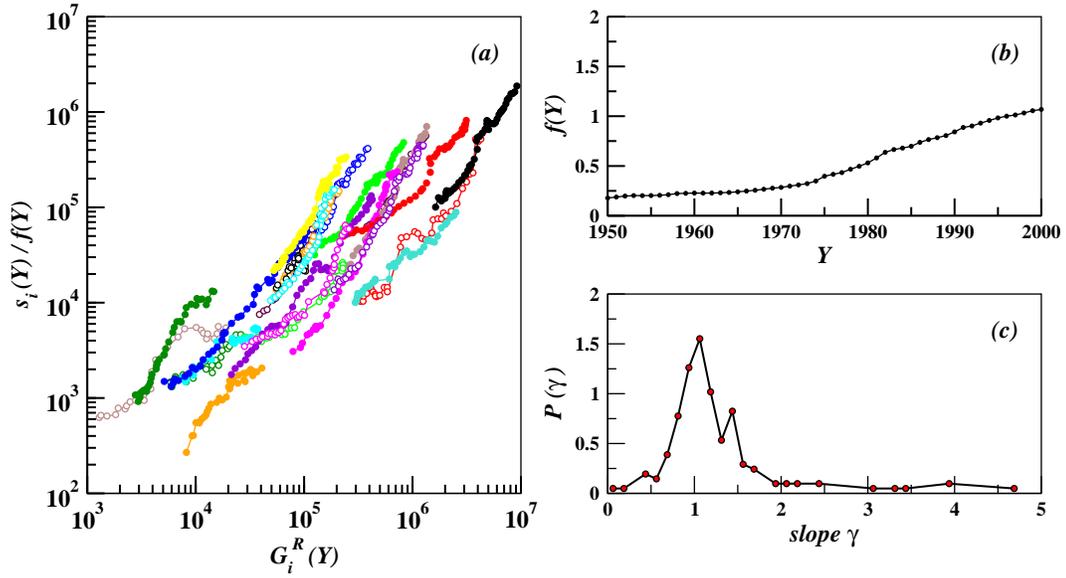
FIGURE 2.13: (a) The dependence of the scaled strength $s_i(Y)/f(Y)$ of a country $i$ on its real GDP $G_i^R(Y)$ in year $Y$, plotted for each country over the 53 year span from 1948 to 2000. (b) The variation of the GDP deflation factor over the period of investigation. (c) The probability distribution of the exponent $\gamma$ associated with individual countries.

function of the total world real GDP to the power of 1.16, along with other factors. In comparison, however, our observation reveals a more detailed picture, indicating that the total trade volumes of individual countries are also approximately power-laws as function of their individual GDPs, with exponents close to this value.

## 2.4.5 Rich-club Behavior

The *rich-club* behavior refers to a non-trivial correlation that is seen to exist among the nodes of different real-world networks like the Internet [94]. For an unweighted network this means that large degree nodes, referred to as rich nodes, are strongly connected among themselves forming a club. Precisely such a club consists of a subset of $n_k$ nodes whose degree values are at least $k$ and the rich-club coefficient (RCC) is measured as,

$$\phi(k) = \frac{2E_k}{n_k(n_k - 1)}, \tag{2.4}$$

where $E_k$ is the number of links that actually exist in the club and $[n_k(n_k - 1)]/2$ is the total number of node pairs in the club [94]. When the RCC $\phi(k)$ increases with the degree $k$, it implies that rich nodes are indeed tightly connected.

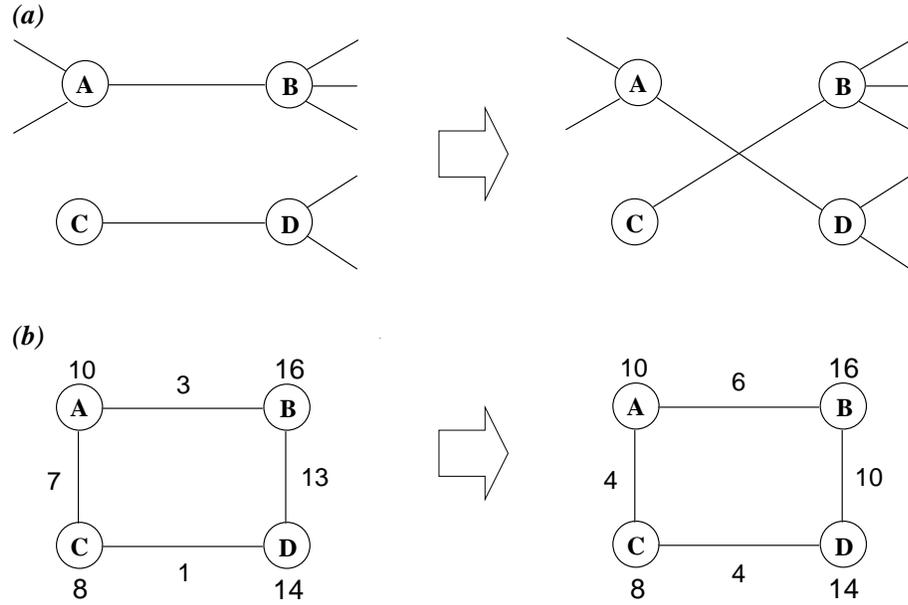However it has been realized that only this definition is not enough, since with this measure

FIGURE 2.14: (a) A typical step of the *local rewiring algorithm* [98, 99]. A pair of links A-B and C-D is randomly selected and rewired in such a way that two new links A-D and B-C are formed and the original connections A-B and C-D are erased form the network. During this process it is taken care are of that no multiple edges or self loops are formed. (b) A small network is shown to illustrate the process of weight randomization. The original network has four nodes and four links. The weights on the links are $W_{AB} = 3$, $W_{BD} = 13$, $W_{CD} = 1$ and $W_{AC} = 7$ such that the strength values are $s_A = 10$, $s_B = 16$, $s_C = 8$ and $s_D = 14$. After randomization, a new set of weight values are obtained *viz.* $W_{AB} = 6$, $W_{BD} = 10$, $W_{CD} = 4$ and $W_{AC} = 4$ which are consistent with the original strength values.

even uncorrelated graphs like the ones obtained by the Molloy-Reed (MR) algorithm [95, 96] show some rich-club effect as well [97]. It is suggested [97] that to obtain a proper benchmarking one needs to define a 'null model' or the maximally random network (MRN). The MRN can be constructed by the *local rewiring algorithm* [97–99] that randomizes a network preserving the nodal degree values $\{k_i\}$. This algorithm is illustrated in Fig 2.14(a). The repeated application of the rewiring step, starting with original graph, generates an ensemble of graphs corresponding to the original. Measuring the corresponding RCC $\phi_{ran}(k)$ on this ensemble and observing the variation of the *normalized* rich-club coefficient i.e., the ratio,

$$\rho(k) = \frac{\phi(k)}{\phi_{ran}(k)}, \qquad (2.5)$$

one is able to truly characterize the rich-club phenomenon. The ratio $\rho(k)$ greater than unity signifies that the high degree nodes are indeed tightly interconnected due to some non-trivial organizational principle in the network. For uncorrelated graphs it is found that $\rho(k) = 1$ for all $k$ [97]. We have executed the same analysis for the ITN for different years. However, it is observed
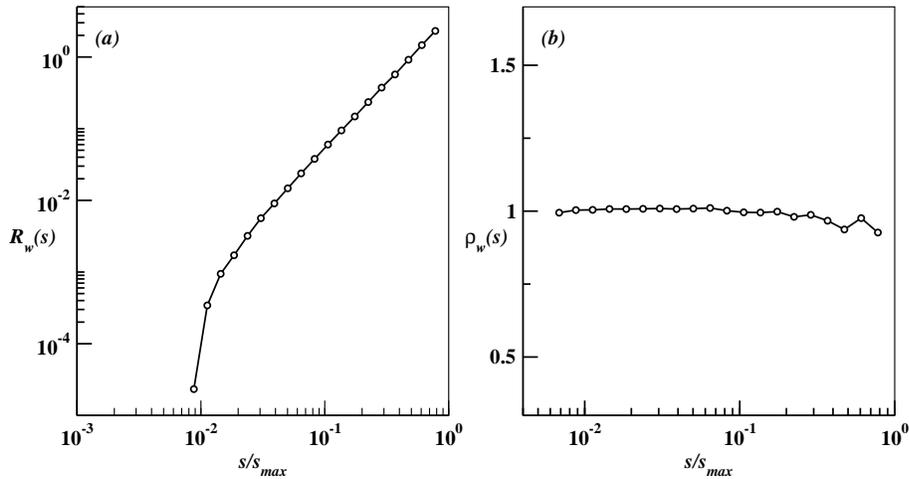
FIGURE 2.15: (a) The weighted rich-club coefficient $R_w(s)$ and (b) the normalized counterpart $\rho_w(s)$, for a model network constructed along the lines of [100]. The network for which $R_w(s)$ is calculated has a scale-free topology with exponent $\gamma = 2.5$ and the strength-topology relation $s \sim k^\beta$ is satisfied on average with $\beta = 1.5$.

that the variations of $\phi(k)$ and $\phi_{ran}(k)$ with $k$ are nearly same and consequently $\rho(k)$ is nearly equal to unity for the whole range of degree values.

## Weighted Rich-club Coefficient

We have also studied the rich-club effect of the ITN by considering it as a weighted network. To characterize the rich-club phenomena in weighted networks we have generalized the concepts that are applicable to the unweighted graphs. The rich-club is now defined as the subset of nodes ($n_s$ in number) whose strengths are at least $s$ controlling a major share of the world's trade dynamics. The RCC for the weighted network is defined as:

$$R_w(s) = \frac{2\Sigma_{s_i,s_j>s}w_{ij}}{n_s(n_s-1)}.$$

(2.6)

However, the properly normalized RCC, $\rho_w(s)$ is obtained by designing a null model corresponding to the original network by generating the ensemble which we call the maximally random weighted network (MRWN).

We have generated the MRWN by keeping both the nodal degrees $\{k_i\}$ as well as the nodal strength values $\{s_i\}$ preserved. To generate the MRWN of a given weighted network, we first generate the MRN from the unweighted version of the graph, as described above. Next we use a self-consistent iteration procedure to obtain the link weight distribution consistent with the nodal strength list $\{s_i\}$. We start by assigning arbitrary random numbers as the weights $w_{ij}$ to all links
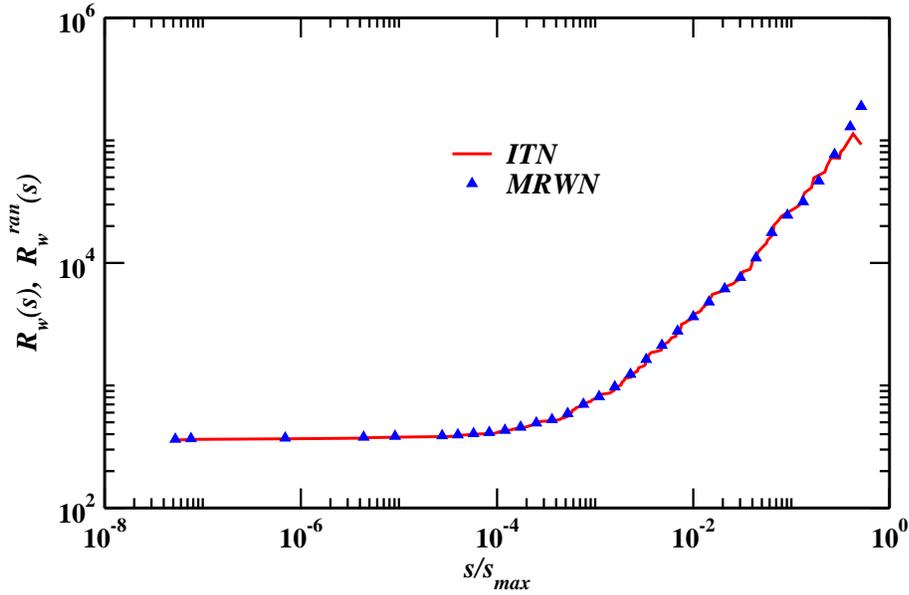
FIGURE 2.16: The weighted rich-club coefficients $R_w(s)$ (solid line) and $R_w^{ran}(s)$ (triangles) corresponding to the ITN of the year 2000.

maintaining that the weight matrix is always symmetric, i.e., $w_{ij} = w_{ji}$. For an arbitrary node $i$, the difference $\delta_i = s_i - \Sigma_j w_{ij}$ is calculated. Weights of all $k_i$ links meeting at the node $i$ are then updated as:

$$w_{ij} \rightarrow w_{ij} + \delta_i \left( w_{ij} / \Sigma_j w_{ij} \right), \tag{2.7}$$

in order to balance $s_i$ and $\Sigma_j w_{ij}$. By repeated iterations the link weights quickly converge and attain consistency with nodal strengths $\{s_i\}$. The Fig 2.14(b) illustrates the effect of the above procedure on a small graph consisting of four nodes and four links. For this graph a new configuration of weights is obtained which is consistent with the strength values of the four nodes. Once we generate this ensemble of different network configurations having fixed degree sequence $\{k_i\}$ and fixed strength sequence $\{s_i\}$, we measure the average weighted RCC $R_w^{ran}(s)$ for this ensemble to obtain the normalized weighted RCC:

$$\rho_w(s) = \frac{R_w(s)}{R_w^{ran}(k)}. \tag{2.8}$$

Similar to that unweighted counterpart, $\rho_w(s)$ greater than unity will signify positive correlation among the nodes in the club.

We verify our procedure for the model of maximally random weighted networks proposed in [100]. To construct such a weighted network we first use the MR [95, 96] algorithm to build an uncorrelated scale-free network with degree distribution $P(k) \sim k^{-\gamma}$. While choosing the degree sequence we limit the maximum degree $k_{max}$ to $\mathcal{O}(N^\alpha)$, where $\alpha = \min[1/2, 1/(\gamma - 1)]$
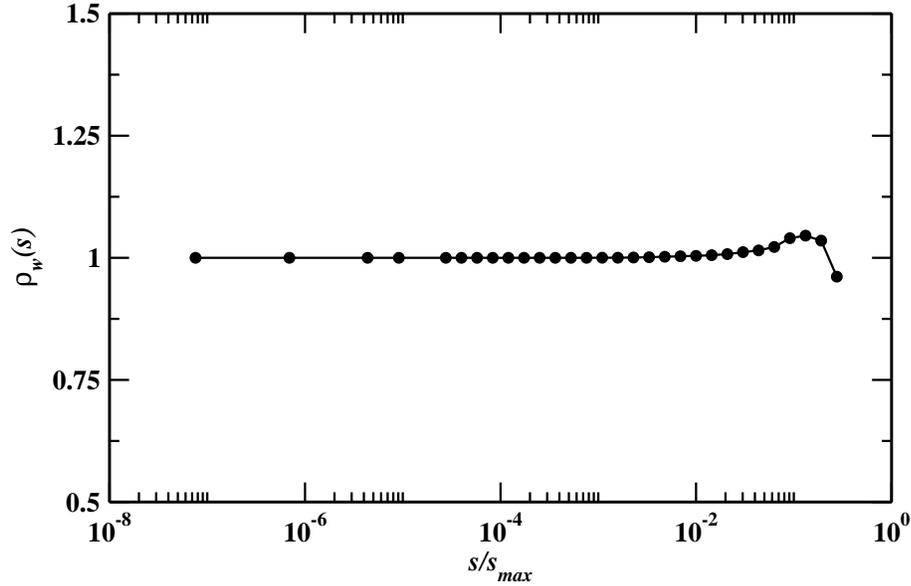
FIGURE 2.17: The ratio $\rho_{ran}(s)$ of the two coefficients $R_w(s)$ and $R_w^{ran}(s)$ for the year 2000 and is nearly equal to unity over the whole range of variation.

[101–103], so that ultimately it is possible to construct the unweighted network devoid of multiple edges and self-loops. We assign expected strengths to the nodes as $s_i \sim k_i^{\beta}$ and then assign the weights on the links using the relation [100]:

$$w_{ij} = \frac{\langle s \rangle k_i k_j}{\langle k \rangle s_i s_j},$$
(2.9)

so that the final strength values become $s_i = \sum_j a_{ij} w_{ij}$ and satisfy the relation $s \sim k^{\beta}$ on the average. For such a network we do not expect any rich-club behavior. The structural correlations [103] that are manifested in these networks due to finite size effects (which includes correlations generated by avoiding self-loops and multiple edges) are also present in the null model and therefore does not affect the ratio $\rho_w(s)$. This is illustrated in Fig. 2.15. The network constructed has $\gamma = 2.5$ and $\beta = 1.5$ (such a value of $\beta$ is seen in many real-world networks like the network of worldwide air transportation network [34]). Whereas the function $R_w(s)$ grows monotonically with strength $s$, the normalized weighted RCC $\rho_w(s)$ is found to be nearly 1 for all $s$ values.

In Fig. 2.16 we plot both $R_w(s)$ of the ITN for the year 2000 and $R_w^{ran}(s)$ for the MRWN with the scaled nodal strength $s/s_{max}$. The two measures are found to be nearly same, grow like $s^{0.85}$ for large $s$ values and their ratio $\rho_{ran}(s)$ is nearly equal to one except for a few values of $s$ near $s_{max}$ (Fig. 2.17).

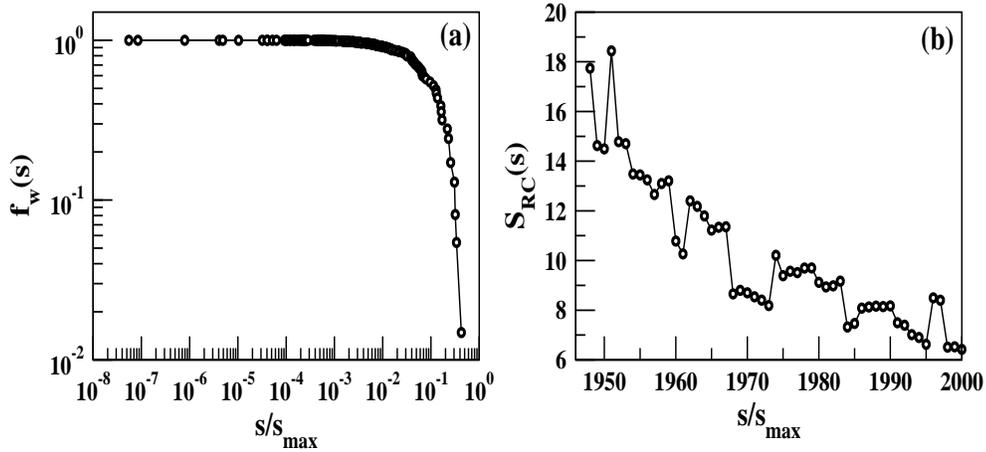To explain the above facts we observe that only 15% elements of the adjacency matrices of

FIGURE 2.18: Variations of the (a) fraction $f_w(s)$ of the total volume of trade taking place among the members of the club having strengths $s$ and above, and (b) percentage of the world countries that make 50% of the world's total trade volume falls from $\approx 19\%$ to $\approx 6\%$ between 1948 to 2000.

the ITN and the MRN are different. Therefore a typical node of ITN retains the links to most of its neighbors even after maximal randomization. This is because of the high value of the link density ($59\%$) of the ITN for the year 2000. As a result $\rho_{ran}(k)$ as well as $\rho_{ran}(s)$ are nearly equal to unity. This implies that the pairwise link connections and the associated link weights of the original ITN are very close to those of the corresponding MRWN. In fact one can say that the original ITN is a typical member of the different random configurations of the MRWN when the $\{k_i\}$ as well as $\{s_i\}$ sets of the ITN are preserved.

Zhou and Mondragón [94] observed a very similar behavior for the Internet statistics. Following them we conclude that rich nodes in the original ITN and in its corresponding MRN and MRWN are tightly connected and the similarity of the rich-club connectivity in the ITN structure (with and without weights) does not imply that ITN lacks a rich-club structure.

In fact the presence of the rich-club effect is evident even if we simply analyze the variation of the fraction $f_w(s)$ of the total volume of trade taking place among the members of the club. We define $f_w(s)$ as the ratio of the total volume of trade a subset of countries make among themselves to the total trade volume $W$ in the ITN. The subset is defined as those countries whose strengths are at least $s$. For this analysis we first arrange the nodes in a sequence of increasing strengths and then delete the nodes in this sequence one by one. When a node is deleted all links meeting at this node are also deleted. Consequently the total volume of trade among the nodes in the subset also decreases.

In the Fig. 2.18(a) we show how $f_w(s)$ decreases with $s/s_{max}$ for the year 2000. Up to a large value of $s/s_{max} \approx 0.01$, $f_w(s)$ effectively remains close to unity beyond which it decreases faster. It is observed that only a few top rich countries indeed trade among themselves one half of the
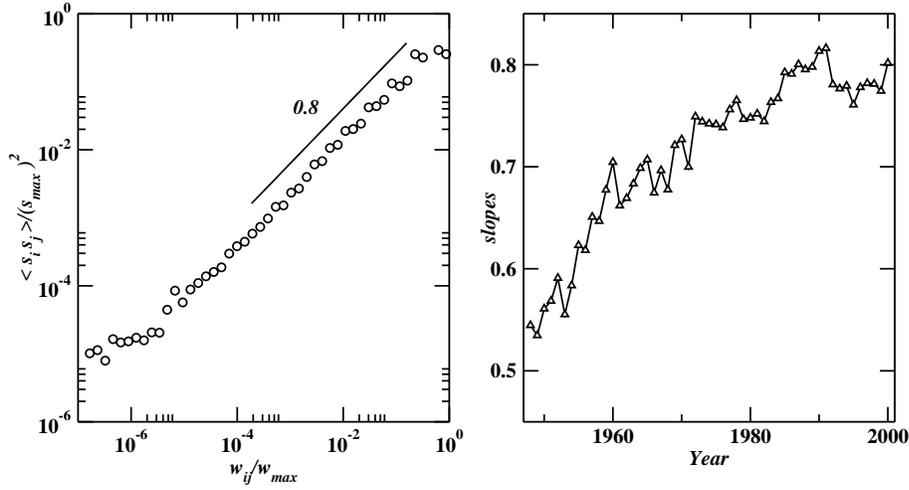
FIGURE 2.19: (a) The strength-strength correlation $\langle s_i s_j \rangle$ as a function of link weight $w_{ij}$ for the year 2000. For a power-law form $\langle s_i s_j \rangle \sim w_{ij}^{\nu}$ of the function, $\nu$ is found to be around $0.8$. (b) The values of $\nu$ for different years.

world's total trade volume, corresponding to $f_w(s) = 1/2$. Evidently these countries are very rich and are the few toppers in the list of strengths - which is said to have formed a 'rich-club'(RC). Therefore we measure the fraction of countries in the RC and calculate how the percentage size of the rich-club varied with time. In Fig. 2.18(b) we plot the year-wise fractional size $S_{RC}$ of the rich-club from 1948 to 2000 and see that it has been decreased more or less systematically from $\approx 19\%$ to $\approx 6\%$. This implies that though the world economy is progressing fast and more and more countries are taking part in the world trade market, yet a major share of the total trade is being done only among a few countries within themselves.

## 2.4.6 Other Correlations

The very heterogeneous distribution of trade volumes in the ITN is also reflected in the average pair correlation function $\langle s_i s_j \rangle$ [34] of nodal strengths and in its power-law dependence on the link weights $w_{ij}$ as shown in Fig. 2.19(a). Links with high weights $w_{ij} \sim w_{max}$ obviously must connect pairs of nodes of high strength, and for them $\langle s_i s_j \rangle \sim s_{max}^2$. On the other hand, for links of weights around unity, $\langle s_i s_j \rangle \sim s_{max}$. Assuming that $w_{max}$ itself is of the order of $s_{max}$, we find an upper bound for the exponent $\nu = 1$ describing the variation of $\langle s_i s_j \rangle \sim w_{ij}^{\nu}$. Our analysis of the ITN yields, however, a somewhat smaller value of $\nu$ being between 0.55 and 0.85 for different financial years between 1948 and 2000. The values of $\nu$ for different years are plotted in Fig. 2.19(b). The dependence of the weight distribution on the underlying topological structure of the ITN is studied by measuring the average strength of a node as a function of its degree [34],
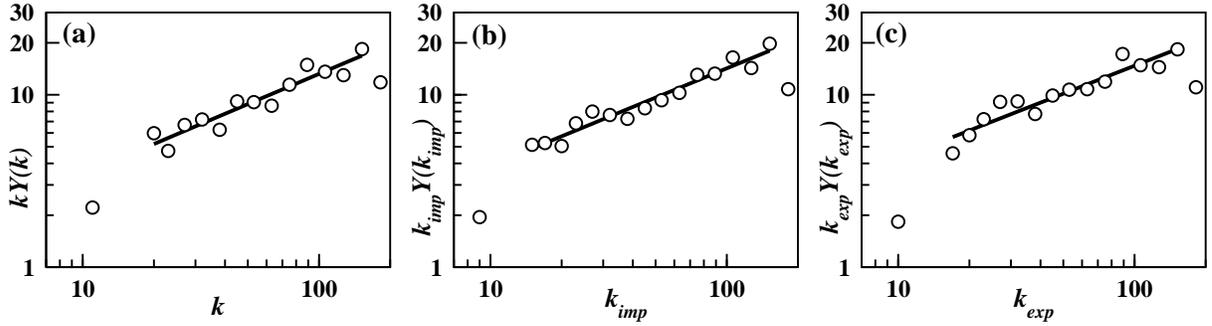
FIGURE 2.20: Binned plot of the nodal disparity measures with degree. Averaged ITN data for the period 1991 to 2000 have been used. The best fit straight lines are (a) $kY(k) \sim k^{0.56}$ for the trade network, (b) $k_{imp}Y(k_{imp}) \sim k_{imp}^{0.58}$ for the import network and (c) $k_{exp}Y(k_{exp}) \sim k_{exp}^{0.54}$ for the export network.

which turn out to exhibit strong degree of non-linearity: $\langle s(k) \rangle \propto k^{\mu}$ where $\mu$ varies between 3.4 and 3.7 for the same period.

## 2.4.7 Disparity

A country makes different volumes of trade with other countries. Therefore the values of the weights associated with the links of a node, both for imports and exports vary quite a lot. A numerical measure of this fluctuation is given by the 'disparity' measure Y [104, 105]. For a node $i$, the disparity is measured by [106, 107]

$$Y_i = \sum_{j=1}^{k_i} \left[ \frac{w_{ij}}{s_i} \right]^2. \tag{2.10}$$

The average disparity measure $Y(k)$ over all nodes of degree $k$ is calculated. If the weights associated with the $k$ links are of the same order then $Y(k) \sim 1/k$ for large $k$ values where as if the weights of a few links strongly dominate over the others then $Y(k)$ is of the order of unity. We have measured three disparity measures, namely $Y(k)$ for the link weights $w_{ij}$ as the total trade, $Y(k_{exp})$ for the link weights $w_{ij}^{exp}$ as the export from the node $i$ to node $j$ and $Y(k_{imp})$ for the link weights $w_{ij}^{imp}$ as the import from the node $j$ to node $i$. These quantities are plotted in Fig. 2.20 on log-log scales and we observe power-law dependencies as: $kY(k) \sim k^{0.56}$, $k_{imp}Y(k_{imp}) \sim k_{imp}^{0.58}$ and $k_{exp}Y(k_{exp}) \sim k_{exp}^{0.54}$. Similar variations are also observed in trade imbalances [82].

## 2.5 Communities

While studying a real network, one faces the problem of understanding and quantifying the nature of organization present in the system. We have already come across this problem while dealing with problem of characterizing rich-club phenomena. Decomposing the whole network into different smaller but highly interconnected subgraphs, called *communities* and characterizing their presence in terms of local correlations has been a challenging subject in the field of complex networks [108, 109]. The methods developed in this context been applied in very different contexts like the Internet [94] and biological webs [111]; and in general the methods have been widely different. For example in [109] the investigation has been done in the structural properties overlapping communities called *k-clique communities*. While the approach in [112, 113] has been to investigate the degree of community structure at different levels of hierarchy called *k-cores*. The first method essentially relies upon determination of all cliques (complete subgraphs) of size $k$ for a fixed value of $k$ whereas the latter is based on application of bootstrap percolation [114] to find subgraphs in which all nodes have at least $k$ edges. In general, however, the value of $k$ in the former method can be varied to probe at different hierarchies.

In this section our aim is to study the trading patterns of the ITN as it has evolved over 53 years [89] from 1948 to 2000 with an approach which is intermediate to that of [109] and [112, 113], and takes into account the bare topological as well as the weighted description. The method we describe below can in general be used to study and extract information from other real evolving networks.

In an unweighted network, a set of nodes will be called strongly interconnected if the number of links within these set of nodes is large. This degree of interconnectedness is maximum when the set of nodes constitute a clique. A node, in general, belongs to one or more independent cliques of different sizes. By an independent clique we mean a clique which is not a part of larger clique. In our method, for a particular node, we only focus on the clique with the largest size that the node belongs to. In general there can be more than one largest clique that the node belongs to. In such a case we determine the complete set of such cliques for a particular node. And we determine the sets for all the nodes in the network. In other words, in the network we determine all independent cliques where each of them is largest for at least one node in the network.

We call such cliques *communities*. In particular, we are interested in the structure of the largest clique (can be more than one) in the network, i.e., by our definition the community with the largest size. The notion of such a community is close to the sense of having a rich-club because we expect the hubs to be participating in such a community [115]. The definition of a completely connected graph as a community also makes sure that any measure of interconnectedness like the rich-club coefficient for such a community, where a null ensemble is used for sampling and eventual normalization, yields a value $\geq 1$, i.e., its presence is statistically recognized.
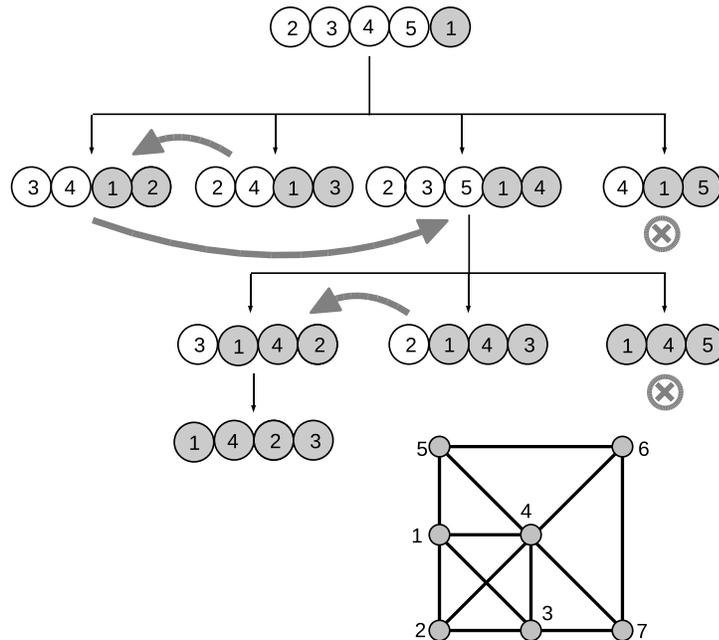
FIGURE 2.21: The illustration of the extraction of the largest clique in a small graph of seven nodes. The example graph is a stable 3-core and therefore it is searched for the presence of a 4-clique. We assume (without the loss of generality) that the searching process begins at the node numbered 1 having four edges, i.e., by searching for those 4-cliques which contain 1. We begin by constructing a set where all the neighbors of 1 as well as the node 1 itself are listed. This set is (as shown above by adjacent circles) therefore:{2,3,4,5,1}. This actually enumerates the subgraph which consists of 1 and its neighbors and the links that exist between these nodes. In the next step, four new sets are generated (sequentially) each of which corresponds to a neighbor of 1. Now when a new set is generated, it is checked against the sets that are generated earlier in the same time step. In this process of comparison if one set is found to be the subset of the other, the former is removed from the process and the latter is only considered for the next time step. Since we are searching for a 4-clique, if the cardinal number of any set is found to be less than 4, it is removed from the process. As seen above, the set {4,1,5} is rejected in the second step. In the figure above the set of shaded circles with a particular set of circles represents a complete subgraph within a larger subgraph. The process is carried out for newer time steps until we arrive at a complete subgraph of size four i.e., a 4-clique.

## 2.5.1 Algorithm

The problem of computing the size of the largest clique is a NP-complete problem [116]. For arbitrary graphs this problem can not be solved in polynomial time. However, our method, which we describe below, is found to be effective for the graphs we are interested in. Primarily because the graphs we investigate here are dense. The average link density being $0.52$ in all the realizations of the ITN corresponding to different years. First we find $k_c$, the largest value of $k$ above which the size of the $k$-core falls to zero. We note that if the size of the largest clique present in the
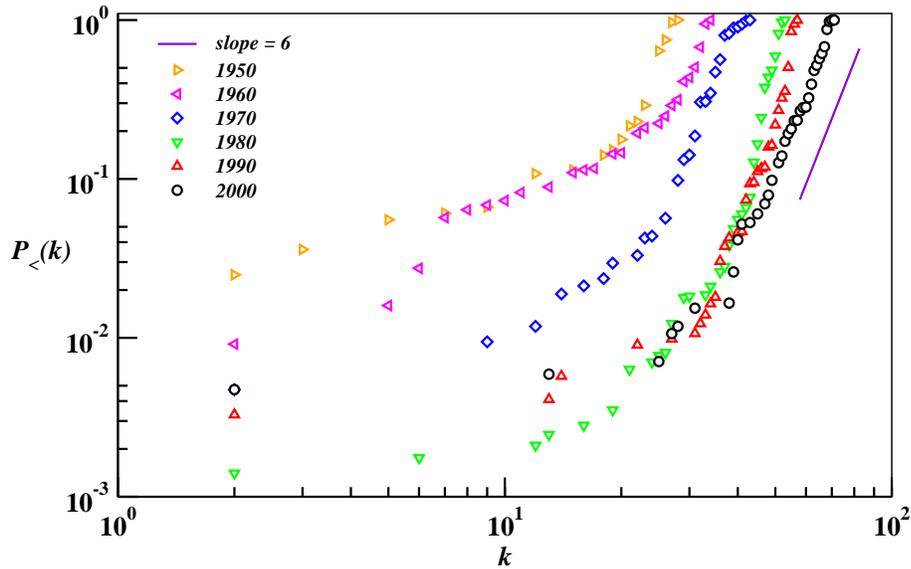
FIGURE 2.22: The probability $P_<(k)$ to find a community of size less than $k$.

graph be $k^{max}$, then $k^{max} \leq k_c + 1$. This upper bound on $k^{max}$ helps in pruning the graph and searching within the graph faster. If the largest clique has size exactly equal to $k_c + 1$ then we know it is a part of the $k_c$-core and we search for its presence within this subgraph (which is in general smaller in size compared to the original graph) without worrying about the rest of the nodes which lie outside. Now if there is no clique of size $k_c + 1$ within the $k_c$-core then we look for the presence of a clique of size $k_c$. And this clique has to be searched in the $(k_c - 1)$-core, which is a larger subgraph. This is because a member of a $k_c$-clique can have exactly $k_c - 1$ edges and will not be a part of $k_c$-core. Like this we go on lowering the value of $k$ to search for $k + 1$-cliques in $k$-cores until we are successful in finding the largest clique.

The search for $k$-cliques within a $(k - 1)$-core is done in the following way. We choose any node $i$ having $k_i$ edges. We construct a list where we put all its neigbours - $l_1$'s and the node itself. This is the first step. Then in the second step there will be $k_i$ new lists generated from this list. Each list will contain the node $i$, one of $i$'s neighbour $l_1$ and all the neighbours of $l_1$ - $l_2$'s, present in the old list i.e., nodes $l_2$ which are neighbours of set $\{i, l_1\}$. Then in the next step newer lists will be generated and each list will contain nodes which are neighbours of the set $\{l_2, l_1, i\}$. This process is continued until we find all lists $\{l_{k-1}, l_{k-2}, ..., l_1, i\}$ which enumerate all $k$-cliques that include the node $i$. During the process whenever the size of a list falls below $k$ no newer lists are generated from this list. Thus if $i$ is not a member of a $k$-clique then the generation of lists will end without detecting one. After finding all the $k$-cliques that include $i$, the node $i$ is removed from graph along with its links. This makes sure that there is no multiple
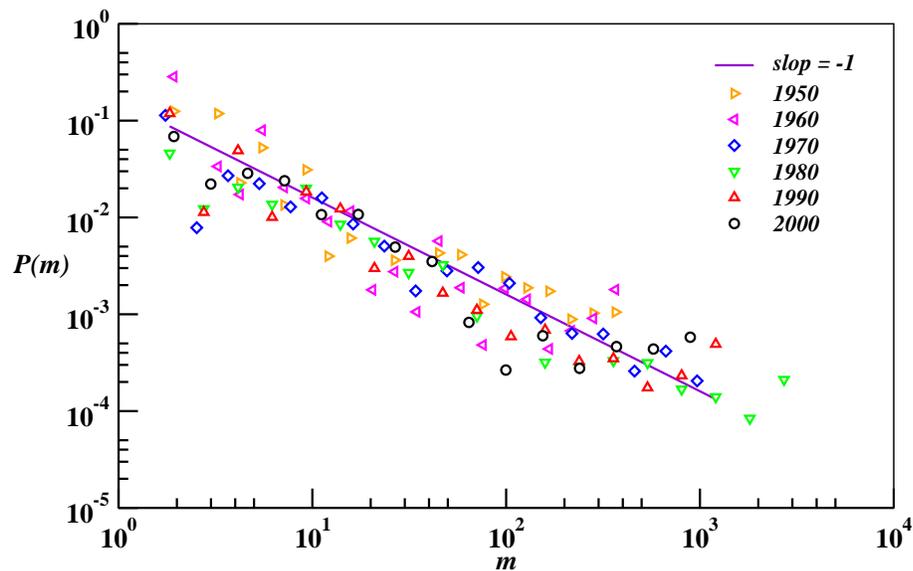
FIGURE 2.23: The probability $P(m)$ that a randomly chosen node participates in $m$ different communities.

detection of the same clique. The pruned subgraph is checked for stability i.e., whether it is still a $(k-1)$-core. If there is a remaining $(k-1)$-core a new node is selected and the above branching process of lists is started. Like this the $(k-1)$-core is explored for detecting $k$-cliques. In practice when we choose a node to carry out the search process we always choose the node with the minimum number of edges. This reduces the memory usage to a great extent and also makes the process faster. The illustration of this process in a graph where the largest clique has four nodes is given in Fig. 2.21.

The algorithm described above is sufficient to determine the set of communities (following our definition) with the maximum size present in the graph. However, if we require enumerating all the communities we have to carry out the process further. We look for communities of size $k$ in the $(k-1)$-core only after the communities of size larger than $k$ have been detected. And while choosing a starting node for a search process or removing nodes by bootstrap method we choose nodes which do not belong to the larger communities. Thus probing the graph at different hierarchies, from the $k_c$-core to the 1-core, all the communities can be found. The ITN grew form a size N=76 in 1948 to a size of N=187 in the 2000. In such a scenario, we probe the organization of the communities and how the overall structure has evolved over the period of investigation. As the communities we investigate here are essentially cliques with the special property stated above, we call such a community '$k$-community' if it has $k$ nodes.
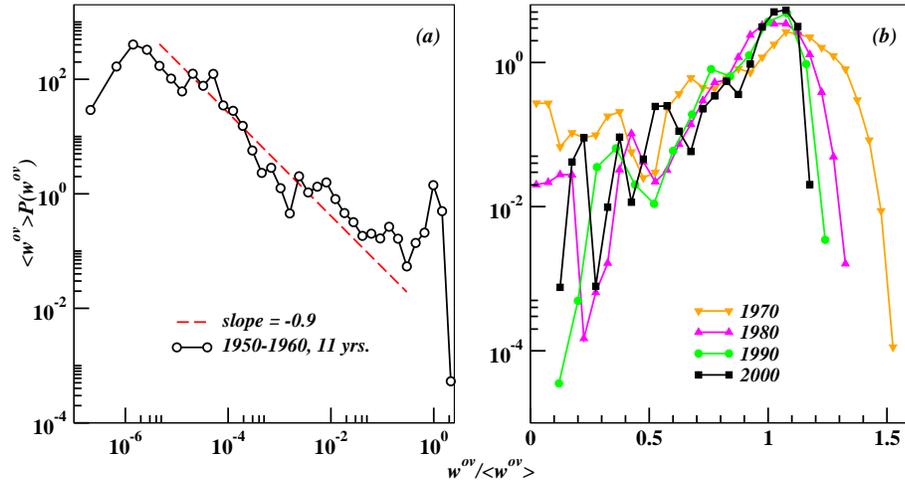
FIGURE 2.24: The plot of scaled probability density $\langle w^{ov} \rangle P(w^{ov})$ versus scaled overlap $w^{ov}/\langle w^{ov} \rangle$ where $P(w^{ov})$ is probability that the amount of overlap between two communities (in terms of weights) is $w^{ov}$ and $\langle w^{ov} \rangle$ is the average overlap. In (a) the probability is calculated over the period from 1950 to 1960 and in (b) the plots are for four calender years 1970, 1980, 1990 and 2000.

## 2.5.2 Analysis

For a particular node $i$ we denote the size of the largest community it belongs to by $k_i^{max}$. Then the size of the largest community in the network is $k^{max} = max\{k_i^{max}, ..., k_N^{max}\}$. In general a node $i$ may be a member of different $k$-communities where $k \leq k_i^{max}$. Looking into different networks realized for different years, the importance of such communities is understood by the fact that in a given network for any node the sum of the weights $w_{ij}$ of its links which belong to $k_i^{max}$ communities is almost $90\%$ of its strength $s_i$. Firstly, we observe that in a ITN for a particular year the number times a $k$-community occurs increases with $k$ and is ultimately cut-off by the value of $k = k^{max}$. In Fig. 2.22 we plot the cumulative function $P_<(k)$ that is the probability to find a community of size less than $k$. We find that $P_<(k)$ increases in the intermediate regions as a power-law before saturating to unity. The Fig. 2.22 suggests that the frequency of $k$-communities goes like $k^\delta$ with $\delta \approx 5$. We define $m_i$ [109] to be the number of communities that a node $i$ is a member of. In Fig. 2.23 we plot probability density $P(m)$ of $m$ treating $m$ as continuous variable. We find a power-law decay over several decades with exponent $-1$. This suggests a scale-free hierarchy of participation of countries in different communities where quite naturally the rich nations sit at the top of the hierarchy.

The ITN being a weighted network, when we study the nature of overlaps between different communities we look at overlaps in terms of weights. We define $w_{ij}^{ov}$ to be the sum of weights on the links which are common to the communities $i$ and $j$. In Fig. 2.24 we plot the probability density $P(w^{ov})$ of $w^{ov}$ for different years. Now the different plots for different realizations of the
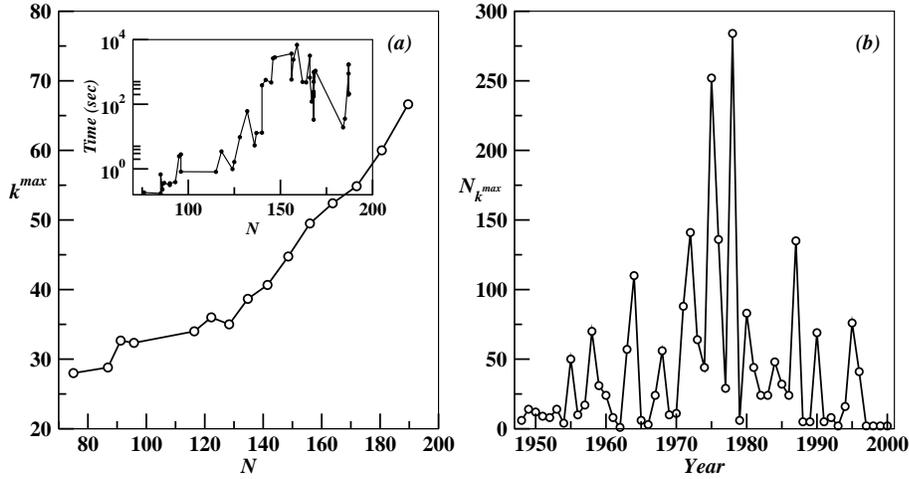
FIGURE 2.25: (a) The size of the largest clique $k^{max}$ versus the size $N$ of the ITN. The inset shows the computer time (in seconds) required to identify the largest cliques. (b) The number $N_{k^{max}}$ of cliques of size $k^{max}$ against different years.

ITN are scaled by the corresponding average overlap $< w^{ov} >$. This normalization is done to take into account the effects of economic growth as well as inflation, weights being originally in millions of US dollars. We observe that the distribution functions show a change in nature as the ITN evolves from the year 1950 to 2000. While plots during the period of 1950 to 1960 show a scale-free region with exponent around $-0.9$ for many decades of $w^{ov}/< w^{ov} >$, the region completely vanishes after 1970. We also note the change is gradual and takes place during the period from 1960 to 1970. This change in nature of overlap from scale free to a modal form (where the most probable value is quite large) suggests the growth of activity in the ITN during this period. Most rich nations develop trade ties amongst each other so that the amount of trade that they make between themselves show up as large overlaps.

Next we focus on the $k^{max}$-communities of different years which quite naturally are constituted by the high degree nodes because these are nodes with very large strengths i.e., the rich nations of the world. In Fig. 2.25(a) we plot the value $k^{max}$ against the number of nodes $N$ in the ITN during the 53 year period of investigation. We find $k^{max}$ to be increasing linearly with $N$. In Fig. 2.25(b) we plot the actual number $k^{max}$-communities found in each year. The number $N_{k^{max}}$ has large fluctuations but is seen to fall to small values during the end of the period of investigation. In the year 2000 the ITN has largest $k^{max}$ which is 71 and the value of $N_{k^{max}}$ is only 2. This is the signature that nations of the world leading in trade have evolved to a strongly interconnected sub-network. Now we look more closely at the trend in trading pattern of such nations. We call $G_{k^{max}}$ as the union of all $k^{max}$ communities. More correctly in a given network $G_{k^{max}}$ is the sub-network composed of all the nodes participating in the $k^{max}$-communities and the links which
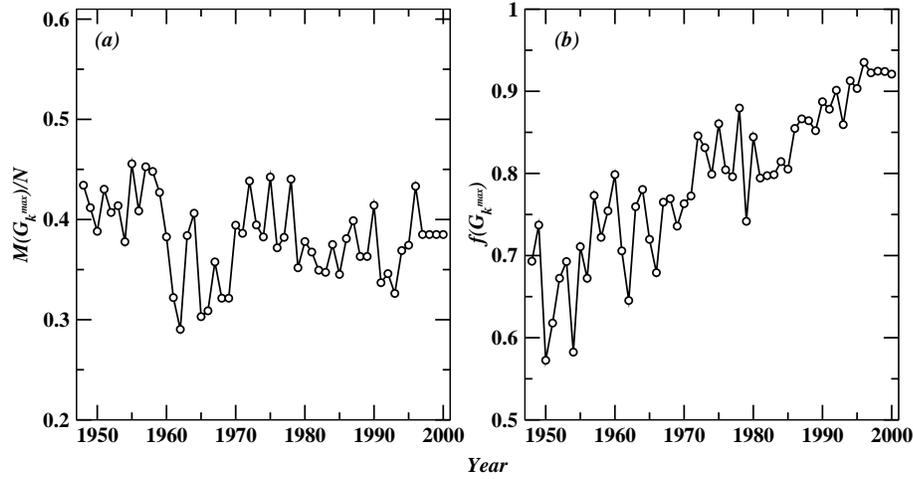
FIGURE 2.26: (a) The number of nodes $M(G_{k^{max}})$ that participate in the formation of the largest cliques in the ITN for a particular year scaled by total number of nodes $N$ in that year is plotted for different years. (b) The trade between the nodes participating in the largest cliques as fraction ($f(G_{k^{max}})$) of the total trade in the network.

are part of the latter. The notion of $G_{k^{max}}$ is similar to a $k^{max}$-core of the $k$-core representation. Interestingly it is found that the $k^{max}$-communities which participate in $G_{k^{max}}$ always form a large (with respect to the number of $k^{max}$-communities present) $k^{max}$-clique percolating cluster [110] and in many cases $G_{k^{max}}$ itself is the percolating cluster. This brings out strong cohesiveness in the structure of $G_{k^{max}}$. We define $M(G_{k^{max}})$ as the number nodes in $G_{k^{max}}$. In Fig. 2.26(a) we plot the fraction $M(G_{k^{max}})/N$ for different years. It shows no overall trend but fluctuates around a value of $0.4$. So as the ITN has grown in size over the years the size of $G_{k^{max}}$ has increased in almost a fixed proportion. However, Fig. 2.26(b) reveals a very different aspect of $G_{k^{max}}$. In Fig. 2.26(b) we plot the sum of weights in $G_{k^{max}}$ as a fraction of total weights present in the graph. It is found to increase as years proceed. This establishes how trade between rich nations has grown. In 1950 where the fraction of trade is around $60\%$, it rises to above $90\%$ in 2000.

## 2.6  Model

We now develop a dynamical model based on well-established gravity models [117] used in social and economic sciences. In a simple version of the model to describe the flow of social interaction between two economic centers $i$ and $j$ as a function of their economic sizes $m_i, m_j$ and distance of separation $\ell_{ij}$: $F_{ij} = Gm_im_j/\ell_{ij}^2$. This equation has been generalized to the parametric
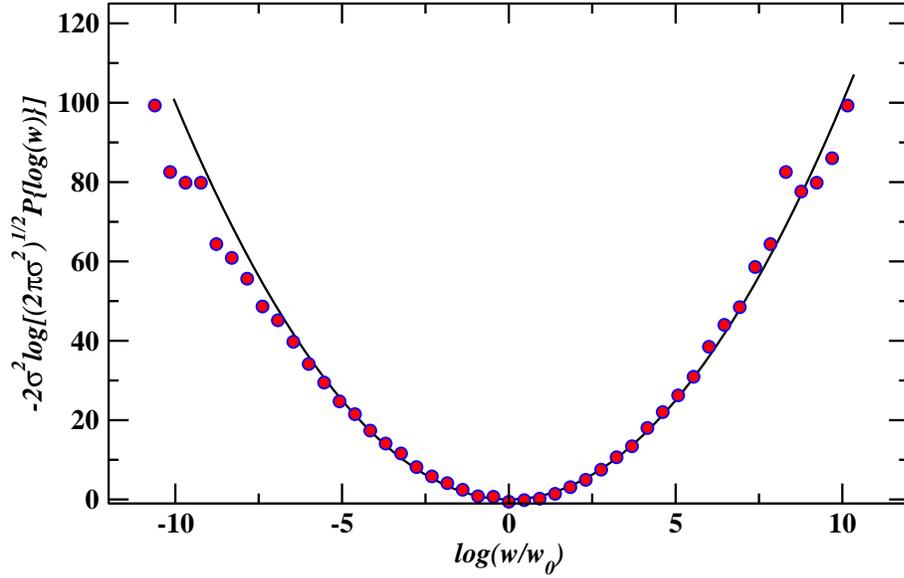
FIGURE 2.27: Model result-1: (a) Scaled weight distribution fits well with the simple parabola $y = x^2$.

form [118]

$$F_{ij} = m_i^{\alpha} \left( \frac{m_j^{\beta}}{\ell_{ij}^{\theta}} / \Sigma_{k \neq i} \frac{m_k^{\beta}}{\ell_{ik}^{\theta}} \right). \tag{2.11}$$

where the exponents $\alpha$ and $\beta$ usually range between 0.7 and 1.1 where as $\theta$ is observed to be around 0.6 [118].

In our model, we assume a unit square to represent the world and N points distributed at random positions representing the capital cities of different countries. Initially the GDP values $m_i (i = 1, N)$ are randomly assigned with uniform probability such that the total GDP is unity: $\Sigma_{i=1,N} m_i = 1$. In Chapter 4 we will investigate some pairwise wealth exchange models which are used to simulate the distribution of wealth in a society [119–121]. In a similar fashion we let the dynamics start, which is essentially a series of pairwise interactions. At every time step a pair of countries $(i, j)$ is randomly selected $(1 \leq i, j \leq N)$ for a transaction. In a transaction, the selected countries invest the amounts $F_{ij}$ and $F_{ji}$ calculated using Eq. (2.11). Then the total amount of investment $\tilde{F}_{ij} = F_{ij} + F_{ji}$ is randomly shared between the two countries as a result of this transaction, as follows:

$$m_i = m_i - F_{ij} + \epsilon \tilde{F}_{ij} + \Delta_i, \tag{2.12}$$
$$m_j = m_j - F_{ji} + (1 - \epsilon) \tilde{F}_{ij} + \Delta_j. \tag{2.13}$$

Here $\epsilon$ is a random fraction freshly drawn for every transaction. The random sharing of $\tilde{F}_{ij}$ is justified by the fact that while the gravity law describes the average interaction in terms of the
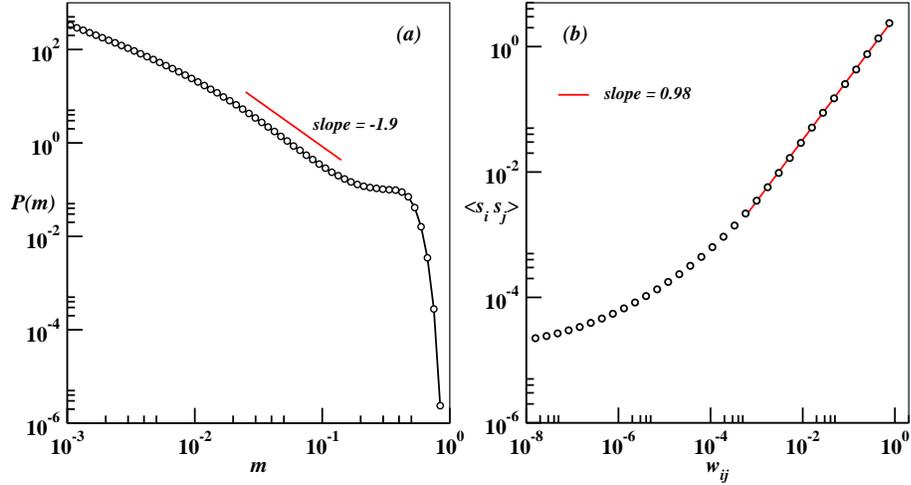
FIGURE 2.28: Model result-2: (a) The GDPs of the individual countries have a broad distribution, which in the tail region seems to follow roughly a power-law behavior (shown as a line with exponent ~1.9). (b) The strength correlation $\langle s_i s_j \rangle$ as a function of link weight is shown to grow approximately as $\langle s_i s_j \rangle \propto w_{ij}^{0.98}$.

strengths and distances of separation, the actual amount of trade depends on other factors, many of them are political.

In this idealized model, countries are not allowed to make debt, which in turn makes the dynamics non-conservative through the parameters $\Delta_i$ and $\Delta_j$. It holds for these parameters that $\Delta_i = 0$ if $F_{ij} < m_i$ and $\Delta_j = 0$ if $F_{ji} < m_j$. However, if for some transaction $F_{ij} > m_i$ or $F_{ji} > m_j$ then we add $\Delta_i = F_{ij} - m_i$ or $\Delta_j = F_{ji} - m_j$ such that after the transaction, GDP balance does not become negative. Also after the transaction, the individual GDP's are rescaled $m_i \rightarrow m_i / \Sigma_j m_j$ for the total GDP to remain unity. It is observed that a large number of pairwise transactions leads to a stationary state where $\langle m^2 \rangle$ fluctuates with time around a steady mean value. Starting at any time after reaching the stationary state, the dynamics is used to construct a model ITN such that links are established between countries $i$ and $j$ whenever there is a transaction between them. We let the dynamics run until a pre-assigned link density (typically 0.3-0.5) has been reached. For example, to generate a network corresponding to the ITN of the year 2000, we take $N = 187$ and continue the exchange dynamics till $L = 10252$ distinct links are dropped corresponding to the link density $0.59$. The weight of a link is then defined as the total amount of investment between pairs of countries in all transactions.

For comparison the weight distribution of our model networks is analyzed in the same way as the real ITN data, and it turns out that an excellent consistency with the simple parabola $y = x^2$ is observed for parameter values $\alpha = 1/2, \beta = 1, \theta = 1/2$, within a tolerance of 0.2 for all exponents as shown in Fig. 2.27. We also find that the resulting GDP distribution (shown in

Fig. 2.28(a)) is broad, showing a power-law like behavior for a short interval of $m$ (with exponent $\sim 1.9$) before finite size effects set in. This is to be compared with the real-world data where the GDP distribution of different countries has been argued to be consistent with the Pareto law [12]. Finally, as in the real ITN, the two-point strength correlation, shown in Fig. 2.28(b), is seen to grow like $\langle s_i s_j \rangle \propto w_{ij}^\nu$ with $\nu \approx 0.98$ in the large weight limit, compared to the range of values 0.6 - 0.8 for the real ITN (Fig. 2.19(b)).

## 2.7 Conclusion

In this chapter we have presented the analysis of the international countrywise trade data and studied the variations of different quantities associated with the International Trade Network. While the ITN is inherently directed, where two opposite flows are associated with the majority of the links, we largely ignored the directedness and analyzed the network as an undirected weighted graph. We also observed how different quantities evolved over time. Our analysis shows that the link weight probability distribution of the undirected ITN fits better to a log-normal distribution. This feature of the ITN remaining unchanged over a span of 53 years indicates robustness and some form of universality. Secondly, the nodal strength measuring the total trade volume associated with a country grows non-linearly with its GDP with a robust exponent.

Here we also develop a suitable null model to measure the rich-club effect in weighted networks and we use this to probe the ITN. Our study reveals the inherent subtleties involved in the definition of the rich-club. We also study the largest cliques in the ITN as it has evolved over the years. Identification of the cliques reveals a scale-free hierarchical structure in the ITN and also how participation in trade increased over the years. The rate of increase being more for the rich countries of the world. Finally, the main features of the real-world ITN have been reproduced by using a simple non-conservative dynamical model starting from the well-known gravity model of social and economic sciences.

# 3 Self-organized Critical Model of Earthquakes

## 3.1 Introduction

We have already discussed in previous chapter that a striking feature of many real-world networks are their fat-tailed degree distributions. It has been argued that these networks, called scale-free networks, self-organize to such architectures. A possibility which has been explored is that the network topology evolves under the feedback from some dynamical process taking place on the network itself. Several groups [122–124] have attempted to explain the emergence of scale-free nature in networks in the framework of self-organized criticality (SOC). Such investigations are prompted by the success of SOC in modeling the fractal structures and scale-free properties ubiquitous in nature [20, 21] where any external control is absent.

In this chapter, based on our publications [125, 126], we present a SOC model for earthquakes with a new boundary condition. This boundary moves with the center of the avalanche and therefore is different for different avalanches. Consequently all measures become free from the non-uniformity with respect to the fixed boundary models; and we investigate the different distributions and scaling, observed in real data, in the context of the model.

SOC has been argued to explain the natural phenomenon of earthquakes where signatures of criticality are revealed by the presence of rich scaling and scale invariant phenomena in absence of any control parameter. Earthquakes are characterized by the very slow build-up and sudden release of stress within the earth's interior and occur as irregular bursts of various magnitudes. A globally driven variant of the sandpile model of SOC, which we have already discussed in the Chapter 1, provide an appropriate platform for modeling where an avalanche in the model is identified with an earthquake.

Earthquakes result in sudden release of energy under the surface of the earth. The energy propagates as waves called *seismic waves*. In general a single earthquake results in very different kinds of vibrations. The waves are essentially classified according to the resulting particle motion relative to the direction of propagation of the wave. These waves propagate at the earth's surface as well as through the interior of the earth. At the surface of the earth these waves produce vibrations and fracture of the ground. Conventionally, the magnitude of an earthquake
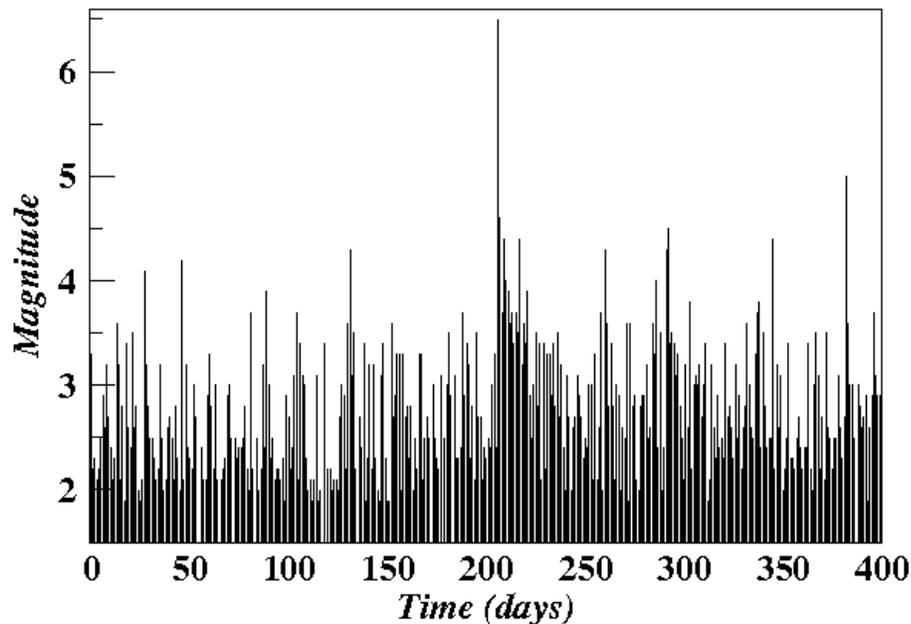
FIGURE 3.1: Time series for earthquake magnitudes in the period of November 1992 to February 1993 for earthquakes recorded by the South California Seismographic Network. Data is available at http://www.data.scec.org/ftp/catalogs/SCSN.

is measured on the Richter Scale. On a particular seismograph i.e., a magnitude measuring instrument, a particular earthquake is assigned a magnitude $m + 1$ if it releases ten times more energy than an earthquake of magnitude of $m$. This estimation is done based on the amplitude of vibration recorded in the seismograph and the difference in time of arrival of different form of waves from where they originated due to a particular earthquake. An earthquake of magnitude $m = 3$ or less will not cause much perturbation at the surface but earthquakes with magnitude larger than 7 will inflict damage to man-made structures like buildings ultimately causing severe loss of human life and property. Fig. 3.1 shows a time series for the magnitude of earthquakes (with magnitude greater than $1.8$) that occurred in the Southern California region in year 1992-1993. The quantity $10^m$ is known as the seismic moment '$s$'. The energy released $E$ is assumed to follow the approximate relation $E \sim s^{3/2}$ [127].

Based on different mechanical properties like the elastic moduli, the earth can be divided into different layers. The outermost layer is the $lithosphere$ which has an average thickness of around 60 kilometers. Under the lithosphere lies the $asthenosphere$ which has relatively less viscosity and shear strength and therefore is able to flow on geological time scales. This layer is another 100 kilometers thick. However, the lithospheric layer is broken up into different pieces called $tectonic\ plates$; and a single plate in general underlies continents as well as oceans(Fig. 3.2). An interplay of transport of thermal energy and matter at the boundary of the lithosphere and the
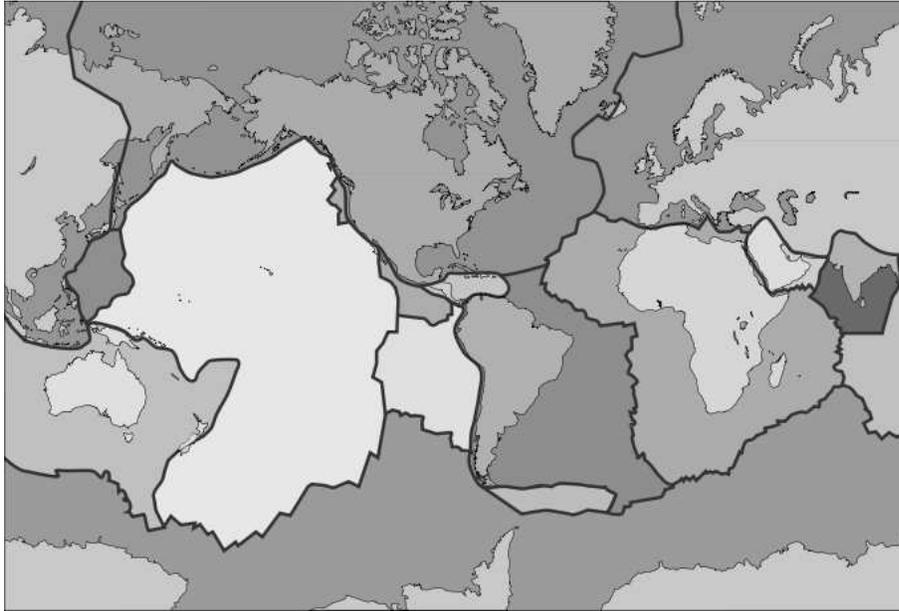
FIGURE 3.2: Picture showing different tectonic plates containing the continents and oceans (courtesy of http://en.wikipedia.org).

asthenosphere gives rise to motion of the tectonic plates which 'float' on the asthenosphere. The plates move very slowly relative to each other. Motion of individual plates range from around 1 cm per year to around 10 cm per year. The relative motion between two adjacent plates often results in their collision at different point along the boundaries and gives rise to a '*stick-slip*' process [128–130]. Such stick-slip processes are the major cause of earthquakes. When two plates have their surfaces (at the plate boundaries) in contact and one plate tries to slide past the other, the motion is rarely smooth. The irregular surfaces with rocky projections provide huge resistance. In fact the structure of boundaries are known to be fractal-like [132, 133]. When the sliding motion is prevented by the irregularities, a stress field develops in the region with accumulation of strain energy within the volume near the surfaces in contact. The upper part of lithosphere is brittle and the process continues until the stress is sufficient to cause fracture in the rocks that compose the surfaces allowing sudden motion along boundaries. The stored strain energy is released instantaneously in the form of seismic waves causing an earthquake. The point at the plate boundaries where stress initiates fracture is called the focus of the earthquake. Generally, the focus lies at some depth under the ground. The point directly above the focus and at the ground level is called the *epicenter* of the earthquake.

Although rare but there are earthquakes in the interior region of a tectonic plate, away from inter-plate boundaries. These are called *intraplate* earthquakes and are found to occur around fracture zones within the tectonic plates. Most earthquakes, however, occur at and around
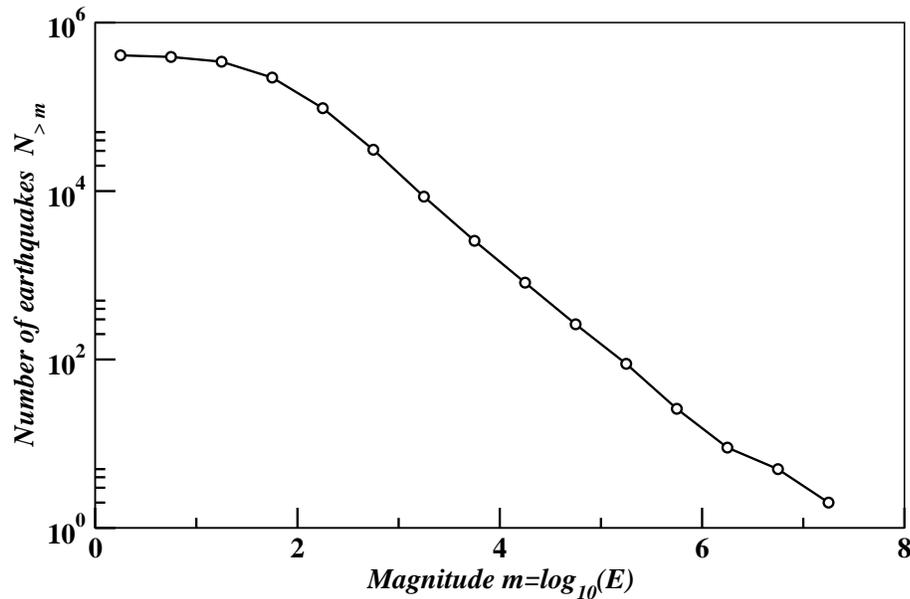
FIGURE 3.3: Plot of the Gutenberg-Richter law from the data from the South California Seismographic Network.

the plate boundaries. The investigations into the pattern of occurrence of earthquakes reveal a clustering effect in space and time. The general observation being earthquakes tending to occur in intermittent bursts but without any average frequency; and successive bursts most of the times separated by long periods of inactivity. A conventional way of analyzing data from such bursts is to divide a cluster of earthquakes into different shocks. The largest of the lot being labeled as the main shock and earthquakes that occur before and after the main shock as the foreshocks and aftershocks, respectively. However, a clear demarcation may not be possible always. According to Omori' law, suggested in 1894 [136], the number of aftershocks $n(t)$, after time $t$ elapses since the main shock in a cluster of earthquake events, decays in time as:

$$n(t) = \frac{k}{(c+t)^p},$$

(3.1)

where $k$, $c$ and $p$ are constants [136–138] that are obtained from a fit of this empirical law to the data for the cluster of events. The value of $p$ is seen to range between $0.7$ and $1.7$ from region to region.

In addition to Omori's law which is a power-law, there emerges many other instances of fractality and scale-invariance in the spatio-temporal behavior. The epicenters are found to be spatially distributed on a fractal pattern [4, 131, 133]. The distances between the epicenters of successive earthquakes are distributed according to a power-law [134]. Estimation of correlation between a pair of shocks, when used for the identification of the main shock of each aftershock, results
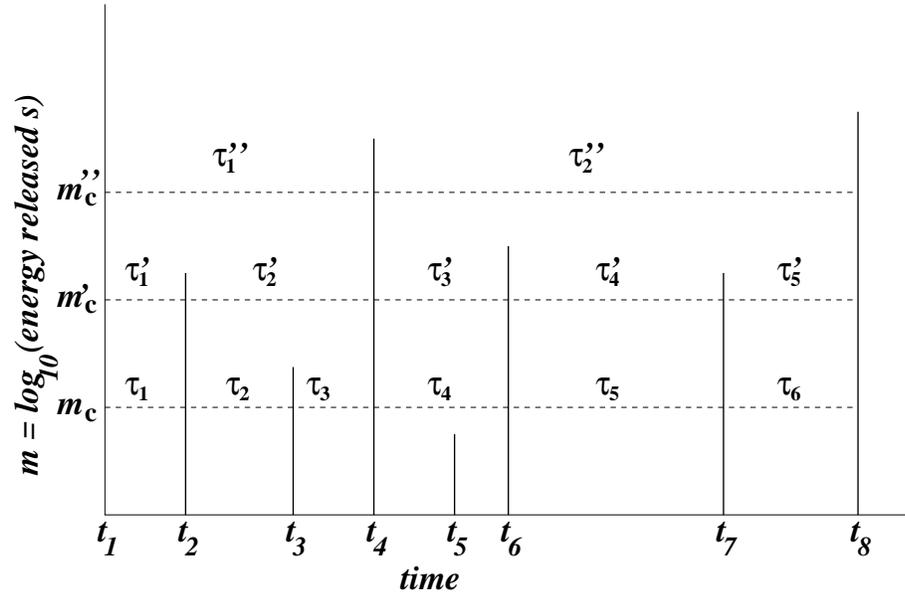
FIGURE 3.4: A sample time series shows how the inter-occurrence time of earthquakes is determined with after the value for magnitude cutoff $m_c$ is chosen.

in a scale-free network of connections [135]. Compared to Omori's law, a much more holistic description encompassing earthquakes from all regions and of all magnitudes is the Gutenberg-Richter law [139]. This empirical law summarizes the fact that emerges from earthquake catalogs all over the world. It is seen that the number of earthquakes $N_{>m}$ of magnitude at least $m$ decays exponentially with $m$ as:

$$\log_{10} N_{>m} = c_1 - c_2 m. \tag{3.2}$$

The plot of $N_{>m}$ versus $m$ from the data recorded in the Southern California region in Fig. 3.3 illustrates the above law. Since the magnitude of an earthquake varies logarithmically with the amount of energy released: $\log_{10} E(m) = c_3 + c_4 m$. Eliminating $m$ one gets, $\log_{10} N = c_1 - (c_2/c_4)\log_{10} E + (c_2 c_3)/c_4$. This implies that the cumulative number $N(E)$ of earthquakes of energy at least $E$ decays like a power-law as:

$$N(E) \propto E^{-b} \tag{3.3}$$

where $b = c_2/c_4$. Therefore the probability density of earthquakes varies as: $\text{Prob}(E) \propto dN(E)/dE \propto E^{-1-b}$. The estimates from different parts of the world give the value of $b$ around $1$.
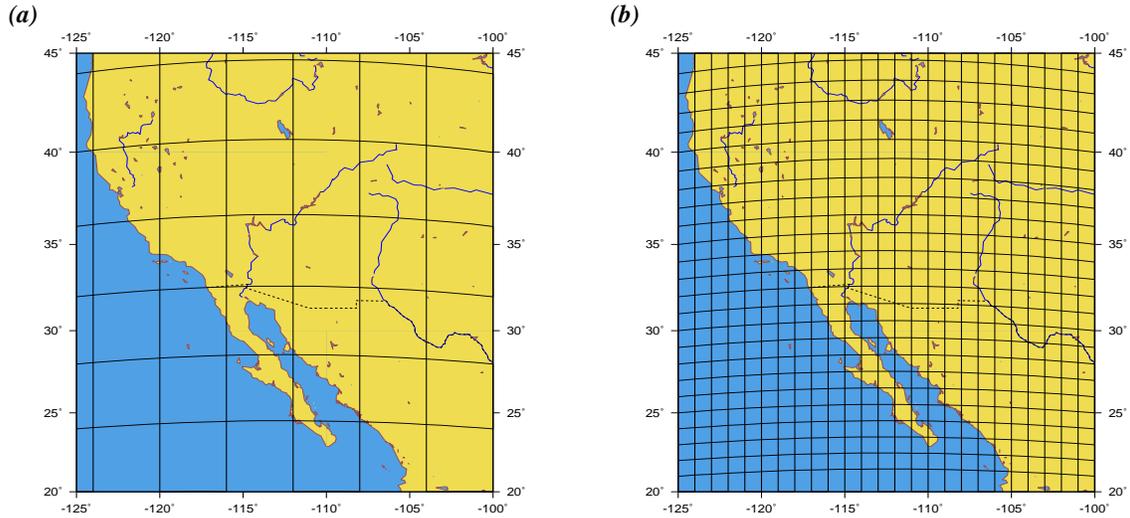
FIGURE 3.5: The South California region originally studied by Bak *et al.* [140]. The region divided into cells of size (a)$L = 4°$ and (b)$L = 1°$. The figures are courtesy of Bak *et al.* [141].

## 3.2 Recurrence Time Distribution

In this chapter of the thesis we focus on one particular aspect of the spatio-temporal behavior of earthquakes where scaling and scale invariance emerges. It is interesting to look at the time intervals between successive shocks. This time is referred to as the recurrence time, interoccurrence time or the waiting time. In a process which is Poissonian in nature the probability of occurrence of an event in a time slice $\Delta t$ is given by $\Delta t / \langle \tau \rangle$, where $\langle \tau \rangle$ is the mean time between occurrence of earthquakes. However, the general observation of intermittent bursts of shocks in space and time and the evidence of scale invariant behavior like the Gutenberg-Richter law suggests to a non-Poissonian process and absence of any characteristic scale.

The recurrence time is defined with respect to the precision $m_c = \log_{10}(s_c)$ with which the magnitudes of different earthquakes are measured as well as the size L of the region where the earthquakes occurred. Consider a model time series (Fig. 3.4) of occurrence of shocks of magnitude at least $m_c$ whose epicenters are located within a region of size $L$. Let the $i$th shock in this sequence occur at time $t_i$. Then the recurrence time is defined as $\tau_i(m_c, L) = t_i - t_{i-1}$. The lower cut-off $m_c$(or $s_c$) of the earthquake magnitudes and the size $L$ have competing effects on the recurrence time distribution. Since the probability of occurrence of an earthquake of size at least $s_c$ decreases with $s_c$, for a fixed $L$ the recurrence time increases with increasing $s_c$. On the other hand for a fixed $s_c$, since the maximum of the earthquake sizes increases with $L$,
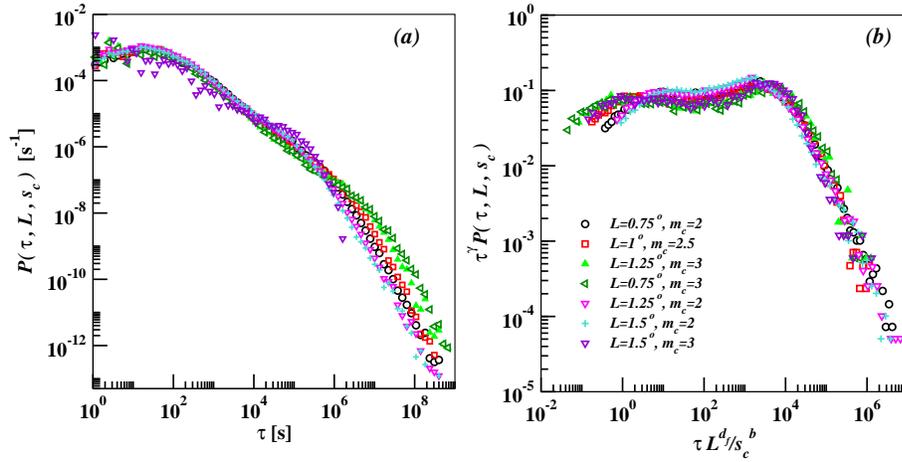
FIGURE 3.6: (a) Recurrence time distributions for earthquakes in Southern California region constructed from *SCSN catalogue* data for time span of 1985 to 2007. (b) Scaling of the distributions according to the prescription in [140, 141].

the probability of occurrence of an earthquake of size at least $s_c$ increases with increasing $L$. Consequently the recurrence time decreases with increasing $L$.

## 3.2.1 The BCDS analysis

The recurrence time distribution of earthquakes was first analyzed by Bak, Christensen, Danon and Scanlon (BCDS) from the viewpoint of earthquake as a self-organized critical phenomenon. BCDS analyzed the earthquake shock data during the period from 1984 to 2000 of the Southern California region considering main events, aftershocks and foreshocks on the same footing [140, 141]. They divided this region spanning $20\,°$N to $45\,°$N latitude and $100\,°$W to $125\,°$W longitude into a grid of cell size $L$ degrees, as is shown in Fig. 3.5, and calculated the recurrence times of all shocks whose epicenters lie within a specific cell. In general these cells are not equivalent with respect to seismic activity since it is already known that the epicenters of earthquakes form a fractal set, therefore some cells within the grid have strong seismic activity with many epicenters where others may have low level of seismic activity with small number of epicenters. BCDS collected together the data of different cells and made a grand sample where recurrence times varied over a long range from small values (highly active cells) to large values (less active cells). They found the probability density for recurrence time $P(\tau, L, s_c)$ to have a power-law region $\tau^{-\gamma}$ till a cut-off decided by the values of $L$ and $s_c$. We reconstructed the probability from the data originally studied by BCDS. This is shown in Fig. 3.6(a). The power-law regime of interoccurrence times signifies a correlated sequence of earthquakes and can be identified with Omori's law for aftershocks. The power-law indicates to an absence of scale and hence to artificiality in the

characterization of earthquakes into foreshocks and main shocks. Two earthquakes separated by a long time-span may be expected to be correlated, the upper limit for such a span being provided by threshold magnitude $s_c$ and size of the region of observation $L$. BCDS chose $x = \tau L^{d_f} s_c^{-b}$ as the scaling variable, where $b$ is the exponent from Gutenberg-Richter law (Eq. (3.3)) and $d_f$ giving the fractal dimension of spatial distribution of epicenters. The quantity $s_c^b/L^{d_f}$ appearing in the definition of the scaling variable actually provided a measure of mean recurrence time $\langle \tau \rangle_{L,s_c}$ of earthquakes since the probability of occurrence of a shock of size at least $s_c$ goes like $s_c^{-b}$ and there are $L^{d_f}$ shocks within a specified period of observation. They proposed a scaling form for probability density:

$$P(\tau, L, s_c) = \tau^{-\gamma} \mathcal{F}\left(\tau \frac{L^{d_f}}{s_c^b}\right).$$

The scaling analysis[140] with value of $b = 1$, $d_f = 1.2$ (which BCDS interpreted as the effective fractal dimension of the San Andreas fault system) and Omori exponent $\gamma = 1$, allowed collapse of probability densities, for different values of $L$ and $s_c$ onto a single curve. The universal function $\mathcal{F}(x)$ was found to be constant for $x < 1$ signifying the correlated Omori's law regime and decaying faster than a power-law in the uncorrelated regime when $x > 1$. The Fig. 3.6(b) shows the nature of data collapse when we performed the scaling according to the above prescription. Taking the value of $\tau$ to be unity we can also recast the scaling proposal in the form:

$$P(\tau, L, s_c) \frac{s_c^b}{L^{d_f}} \sim \mathcal{F}_1(\tau \frac{L^{d_f}}{s_c^b}), \tag{3.4}$$

where $\mathcal{F}_1(x)$ goes like $1/x$ for $x < 1$.

## 3.2.2 The Corral analysis

As mentioned above BCDS constructed the probability distribution $P(\tau, L, s_c)$ by sampling from the different cells. However, the number of earthquakes per cell is a highly variable quantity proven by the fact that distribution of epicenters is a fractal set. Álvaro Corral [142, 143] looked into this heterogeneity in great detail. Corral constructed different probability distributions $P_{x,y}(\tau, L, s_c)$ for different cells (the reference position of a $L \times L$ cell being given by coordinates x,y). The relation with the BCDS probability distribution being given by [143]:

$$P(\tau, L, s_c) \propto \sum_{\forall xy} \int P_{x,y,t}(\tau, L, s_c) R_{x,y,L,s_c}(t) dt, \tag{3.5}$$

where $R_{x,y,L,s_c}(t)$ is the instantaneous rate of shock occurrence in the cell (x,y) at time $t$ such that time average quantity $R_{x,y,L,s_c} = \langle \tau \rangle_{x,y,L,s_c}^{-1}$. Corral looked into earthquake catalogs from different parts of the world including Japan, northern Africa and the Southern California region

(originally studied by BCDS), and was able to scale all the probability distributions $P_{x,y}(\tau, L, s_c)$ according to the equation[142]:

$$P(\tau) = R\mathcal{G}\left(R\tau\right) \tag{3.6}$$

where all quantities in the above equation are functions of x,y,$L$ and $s_c$. The universal scaling function $\mathcal{G}(x)$ was found to have the form of a generalized Gamma function. A power-law region $x < 1$ indicated presence of correlation between consecutive shocks.

## 3.3 Models

After having investigated the signatures of criticality that are manifested over time in the phenomenon of earthquakes, we look into the modeling aspect. The subject of modeling of seismic phenomena has, in general many different facets. However, motivated by the scale-free, features Bak and Tang [144] were among the first to suggest that earthquakes could be modeled in the paradigm of self-organized criticality. The model suggested by them in [144] and [145] is known as earthquake model of SOC and is similar to the BTW sandpile model [66] described in Chapter 1. The sites on the square lattice for the sandpile model were identified with segments of a tectonic plate sliding past another. The variable $z_{i,j}$ at any site $(i, j)$ represented accumulated local stress due to constant tectonic driving and the critical stress $z_c$ represented the maximum static friction that can be sustained at a segment while sliding. But unlike the BTW sandpile model, a constant global driving was introduced in these earthquake models. The avalanches and their sizes were identified with the earthquakes and the energy released therein, respectively.

### 3.3.1 The Burridge-Knopoff Model

The sandpile models were invoked because they were loosely cellular automata based on the *block-spring* picture of earthquake faults. Such a block-spring model was suggested by Burridge and Knopoff [146] to essentially simulate the stick-slip dynamics of the tectonic plate boundaries. A prototype of such a model [146–148] is illustrated in Fig. 3.7. The figure shows a one-dimensional version of the model for a fault-line. The model consists of series of blocks of identical mass $m$ initially resting on a rough surface. Each block is connected to it's nearest neighbors through harmonic springs of strength $k_1$. In addition each block is connected to a movable plate by a set of "pulling springs" with strength $k_L$. The movable plate is driven with uniform speed $v$ in the positive $X$-direction. Let $x_i$ denote the position of a block $i$ at a time $t$. The force on the $i$th block due the harmonic couplings is:

$$F_i^k = k_1\left(x_{i+1} + x_{i-1} - 2x_i\right) - k_L\left(x_i - vt\right). \tag{3.7}$$
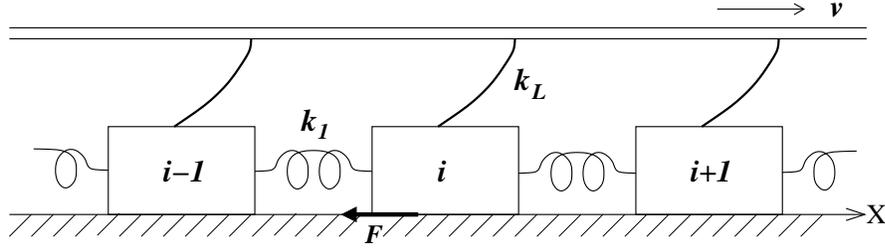
FIGURE 3.7: Figure shows a typical *spring-block* model with $k_1$ and $k_L$ as different spring constants and friction force offered by the surface to the blocks $F$.

Then the equation of motion is:

$$m\ddot{x}_i = F_i^k - F. \tag{3.8}$$

Here '$F$' is the friction force offered by the rough surface to the block $i$. The two plates moving relative to each other with speed $v$ represent the motion of two tectonic plates sliding past each other and the blocks simulate the dynamics of points of contact between the tectonic plates. The spring constants $k_1$ and $k_L$ mimic the response of actual contact regions to compression and shear, respectively.

The friction force is a very significant part of the model and is the main mechanism behind the stick-slip dynamics of the blocks. Almost parallely to Bak *et al.* [144], Carlson and Langer [149, 150] made a detailed study of this model taking into consideration the velocity dependence of the friction, i.e., $F = F(\dot{x}_i)$ (to be particular a decaying function). This made the friction less effective and increased the inertia of the blocks in the sense that fast moving blocks were less likely to stop. They found each block to slip (until there is sufficient force on it to overcome maximum static friction) and stick (mainly due to the effect of pull from the springs) quasi-periodically. They also identified 'events' where group of blocks slip almost simultaneously. The word 'simultaneously' is used with the sense of probing in the time-scale of driving due to the movable plate [149–151]. Such events were identified with earthquakes. A quantity analogous to the energy released was defined as:

$$E = c \sum_i \Delta x_i, \tag{3.9}$$

where $\Delta x_i$ refers to the displacement suffered by the $i$th block during the event and $c$ is a constant. Such a model produced the Gutenberg-Richter law for intermediate size events. The very large earthquakes were found to be periodic. The first simulations of a two-dimensional Burridge-Knopoff model was done by Ostuka[154].

Experiments have also shown dependence of rock friction on velocity to be weak [152, 153] and different groups [144, 155, 157, 158] ignored such a dependence on velocity to put in the stick-slip behavior *ad-hoc* into their models. These models considered a maximum static friction

$F_{th}$. When spring forces $F_i^k$ on block $i$ would exceed the threshold value $F_{th}$, the block would slip and when $F_i^k$ fell below $F_{th}$ the block would come to a stop. Although these models were ideally aimed at modeling the stick-slip process of tectonic segments, these models closely resembled the laboratory experiments on rice piles. Piles consisted by rice grains of rice with less inertia (due stickiness or large aspect ratio) exhibited self-organized critical behavior [159].

### 3.3.2 The Olami-Feder-Christensen Model

In 1992, Zeev Olami, Hans Jacob Feder and Kim Christensen (OFC) derived a non-conservative continuous cellular automata model from Burridge Knopoff spring-block mechanism. The model described in [160] is a two-dimensional spring-block setup such that there were four nearest neighbors to each block $(ij)$. The spring force $F_{ij}^k$ on block $(ij)$ is:

$$F_{ij}^k = k_1 \left( x_{i+1,j} + x_{i-1,j} - 2x_{i,j} \right) + k_2 \left( x_{i,j+1} + x_{i,j-1} - 2x_{ij} \right) - k_L \left( x_i - vt \right). \qquad (3.10)$$

If $F_{ij}^k$ exceeds $F_{th}$, the block $(ij)$ slips to a fully relaxed position and the whole amount of stress is distributed to the neighboring blocks:

$$F_{i\pm1,j}^k \rightarrow F_{i\pm1,j}^k + \delta F_{i\pm1,j}^k, \quad F_{i,j\pm1}^k \rightarrow F_{i,j\pm1}^k + \delta F_{i,j\pm1}^k, \quad F_{i,j}^k \rightarrow 0.$$

The stress increments on the neighboring blocks are given by:

$$\begin{aligned} \delta F_{i\pm1,j}^k &= \frac{k_1}{2k_1 + 2k_2 + k_L} F_{i,j}^k, \quad \text{and} \\ \delta F_{i,j\pm1}^k &= \frac{k_2}{2k_1 + 2k_2 + k_L} F_{i,j}^k. \end{aligned}$$

The situation where $k_L > 0$, the distribution of stress among the system of blocks is non-conservative so that only a fraction and not the whole amount of the total stress released is distributed. In an isotropic situation of $k_1 = k_2 = k$, the parameter $\alpha = k/(4k + k_L)$ determines the level of non-conservation. Evidently the conservative case corresponds to $k_L = 0$ or $\alpha = 1/4$.

OFC converted this spring-block model into a discrete time, continuous stress cellular automata. At every site of a square lattice a continuous variable $f$ represents the accumulated local stress at that site. The system is globally driven, so that in the inactive state of no avalanches (earthquakes), the stress at all sites increases uniformly. A site relaxes when $f_{i,j} \geq f_c$, a pre-assigned threshold value. In a relaxation the stress at the site is reset to zero and the whole amount of stress is transferred equally to the neighboring sites:

$$\text{If} \quad f_{i,j} \geq f_c \quad \text{then} \quad f_{i,j} \rightarrow 0 \quad \text{and} \quad f_{n,n} \rightarrow f_{n,n} + \alpha f_{i,j}, \qquad (3.11)$$

where $f_{n,n}$ are the local stress at the four neighboring sites of $(ij)$ and $\alpha$ varies continuously within the range $0 < \alpha \leq \frac{1}{4}$ [160]. Consequently, stress values at some neighboring sites may
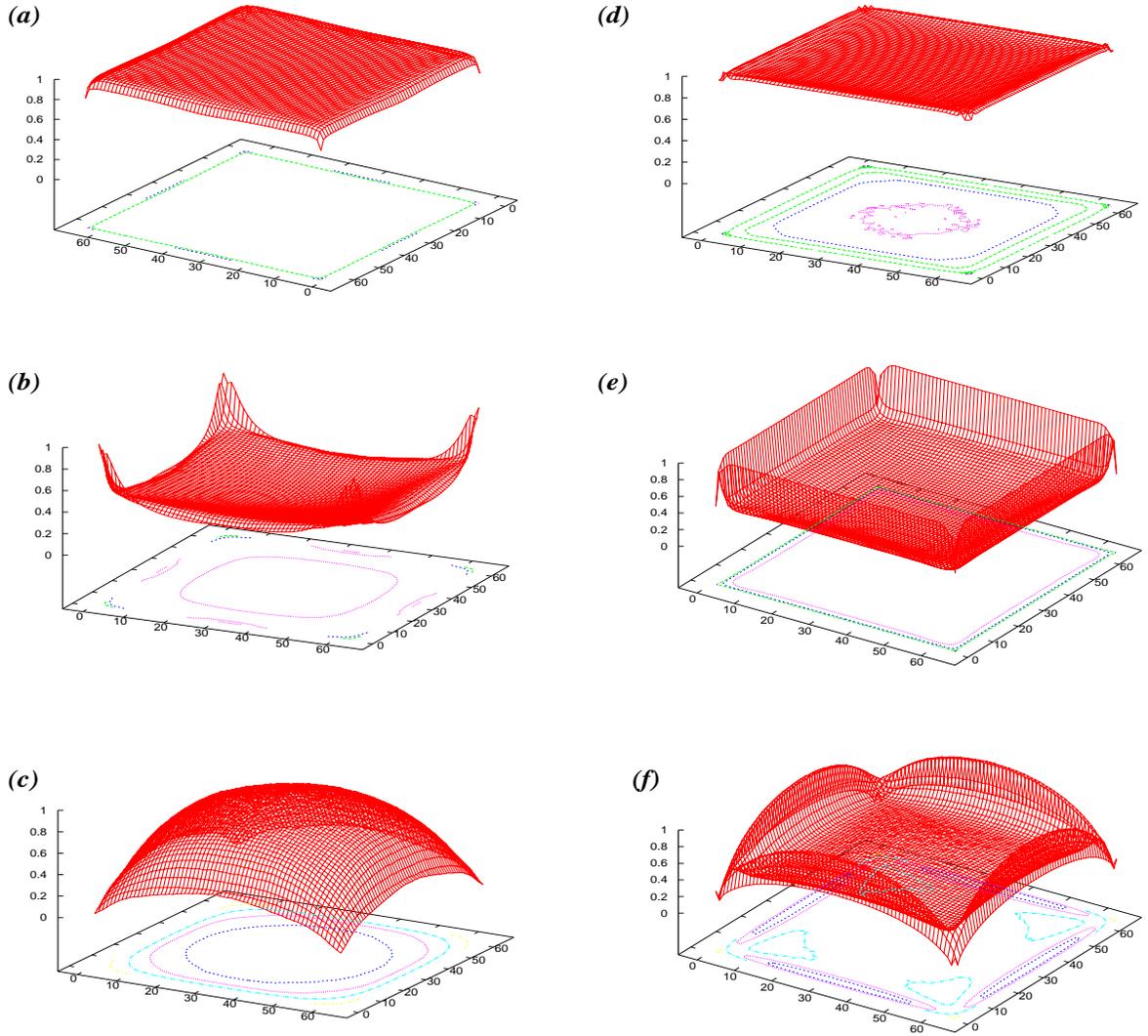
FIGURE 3.8: Surface profiles for the OFC model on a square lattice of size $L = 64$ for with open boundary conditions. The average stress per site for $\alpha = 0.25$ (a) and $0.20$ (d), the fraction of avalanche origins per site for $\alpha = 0.25$ (b) and $0.20$ (e) and the average avalanche size per site for $\alpha = 0.25$ (c) and $0.20$ (f).

exceed $f_c$ which also relax so that a cascade of site relaxations propagates in the system, causing an avalanche. In the limit of $\alpha \to 0$, the avalanche sizes are small and the system is therefore in a sub-critical state. On the other hand in the conservative limit of $\alpha \to 0.25$, the avalanches have all length and time scales. In between, a critical value $\alpha_c$ exists so that for $\alpha < \alpha_c$ the system is in a sub-critical state whereas for $\alpha > \alpha_c$ the system is in a critical state. Different values of $\alpha_c$ have been suggested as $0.05$ [160], around $0.20$ [161], equal to $\frac{1}{4}$ [162]. It has also
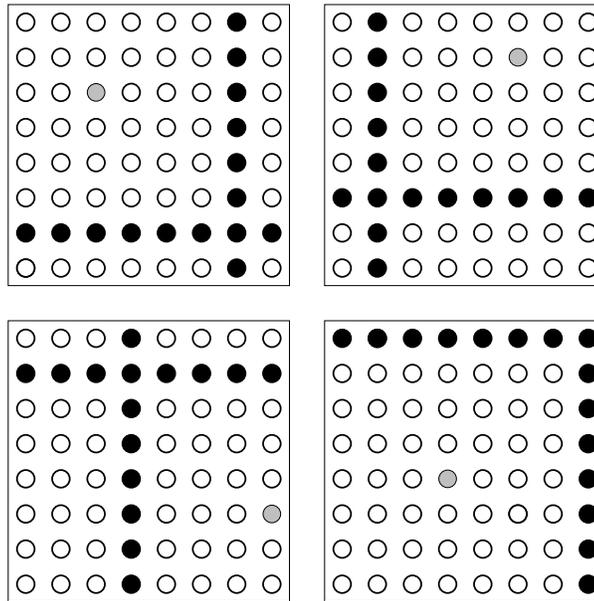
FIGURE 3.9: Four examples show the positions of the avalanche origins (shaded circle) and the corresponding boundaries sites (filled circles) on a $8 \times 8$ square lattice.

been argued that the avalanche size distribution has a multifractal scaling [163].

## 3.4 Our Work

We argue that assigning a fixed boundary in the SOC models of earthquakes is rather artificial. In nature there is no fixed boundary for the earthquakes which absorbs earth's vibrations, the seismic waves propagate in all directions till they slowly damp out at long distances. Presence of a fixed boundary introduces a strong non-uniformity in the system, i.e., all measurable quantities show strong dependence on the distance from the boundary. This effect is present in both conservative as well as non-conservative versions of the OFC model, but it is so strong in the latter case that even arriving at the stationary state becomes very difficult [161]. Surface profiles for the averaged stress per site $\langle f \rangle$, the average fractional number of avalanches $\langle e \rangle$ that originates at each site and average size of the avalanche per site $\langle s \rangle$ in the OFC model with fixed boundary in the conservative case ($\alpha = 0.25$) and in a non-conservative case ($\alpha = 0.20$ corresponding to the case when all couplings in the Burridge-Knopoff model are of same order) are shown in Fig 3.8. It is therefore desirable that all avalanches are on the same footing with respect to the boundary and at the same time the origin of the avalanche should be at the deepest interior point of the system.
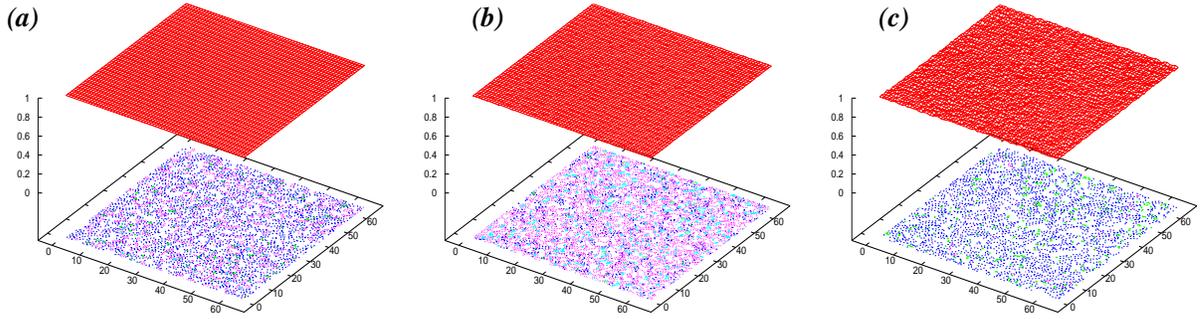
FIGURE 3.10: Surface profiles for the OFC model on a square lattice of size $L = 64$ for $\alpha = 0.25$ with moving boundary conditions, (a) the average stress per site (b) fraction of avalanche origins per site and (c) average avalanche size per site.

## 3.4.1 The Moving Boundary Condition

These arguments prompted us to formulate a new boundary condition. Here, a globally fixed set of lattice sites does not constitute the boundary for all avalanches. In contrast, boundaries are different for different avalanches depending on the positions of the avalanche origins, and its position is constantly moved from one avalanche to the other.

First we make the square lattice periodic in both directions to get the topology of a torus. An arbitrary random distribution of forces $f_{i,j}$, drawn from a set of independent and identically distributed random numbers within $\{0, 1\}$ are assigned at all $L^2$ sites. The maximum force $f_{max}$ among all $L^2$ sites is found to be at some specific location $(i_o, j_o)$ and the difference from the threshold force is estimated: $\delta = f_c - f_{max}$. Forces at all sites are then enhanced by $\delta$ so that at the origin $(i_o, j_o)$ the force reaches the threshold $f_c$. The avalanche then starts from the origin and a cascade of relaxations propagates away from the origin.

Now, for this avalanche, we select a specific set of lattice sites as the boundary such that the origin is at the center position with respect to these boundary sites. More precisely, on a $L \times L$ square lattice and with respect to the origin located at $(i_o, j_o)$ the boundary sites form two transverse rings on the torus defined by one column and one row of lattice sites as (Fig. 3.9):

$$
\begin{aligned}
i &= i_o + L/2 \quad \mathrm{mod}(L) \quad \text{and} \\
j &= j_o + L/2 \quad \mathrm{mod}(L).
\end{aligned}
\tag{3.12}
$$

When a site adjacent to the boundary relaxes, it transfers $\alpha f_{i,j}$ force to every non-boundary neighbor but no force to the neighbor on the boundary. Therefore corresponding to each boundary
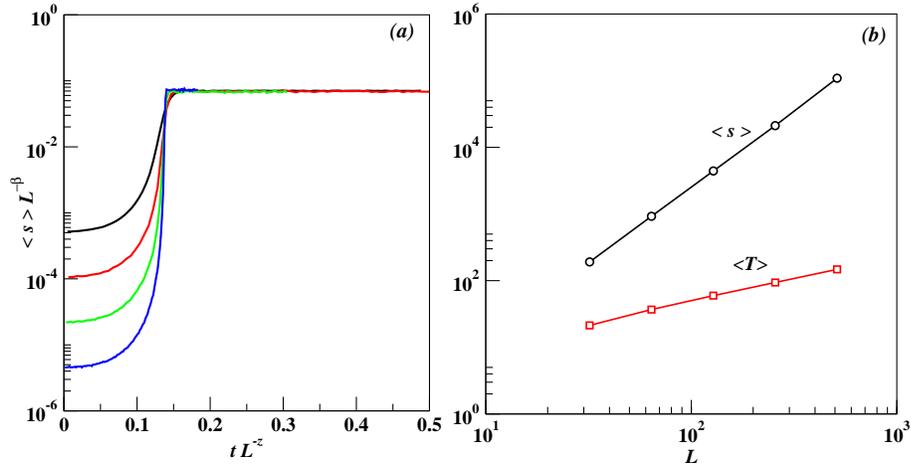
FIGURE 3.11: (a) Scaling of the times to reach the steady state for different system sizes L=64(black), 128(red), 256(green) and 512(blue). The values of $z$ and $\beta$ has been found to be 2 and 2.28, respectively. (b) The plot of the average avalanche size $\langle s \rangle$ (circles) and the avalanche duration $\langle T \rangle$ with system size.

neighbor $\alpha f_{i,j}$ disappears from the system and in this way the system looses force. Since the system is otherwise periodic in all directions all lattice sites are equivalent. Consequently all avalanches are also equivalent since all of them grow in similar surroundings. In a way this is similar to elimination of surface effects in a finite size system. Surface profiles for the averaged force per site $\langle f \rangle$, number of avalanche origins at each site $\langle e \rangle$ and average size of the avalanche per site $\langle s \rangle$ show uniform flat surfaces (Fig. 3.10) but within a very small fluctuation for all sites within the lattice $L \times L$.

Since in a single relaxation, the force at the site is reduced to zero, it creates the possibility that more than one site (typically two) can reach the threshold simultaneously. However, such situations occur with very low probability and in these cases we choose randomly one of the sites as the origin and construct boundaries with respect to this site but relaxation starts from both the unstable sites. Since the forces are continuously varying real numbers, the precision of the numbers is important as observed in [164]. To ensure that the system has indeed reached the stationary state, we calculated the average avalanche size $\langle s(L) \rangle$ for every $10000$ avalanches and monitored its variation with time. This quantity first grows with time but eventually saturates. Repeating this calculation for different system sizes, it is observed that the relaxation time grows as $L^z$ with $z = 2$ as shown in Fig. 3.11(a).
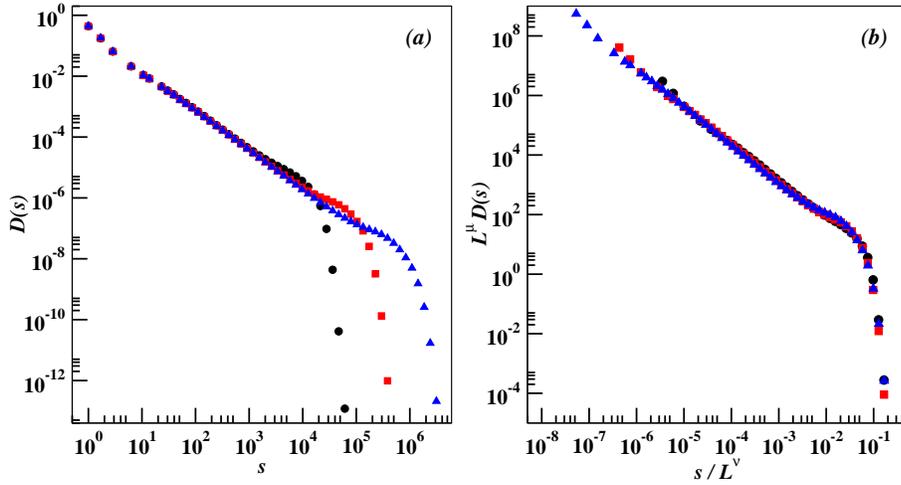
FIGURE 3.12: The avalanche size distributions for three different system sizes $L = 64$ (circles), 128 (squares) and 256 (triangles) have been plotted on a double logarithmic scale in (a). The finite size scaling of the same data is shown in (b).

## 3.4.2 Results

We concentrate on the case $\alpha = 1/4$ where stress is locally conserved. The avalanche size $s$ is the total number of relaxations in an avalanche and represents the total energy release in our model earthquake. Let $D(s)$ be the probability density for a randomly selected avalanche to have a size between $s$ and $s + ds$. While for the infinitely large system size the distribution should indeed be a simple power-law; for the finite size systems, a finite size scaling of the distribution is required (the following relation can obtained by recasting the ansatz in Eq. (1.19)):

$$D(s) = L^{-\mu}\mathcal{H}(s/L^{\nu}), \tag{3.13}$$

where the scaling function $\mathcal{H}(x) \sim x^{-1-b}$ for $x \to 0$ and for $x >> 1$, $\mathcal{H}(x)$ decreases faster than a power-law so that, $b = \mu/\nu - 1$. The system size dependence of the average avalanche size and durations are observed (Fig. 3.11(b)) to be $\langle s(L) \rangle \sim L^{\beta}$ with $\beta = 2.28$ (the value of $\beta$ is also verified from Fig. 3.11(a)) and $\langle T(L) \rangle \sim L^{0.63}$. This shows that the avalanche dynamics is sub-diffusive. We believe that this is due to fact that force is always reset to zero in a relaxation which initiates more relaxations and thus increases the size of the avalanche.

In Fig. 3.12(a) we show the plot of avalanche size distribution for three different system sizes $L = 64$, 128 and 256 on the double logarithmic scale. All of them have very large portions of straight regions starting from very small sizes to the cut-off sizes. A scaling of the data with an excellent data collapse is shown in Fig. 3.12(b) yielding the values of $\nu = 3.02$ and $\mu = 3.78$ giving $b \approx 0.26$. Such a good power-law behavior as well as the excellent finite size scaling have been achieved only due to the moving boundary condition where all lattice sites as well as the
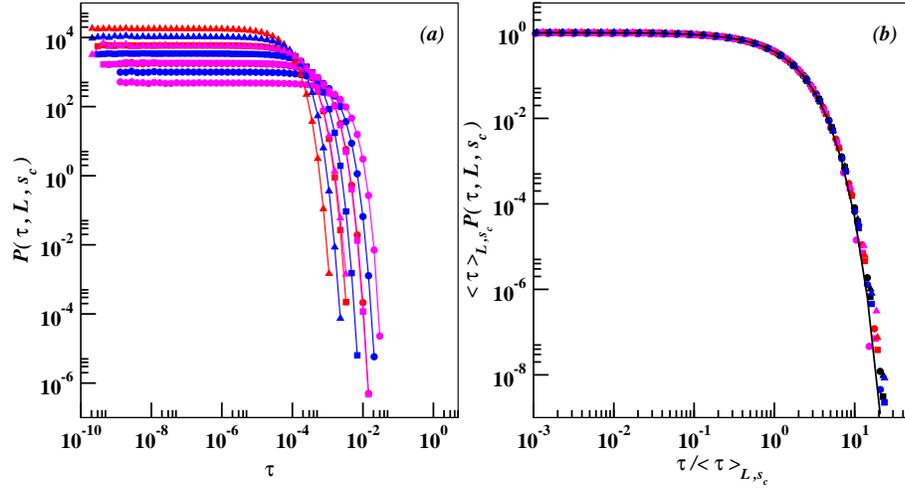
FIGURE 3.13: (a) The waiting time distributions $P(\tau, L, s_c)$ for different systems sizes $L$ and minimal avalanche sizes $s_c$: $L = 64$ (circle), 128 (square), 256 (triangle), $s_c = 0$ (black), 8 (red), 64 (blue) and 512 (magenta). (b) Scaling of the waiting time distributions by the Corral method. The continuous line is the best fit by the functional form in Eq. (3.14).

avalanches are equivalent and have not been observed in fixed boundary cellular automata models of earthquakes before [160, 161].

Since we have assumed that forces at all sites increase uniformly at unit rate, the time difference between successive avalanches is exactly equal to $\delta$. With this definition, the recurrence time distribution (RTD) $P(\tau, L, s_c)$ has been calculated for different system sizes $L$ as well as different $s_c$ values. The plots are shown in Fig. 3.13(a). The effects of $s_c$ and $L$ on RTD are competitive. For $s_c = 0$, the RTD is simply the distribution of force increments $\delta$ only. Since the probability of occurrence of an avalanche of size at least $s_c$ decreases with $s_c$, for a fixed $L$ the recurrence time increases with increasing $s_c$. On the other hand for a fixed $s_c$, since the maximum of the avalanche sizes increases with $L$, the probability of occurrence of an avalanche of size at least $s_c$ increases with increasing $L$. Consequently the recurrence time decreases with increasing L.

In Fig. 3.13(b) we show an unified scaling of twelve different plots with the minimal value of the avalanche sizes measured $s_c = 0, 8, 64$ and $512$ for three different system sizes $L = 64$, 128 and 256. Logarithmic binning is used for coarse-graining of the data. The average waiting time $\langle \tau \rangle_{L,s_c}$ is calculated for each plot. Following Eq. (3.6) we then scale every plot with corresponding $\langle \tau \rangle_{L,s_c} = 1/R$ and observe an excellent collapse of all twelve plots. This confirms the Corral scaling in our model. We tried to verify the Corral scaling form:

$$\mathcal{G}(x) \sim x^{-a_1} \exp(-a_2 x^{a_3}), \qquad (3.14)$$

and obtained $a_1 = 0.003$, $a_2 = 1.02$ and $a_3 = 0.99$ compared to $a_1 = 0.33$, $a_2 = 0.63$
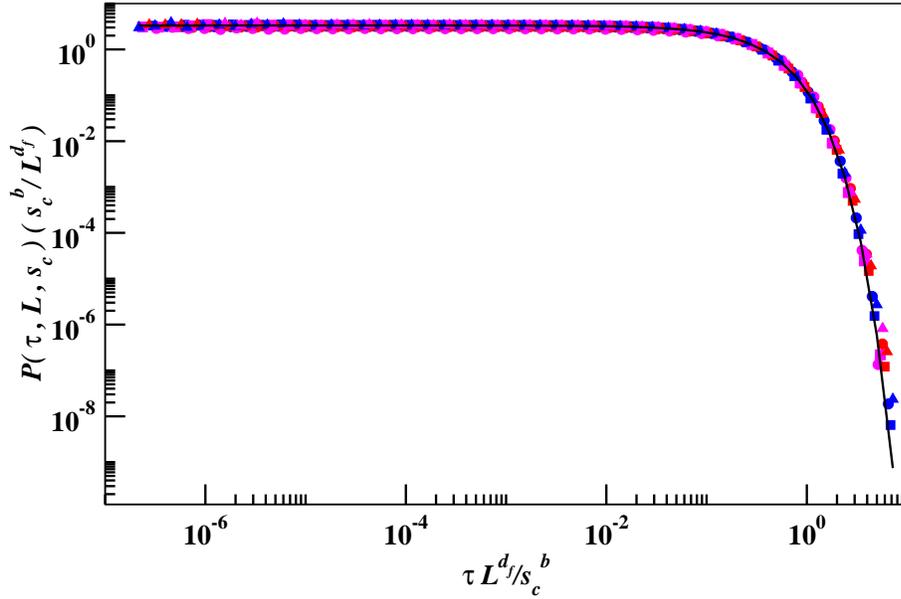
FIGURE 3.14: Scaling of the waiting time distribution by the BCDS method. Symbols used for: $L = 64$ (circle), 128 (square), 256 (triangle) and for $s_c = 8$ (red), 64 (blue) and 512 (magenta). Values of the scaling exponents used are $d_f=1.67$ and $b=0.29$. The continuous line is the best fit by the functional form in Eq. (3.14).

and $a_3 = 0.98$ observed in [142]. The exponential tail in $\mathcal{G}(x)$ is consistent with the Gamma distribution observed by Corral but the observed power-law decay component for small values of waiting times is rather absent in our model.

To verify whether BCDS scaling is valid for our model, we plotted $P(\tau, L, s_c)(s_c^b/L^{d_f})$ vs. $\tau L^{d_f}/s_c^b$ (shown in Fig. 3.14) and obtained a scaling form similar to Eq. (3.4). Here also we see a very good collapse of the nine sets of data for three system sizes $L = 64$, 128 and 256 and for $s_c = 8, 64$ and 512. The scaling exponents that gave the best collapse were tuned to $d_f = 1.67$ and $b = 0.29$. The best fit with the functional form in Eq. (3.14) gives $a_1 = 0.001$, $a_2 = 3.21$ and $a_3 = 0.99$ again showing an exponential tail similar to that obtained from real data analysis [142] but without any power-law component.

We therefore conclude that both the scaling forms used by Corral as well as BCDS are valid for scaling of the RTD data in our model. The scaling functions in both cases were observed to be very close to simple exponential decay and the power-law part representing the RTD for small values of the recurrence times turned out to be absent. This result may also be compared with two recent analytical calculations: (i) a pure exponential decay of the RTD [165] (ii) an approximate unified law compatible with the empirical observations incorporating the Omori law [166].
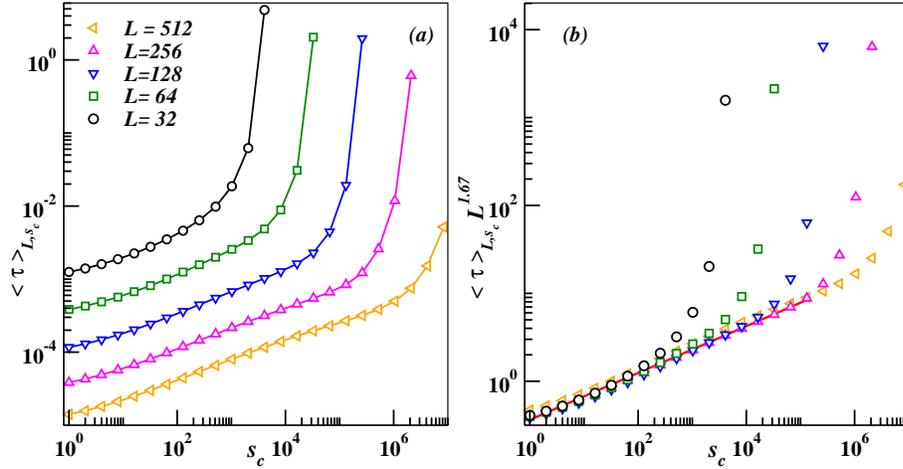
FIGURE 3.15: (a) The average recurrence time $\langle\tau\rangle_{L,s_c}$ has been plotted for different values of $s_c$ for various system sizes; (b) $\langle\tau\rangle_{L,s_c}$ multiplied by the system size dependent factor $L^{d_f}$ is plotted against $s_c$. On increasing system size the plot approaches to the variation mentioned in Eq. (3.15) with $b = 0.30$.

For Corral's analysis it is the single parameter scaling i.e., the mean recurrence time $\langle\tau\rangle_{L,s_c}$. However this parameter in turn also depends jointly on the another two competitive parameters of the distribution, namely the system size $L$ and the avalanche size cut-off $s_c$ in the following way:

$$\langle\tau\rangle_{L,s_c} \propto \frac{s_c^b}{L^{d_f}}. \tag{3.15}$$

To check if it is really true we plotted $\langle\tau\rangle_{L,s_c}L^{d_f}$ with respect to $s_c$ for $L = 32, 64, 128$ and $256$ using $d_f = 1.67$ in Fig. 3.14. A nice collapse of the data for the four different system sizes are observed for small and intermediate values of $s_c$. Collapse of the data between two successive system sizes increased with the system size. The slope of the curve in the longest straight region corresponds to $b = 0.30$.

Finally, we studied the OFC model using values of $\alpha < 1/4$ again on a square lattice of size $L$ using open but moving boundary condition. To our surprise we see that the dynamics become periodic after a short relaxation time of the order of $L^2$. This is checked by looking at the 'hamming distance'. Starting from a random distribution of forces as before we skip some $10L^2$ initial avalanches and store the force configuration in an array $f_{store}$. After that, at the end of every avalanche, we calculated the maximal site difference $\max|f_{i,j} - f_{store}(i,j)|$ and measure the time when this maximal difference becomes less than a small number $\epsilon = 10^{-12}$. The periodic time is of the order of $L^2$ but less than it, and found to depend on the initial distribution of force values.

## 3.5 Conclusion

To summarize, we have studied in a model, the scale invariance properties observed in the real data of earthquakes over last several years by different groups. More specifically, we studied a self-organized critical model of earthquakes using a square lattice cellular automaton. Using a moving boundary condition we could eliminate all boundary effects. We first observe that the avalanche size distribution of this model follow excellent finite size scaling. Further, the recurrence time distribution was analyzed in two ways, i.e., using Corral as well as BCDS scalings. We observe that our simulated data of the RTD support both scalings very well which leads us to conclude that the mean recurrence time is actually a joint function of both the system size as well as the avalanche size cut-off as used to measure the waiting times.

# 4 Econophysics of Wealth Distributions

## 4.1 Introduction

Of all systems present in nature the society is perhaps one of the most complex ones. While conventional physical systems follow some universal laws there is an apparent *lawlessness* in the socio-economic systems. However, in Chapter 1 we described some recent research work which leads to the fact that even in such systems emergent behavior can be found which are suitably characterized by statistical *laws*. In this connection we discussed the Pareto law. In this chapter, based on [167], we look into this aspect in greater detail and we try to develop an understanding at a certain level by studying three different yet related models which try to explain the nature of wealth distribution in societies. The models we discuss here are mostly concerned with agents who trade amongst themselves according to certain rules. The features of real systems such as rationality of agents or the influence of the environment are treated by incorporating stochasticity.

Income and wealth are related economic quantities. However, the nature of these economic variables are different. While the former is characterized as *stock*, the latter is characterized as *flow*. Different members in a society possess different amounts of wealth. Individual members often make economic transactions (income of an individual being such a mode of transaction) with other members of the society. Therefore in general the wealth of a member fluctuates with time and this is true for all other members of the society as well. Over a reasonably lengthy time interval of observation, which is small compared to the inherent time scales of the economic society this situation may be looked upon as a stationary state which implies that statistical properties like the individual wealth distribution, mean wealth, its fluctuation etc. are independent of time. In 1897 Vilfredo Pareto published [12] his findings about the distribution of income across different European countries. Pareto observed that the individual income $(m)$ distribution in a society is characterized by a power-law tail like: $P(m) \sim m^{-(1+\nu)}$. The value of $\nu$ was found to lie around $1.5$. More recently, several groups have investigated the nature of distributions of wealth and income in different countries across the globe. These empirical studies [168–171] have indeed confirmed that the nature of high-income distribution is a power-law with the Pareto exponent $\nu$ varying across different scenarios. Although most of these studies were done with data from countries with *capitalist* economies like the USA,Japan or UK, Pareto law was observed in a more controlled economy like that of India [172]. The Pareto law, however, describes the distribution in
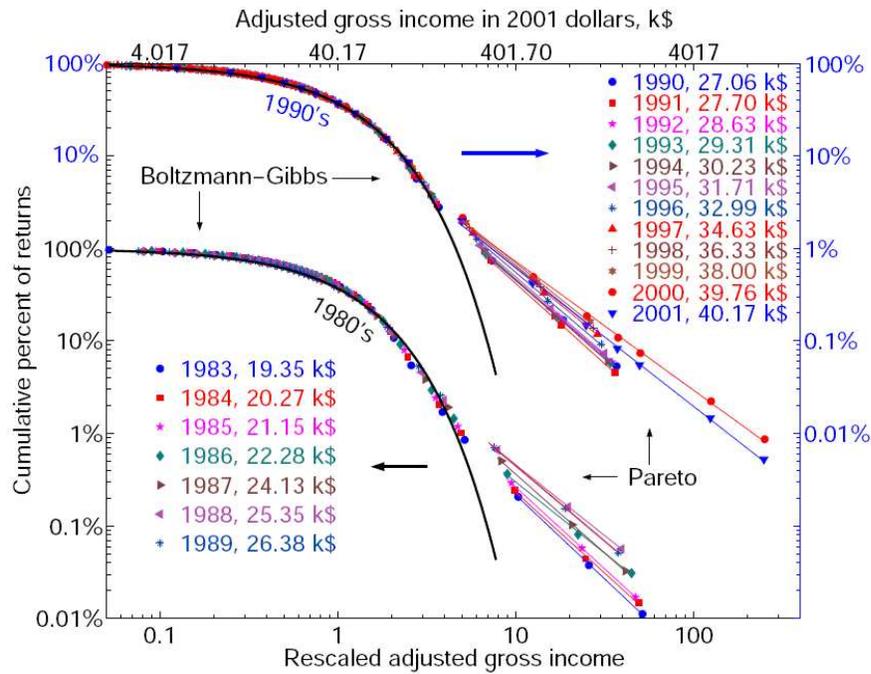
FIGURE 4.1: Plots of cumulative probability of income vs. income in the United States of America for different years. The variable on the horizontal axis is actually the income scaled by the average income. The average incomes are indicated in k$ beside the corresponding years. This figure is courtesy of Silva et al. [178] where the authors analyzed the data on personal income distribution compiled by the Internal Revenue Service, USA from the tax returns in the USA for the period 1983-2001.

the high-income range. The distribution in the low and middle-income range (comprising of over 90% of the total population) is found to be described by distributions like log-normal [173–177]or exponential distribution [169, 171, 179]. In Fig. 4.1 the distribution of incomes in the USA are shown for different years. The two different regions become evident from the plot.

## 4.2 Recent Models of Wealth Distributions

Models of wealth distributions aim to produce a stationary distributions with a power-law tail. This presents a scope within the viewpoint of non-equilibrium statistical physics where the paradigm of power-laws in stationary state of systems (which are out of equilibrium) is already present [20]. The models which we discuss in this chapter belong to a class of models popularly known as *asset-exchange models*. Such a model considers a society to be composed of $N$ individuals where each of them possess wealth (or money) $m_i(t), i = 1, N$ at a certain time $t$. The distribution of wealth in this society evolves through mutual economic transactions taking place between different pairs of individuals. In a typical interaction at a certain time step one individual '$j$'

provides goods or services to another individual '$i$' against a payment of $\Delta m$. By this process the wealth of $i$ and $j$ changes as:

$$m_i(t+1) = m_i(t) - \Delta m$$
$$m_j(t+1) = m_j(t) + \Delta m. \tag{4.1}$$

However, the total amount of wealth possessed by the two individuals remains conserved during the transaction process,

$$m_i(t+1) + m_j(t+1) = m_i(t) + m_j(t). \tag{4.2}$$

An analogy [180] can be drawn with this exchange mechanism with the scattering process that takes place in gases or particle-suspensions in fluids where two molecules or atoms interact via an elastic or in-elastic collision and this has encouraged explanations [119] similar to kinetic theory of gases for the stationary wealth distributions generated by models.

   All the models we discuss below can be cast in the form of the rule (4.1) and hence obey the conservation law described in Eq. (4.2). To be particular we report detailed simulation results on three models of wealth distribution. These models are: (i) the model of Drăgulescu and Yakovenko (DY) [119] which gives an exponential decay of the wealth distribution, (ii) the model of Chakraborti and Chakrabarti (CC) [120] with a constant global *saving propensity* giving a Gamma distribution for the wealth distribution and (iii) the model of Chatterjee, Chakrabarti and Manna (CCM) [121] with a distribution of quenched individual saving propensities giving a Pareto law for the tail of the wealth distribution.

## 4.2.1 The Drăgulescu-Yakovenko (DY) Model

In this model at any instant of time two randomly selected individuals $i$ and $j$, $(i \neq j)$ make transactions by a random bipartitioning of their total wealth $m_i + m_j$ and then receiving one part each:

$$m_i(t+1) = \epsilon(t)(m_i(t) + m_j(t))$$
$$m_j(t+1) = (1 - \epsilon(t))(m_i(t) + m_j(t)). \tag{4.3}$$

Here $\epsilon(t)$ is the $t$-th random fraction with a uniform distribution drawn for the $t$-th transaction. The system dynamically evolves to a stationary state which is characterized by a time independent probability distribution $\mathrm{Prob}(m)$ of wealth irrespective of the details of the initial distribution of wealth to start with. Typically in our simulations a fixed amount of wealth is assigned to all members of the society, i.e. $\mathrm{Prob}(m, t = 0) = \delta(m - \langle m \rangle)$. The model described so far is precisely the DY model in [119]. The stationary state wealth distribution for this model is
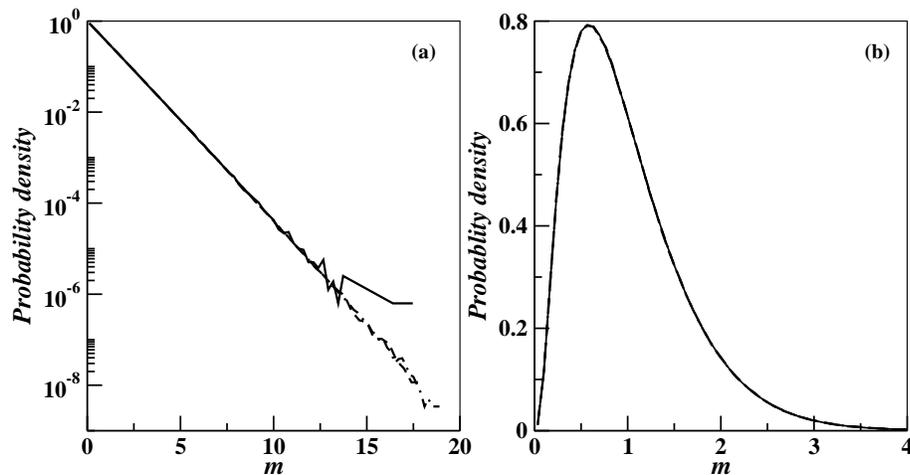
FIGURE 4.2: The three probability densities of wealth distribution, namely $\mathrm{Prob}_1(m)$ (solid line), $\mathrm{Prob}_2(m)$ (dashed line) and $\mathrm{Prob}(m)$ (dot-dashed line) are plotted with wealth $m$ for $N = 256$ in (a) for the DY model and in (b) for the CC model for $\lambda = 0.35$. The excellent overlapping of all three curves indicate that both the DY and CC models are ergodic as well as self averaging.

[119, 182, 187]:

$$\mathrm{Prob}(m) = \frac{1}{\langle m \rangle} \exp(-m/\langle m \rangle). \tag{4.4}$$

Typically $\langle m \rangle$ is chosen to be unity without any loss of generality.

The appearance of the Boltzmann-Gibbs distribution (Eq. (4.4)) as the stationary wealth distribution in the DY Model is a consequence of the rule (4.3). Rule (4.3) is a very special form of rule (4.1) where there is time-reversal symmetry i.e., during the exchange process the probability of transfer of amount $\Delta m$ (rule (4.1)) from one individual $i$ to another individual $j$ is the same as probability of transfer of $\Delta m$ from $j$ to $i$. Historically, asset-exchange models first appeared in physics literature in Ref. [183]. However, the models considered in [183] did not preserve time reversal symmetry and in fact did not yield any stationary distribution like the Boltzmann distribution. The models resulting in the process of aggregation of wealth by few members in a society was shown to obey scaling relations similar to phenomenon of aggregation of particles forming clusters [186]. Such a model for wealth distribution, called the Inequality Process was also considered by sociologist John Angle [184, 185]. The other two models that we describe below although do not obey time-reversal symmetry, produce stationary wealth distributions. On the theoretical side open economies have also been considered [180] where interaction of agents can cause increase in the wealth of the two agents thus violating Eq. (4.2).
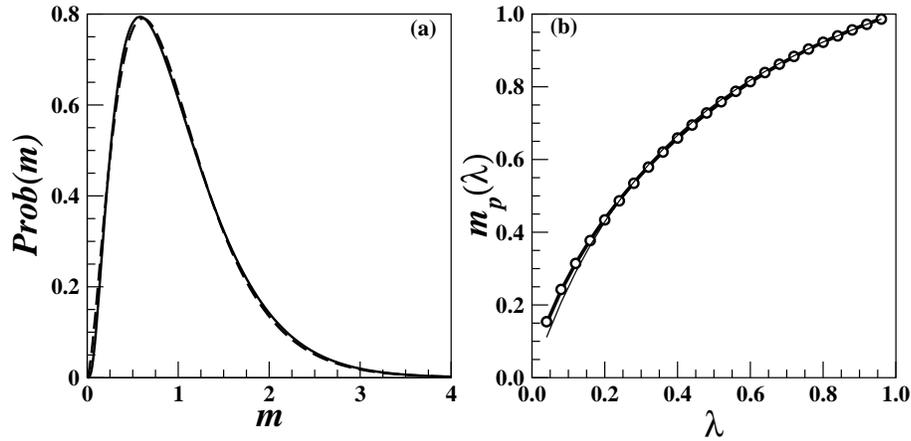
FIGURE 4.3: For the CC model with $N = 256$ and $\lambda = 0.35$ these plots show the functional fits of the wealth distribution in (a) and the variation of the most probable wealth $m_p(\lambda)$ in (b). In (a) the simulation data of $\mathrm{Prob}(m)$ is shown by the solid black line where the fitted Gamma function of Eq. (4.7) is shown by the dashed line. In (b) the $m_p(\lambda)$ data for 24 different $\lambda$ values denoted by circles is fitted to the Gamma function given in Eq. (4.8) (solid line). The thin line is a comparison with the $m_p(\lambda)$ values obtained from the analytical expression of $a(\lambda)$ and $b(\lambda)$ in [188].

## 4.2.2 The Chakraborti-Chakrabarti (CC) Model

A fixed global saving propensity is introduced in the CC model [120]. During the pairwise economic transaction each member saves a fixed fraction $\lambda$ of his wealth [181]. The total sum of the remaining wealth of both the traders is then randomly partitioned and obtained by the individual members as follows:

$$m_i(t + 1) = \lambda m_i(t) + \epsilon(t)(1 - \lambda)(m_i(t) + m_j(t))$$
$$m_j(t + 1) = \lambda m_j(t) + (1 - \epsilon(t))(1 - \lambda)(m_i(t) + m_j(t)). \tag{4.5}$$

The stationary state wealth distribution is an asymmetric distribution with a single peak. The distribution vanishes at $m = 0$ as well as for large $m$ values. The most probable wealth $m_p(\lambda)$ increases monotonically with $\lambda$ and the distribution tends to the delta function again in the limit of $\lambda \to 1$ irrespective of the initial distribution of wealth.

## 4.2.3 The Chatterjee-Chakrabarti-Manna (CCM) Model

In the third CCM model different members have their own fixed individual saving propensities and therefore $\lambda_i(i = 1, N)$ is a quenched variable in the model. Economic transactions therefore
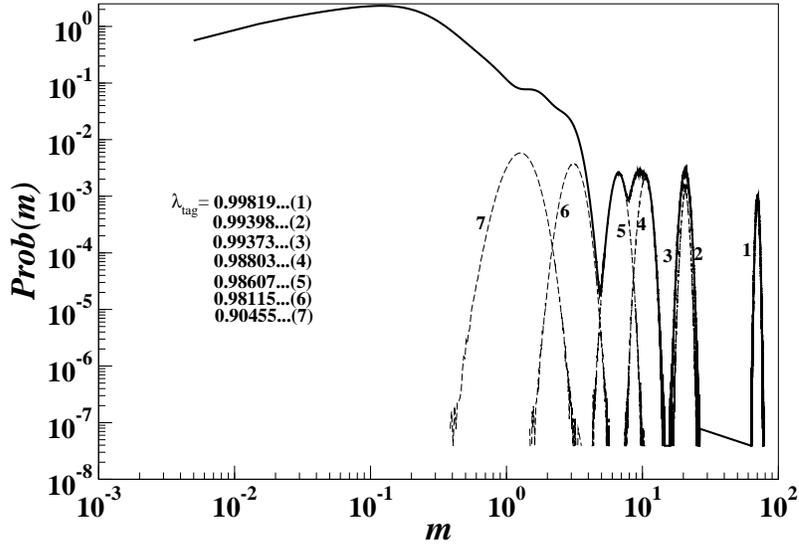
FIGURE 4.4: The wealth distribution $\mathrm{Prob}(m)$ in the stationary state for the CCM model for a single initial configuration of saving propensities $\{\lambda_i\}$ with $N=256$ is shown by the solid line. Also the wealth distributions of the individual members with seven different tagged values of $\lambda_{tag}$ are also plotted on the same curve with dashed lines. This shows that the averaged (over all members) distribution $\mathrm{Prob}(m)$ is the convolution of wealth distributions of all individual members.

take place following these equations:

$$m_i(t+1) = \lambda_i m_i(t) + \epsilon(t)[(1-\lambda_i)m_i(t) + (1-\lambda_j)m_j(t)]$$
$$m_j(t+1) = \lambda_j m_j(t) + (1-\epsilon(t))[(1-\lambda_i)m_i(t) + (1-\lambda_j)m_j(t)] \qquad (4.6)$$

where $\lambda_i$ and $\lambda_j$ are the saving propensities of the members $i$ and $j$. The stationary state wealth distribution shows a power-law decay with a value of the Pareto exponent $\nu \approx 1$ [121].

## 4.3 Analysis and Discussions

Below we present the detailed numerical evidence to argue that while the first two models are ergodic and self-averaging, the third model is not. This makes the third model difficult to study numerically.

We simulated DY model with $N = 256, 512$ and $1024$. Starting from an initial equal wealth distribution $\mathrm{Prob}(m) = \delta(m-1)$ we skipped some transactions corresponding to a relaxation time $t_\times$ to reach the stationary state. Typically $t_\times \propto N$. In the stationary state we calculated the three different probability distributions, namely: (i) the wealth distribution $\mathrm{Prob}_1(m)$ of an arbitrarily selected tagged member (ii) the overall wealth distribution $\mathrm{Prob}_2(m)$ (averaged over all members of the society) on a long single run (single initial configuration, single sequence of
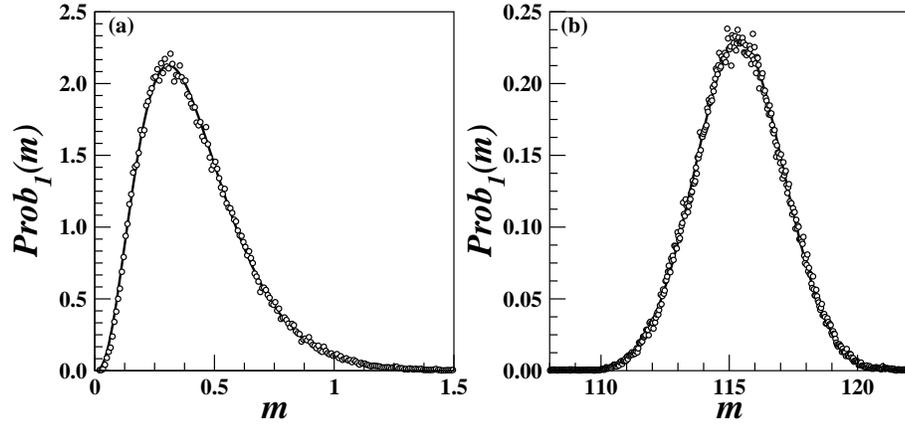
FIGURE 4.5: The individual member's wealth distribution in the CCM model. A member is tagged with a fixed saving propensity $\lambda_{tag}$=0.05 in (a) and 0.999 in (b) for $N$=256. In the stationary state the distribution $\mathrm{Prob}_1(m)$ is asymmetric in (a) and is fitted to a Gamma function. However for very large $\lambda$ the distribution in (b) is symmetric and fits very nicely to a Gaussian distribution.

random numbers) and (iii) the overall wealth distribution $\mathrm{Prob}(m)$ averaged over many initial configurations. In Fig. 4.2(a) we show all three plots for $N = 256$ and observe that overlap of these three plots is excellent, i.e., these distributions are same. This implies that the DY model is ergodic as well as self-averaging.

Similar calculations are done for the CC model as well (Fig. 4.2(b)). We see a similar collapse of the data for the same three probability distributions. This leads us to conclude again that the CC model is also ergodic and self-averaging. Further we fit in Fig. 4.3(a) the CC model distribution $\mathrm{Prob}(m)$ using a Gamma function as cited in [188] as:

$$\mathrm{Prob}(m) \sim m^{a(\lambda)} \exp(-b(\lambda)m) \tag{4.7}$$

which gives satisfactory non-linear fits by for all values of $\lambda$ in the range between say 0.1 to 0.9. Once fitting is done the most-probable wealth is estimated by the relation: $m_p(\lambda) = a(\lambda)/b(\lambda)$ using the values of fitted parameters $a(\lambda)$ and $b(\lambda)$. Functional dependence of $a$ and $b$ on $\lambda$ are also predicted in [188]. We plot $m_p(\lambda)$ so obtained with $\lambda$ for 24 different values of $\lambda$ in Fig. 4.3(b). We observe that these data points fit very well to another Gamma function as:

$$m_p(\lambda) = A\lambda^\alpha \exp(-\beta\lambda). \tag{4.8}$$

The values of $A \approx 1.46$, $\alpha \approx 0.703$ and $\beta \approx 0.377$ are estimated for $N = 256$, 512 and 1024 and we observe a concurrence of these values up to three decimal places for the three different system sizes. While $m_p(0) = 0$ from Eq. (4.8) is consistent, $m_p(1) = 1$ implies $A = \exp(\beta)$ is also consistent with estimated values of $A$ and $\beta$. Following [188] we plotted $m_p(\lambda) = 3\lambda/(1 + 2\lambda)$
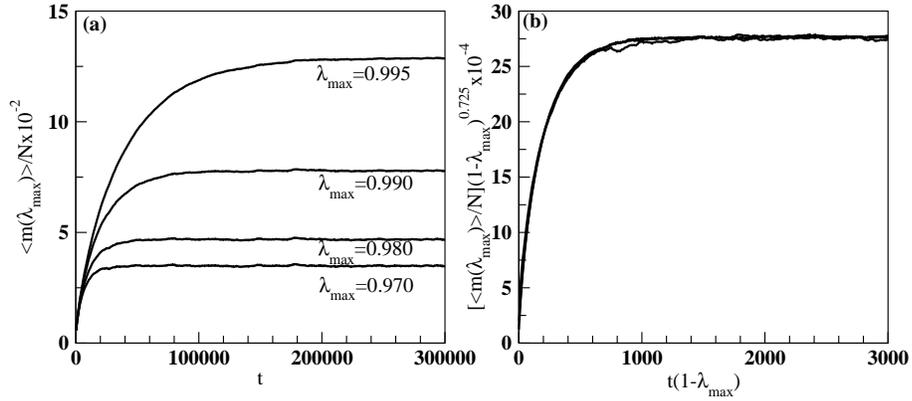
FIGURE 4.6: (a) The mean wealth of a tagged member who has the maximal saving propensity is plotted as a function of time for four different values of $\lambda_{max}$. In (b) this data is scaled to obtain the data collapse.

in Fig. 4.3(b) for the same values of $\lambda$ and observe that these values deviate from our points for the small values of $\lambda$.

However, for the CCM model many inherent structures are observed. We argue that this model is neither ergodic nor self-averaging. For a society of $N = 256$ members a set $\{0 \leq \lambda_i < 1, i = 1, N\}$ of quenched individual saving propensities are assigned, drawing these numbers from an independent and identical distribution of random numbers. The system then starts evolving with random pairwise conservative exchange rules cited in Eq. (4.6). First we reproduced the $\mathrm{Prob}(m)$ vs. $m$ curve given in [121] by averaging the wealth distribution over 500 uncorrelated initial configurations. The data looked very similar to that given in [121] and the Pareto exponent $\nu$ is found to be very close to 1.

Next we plot the same data for a single quenched configuration of saving propensities as shown in Fig. 4.4. It is observed that the wealth distribution plotted by the continuous solid line is far from being a nice power-law as observed in [121] for the configuration averaged distribution. This curve in Fig. 4.4 has many humps, especially in the large wealth limit. To explain this we made further simulations by keeping track of the wealth distributions of the individual members. We see that the individual wealth distributions are significantly different from being power-laws, they have single peaks as shown in Fig. 4.5. For small values of $\lambda$, the $\mathrm{Prob}_1(m)$ distribution is asymmetric and has the form of a Gamma function similar to what is already observed for the CC model (Fig. 4.5(a)). On the other hand as $\lambda \to 1$ the variation becomes more and more symmetric which finally attains a simple Gaussian function (Fig. 4.5(b)). The reason is for small $\lambda$ the individual wealth distribution does feel the presence of the infinite wall at $m = 0$ since no debt is allowed in this model, where as for $\lambda \to 1$ no such wall is present and consequently the distribution becomes symmetric. This implies that the wealth possessed by an individual varies
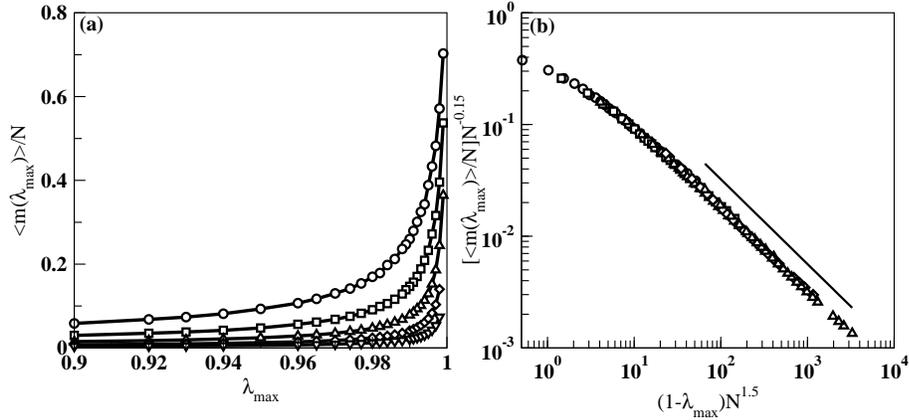
FIGURE 4.7: In the stationary state the mean value of the wealth of the member with maximum saving propensity $\lambda_{max}$ is plotted with $\lambda_{max}$. This value diverges as $\lambda_{max} \to 1$ for $N = 64$ (circle), 128 (square), 256 (triangle up), 512 (diamond) and 1024 (triangle down). (b) This data is scaled to obtain a data collapse of the three different sizes.

within a limited region around an average value and certainly the corresponding phase trajectory does not explore the whole phase space. Therefore we conclude that the CCM model is not ergodic.

Seven individual wealth distributions have been plotted in Fig. 4.4. corresponding to six top most $\lambda$ values and one with somewhat smaller value. We see that top parts of these $\mathrm{Prob}_1(m)$ distributions almost overlap with the $\mathrm{Prob}_2(m)$ distribution. This shows that $\mathrm{Prob}_2(m)$ distribution is truly a superposition of $N$ different $\mathrm{Prob}_1(m)$ distributions. In the limit of $\lambda \to 1$, large gaps are observed in the $\mathrm{Prob}_2(m)$ distribution due to slight differences in the $\lambda$ values of the corresponding individuals. These gaps remain there no matter whatever large sample size is used for the $\mathrm{Prob}_2(m)$ distribution.

We further argue that even the configuration averaging may be difficult due to very slow relaxation modes present in the system. To demonstrate this point we consider the CCM model where the maximal saving propensity $\lambda_{max}$ is continuously tuned. The $N$-th member is assigned $\lambda_{max}$ and all other members are assigned values $\{0 \leq \lambda_i < \lambda_{max}, i = 1, N - 1\}$. The average wealth $\langle m(\lambda_{max}) \rangle / N$ of the $N$-th member is estimated at different times for $N = 256$ and they are plotted in Fig. 4.6(a) for four different values of $\lambda_{max}$. It is seen that as $\lambda_{max} \to 1$ it takes increasingly longer relaxation times to reach the stationary state and the saturation value of the mean wealth in the stationary state also increases very rapidly. In Fig. 4.6(b) we made a scaling of these plots like

$$[\langle m(\lambda_{max}) \rangle / N](1 - \lambda_{max})^{0.725} \sim \mathcal{G}[t(1 - \lambda_{max})]. \tag{4.9}$$

This implies that the stationary state of the member with maximal saving propensity is reached

after a relaxation time $t_\times$ given by

$$t_\times \propto (1 - \lambda_{max})^{-1}. \tag{4.10}$$

Therefore we conclude that in CCM the maximal $\lambda$ member takes the longest time to reach the stationary state where as rest of the members reach their individual stationary states earlier.

This observation poses a difficulty in the simulation of the CCM model. Since this is a problem of quenched disorder it is necessary that the observables should be averaged over many independent realizations of uncorrelated disorders. Starting from an arbitrary initial distribution of $m_i$ values one generally skips the relaxation time $t_\times$ to reach the stationary state and then collect the data. In the CCM model the $0 \leq \lambda_i < 1$ is used. Therefore if $M$ different quenched disorders are used for averaging it means the maximal of all $M \times N$ $\lambda$ values is around $1 - 1/(MN)$. From Eq. (4.10) this implies that the slowest relaxation time grows proportional to $MN$. Therefore the main message is more accurate simulation one intends to do by increasing the number of quenched configurations, larger relaxation time $t_\times$ it has to skip for each quenched configuration to ensure that it had really reached the stationary state.

Next, we calculate the variation of the mean wealth $\langle m(\lambda_{\max})\rangle/N$ of the maximally tagged member in the stationary state as a function of $\lambda_{max}$ and for the different values of $N$. In Fig. 4.7(a) we plot this variation for $N = 64$, 128, 256, 512 and 1024 with different symbols. It is observed that larger the value of $N$ the $\langle m(\lambda_{max})\rangle/N$ is closer to zero for all values of $\lambda_{max}$ except for those which are very close to 1. For $\lambda_{max} \to 1$ the mean wealth increases very sharply to achieve the condensation limit of $\langle m(\lambda_{max} = 1)\rangle/N = 1$.

It is also observed that the divergence of the mean wealth near $\lambda_{max} = 1$ is associated with a critical exponent. In Fig. 4.7(b) we plot the same mean wealth with the deviation $(1 - \lambda_{max})$ from 1 on a double logarithmic scale and observe power-law variations. A scaling of these plots is done corresponding to a data collapse like:

$$[\langle m(\lambda_{max})\rangle/N]N^{-0.15} \sim \mathcal{F}[(1 - \lambda_{max})N^{1.5}]. \tag{4.11}$$

Different symbols representing the data for the same five system sizes fall on the same curve which has a slope around 0.76. The scaling function $\mathcal{F}[x] \to x^{-\delta}$ as $x \to 0$ with $\delta \approx 0.76$. This means $\langle m(\lambda_{max})\rangle N^{-1.15} \sim (1 - \lambda_{max})^{-0.76}N^{-1.14}$ or $\langle m(\lambda_{max})\rangle \sim (1 - \lambda_{max})^{-0.76}N^{0.01}$. Since for a society of $N$ traders $(1 - \lambda_{max}) \sim 1/N$ this implies

$$\langle m(\lambda_{max})\rangle \sim N^{0.77}. \tag{4.12}$$

This result is therefore different from the claim that $\langle m(\lambda_{max})\rangle \sim N$ [121].

## 4.4 Conclusion

To summarize, we have revisited the three recent models of wealth distribution in econophysics. Detailed numerical analysis yields that while the DY and CC models are ergodic and self-averaging, the CCM model with quenched saving propensities does not seem to be so. In CCM existence of slow modes proportional to the total sample size makes the numerical analysis difficult.

# References

[1] M. Tinkham, *Introduction to Superconductivity : Second Edition* (Dover Publications, 2004).

[2] K. G. Wilson, Rev. Mod. Phys. **47**, 773 (1975).

[3] B. B. Mandelbrot, *The Fractal Geometry of Nature* (W. H. Freeman and Company, New York, 1982).

[4] D. L. Turcotte, *Fractals and Chaos in Geology and Geophysics* (Cambridge University Press, Cambridge, 1997).

[5] S. Havlin, S. V. Buldyrev, A. L. Goldberger, R. N. Mantegna, S. M. Ossadnik, C. K. Peng, M. Simons and H. E. Stanley, Chaos Solitons Fractals **6**, 171 (1995)

[6] G. K. Zipf, *Human Behavior and the Principle of Least Effort* (Addison-Wesley, Reading, MA, 1949).

[7] G. K. Zipf, *The Psychobiology of Language* (Houghton-Mifflin, Boston, MA, 1935).

[8] R. N. Mantegna and H. E. Stanley, *An Introduction to Econophysics : Correlations and Complexity in Finance* (Cambridge University Press, Cambridge, England, 2000).

[9] G. B. West, J. H. Brown and B. J. Enquist, Science **284**, 1677 (1999).

[10] M. E. J. Newman, arxiv:cond-mat/0412002.

[11] R. Pastor-Satorras and A. Vespignani, *Evolution and Structure of the Internet: A Statistical Physics Approach* (Cambridge University Press, Cambridge, 2004).

[12] V. Pareto, *Cours d'economie Politique* (F. Rouge, Lausanne, 1897).

[13] J. L. Mccauley, Discrete Dynamics in Nature and Society **1**, 17 (1997).

[14] K. Huang, *Statistical Mechanics* (John Wiley & Sons, Singapore, 2000).

[15] J. C. Ferrero in *Econophysics of Wealth Distributions* ed. by A. Chatterjee, S. Yarlagadda and B. K. Chakrabarti (Springer Milan, 2005).

[16] A. Rubinstein, *Modeling Bounded Rationality* (MIT Press, 1998).

[17] J. Voit, *The Statistical Mechanics of Financial Markets* (Springer-Verlag, Heidelberg, 2001).

[18] S. N. Dorogovtsev and J. F. F. Mendes, *Evolution of Networks : From Biological Nets to the Internet and WWW* (Oxford University Press, Oxford, 2003).

[19] R. Albert and A.-L. Barabási, Rev. Mod. Phys. **74**, 47 (2002).

[20] P. Bak, *How Nature Works* (Oxford University Press, Oxford, 1997)

[21] H. J. Jensen, *Self-Organized Criticality* (Cambridge University Press, Cambridge, 1998)

[22] D. J. Watts and S.H. Strogatz, Nature **393**, 440 (1998).

[23] R. Pastor-Satorras, A. Vazquez and A. Vespignani, Phys. Rev. Lett. **87**, 258701 (2001).

[24] M. Huxham, S. Beaney, and D. Raffaelli, Oikos **76**, 284 (1996).

[25] N.D. Martinez, Ecol. Monogr. **61**, 367 (1991).

[26] A. K. Nandi and S. S. Manna, New J. Phys. **9**, 30 (2007).

[27] M. Á. Serrano and M. Boguñá, Phys. Rev. E **68**, 015101 (2003).

[28] L. Euler, it Solutio Problematis ad Geometriam Situs Pertinantis, Academimae Petropolitance, **8**, 128 (1736). English translation in Sci. Am., July, 66 (1953).

[29] A.-L. Barabási and R. Albert, Science **286**, 509 (1999).

[30] B. Bollobás, *Modern Graph Theory, Graduate Texts in Mathematics* (Springer, New York, 1998).

[31] D. B. West, *Introduction to Graph Theory* (Prentice-Hall, Englewood Cliffs, NJ, 1995).

[32] F. Harary, *Graph Theory*, (Addison-Wesley Publishing Company, Inc., Reading, Mass., 1969).

[33] M. E. J. Newman, SIAM Rev. **45**, 167 (2003).

[34] A. Barrat, M. Barthélémy, R. Pastor-Satorras and A. Vespignani, Proc. Natl. Acad. Sci. (USA) **101**, 3747 (2004).

[35] P. Sen, S. Dasgupta, A. Chatterjee, P. A. Sreeram, G. Mukherjee and S. S. Manna, Phys. Rev. E. **67**, 036106 (2003).

[36] A. D. Montis, M. Barthélémy, M. Campagna, A. Chessa and A. Vespignani in *Congress of the European Regional Science Association*, Free University of Amsterdam (2005).

[37] S. Boccaletti, V. Latora, Y. Moreno, M. Chavez and D.-U. Hwang, Phys. Rep. **424** 175 (2006).

[38] C. L. Freeman, Sociometry **40**, 35 (1977).

[39] L. C. Freeman, Social Networks **1**, 215 (1979).

[40] S. Wasserman and K. Faust, *Social Networks Analysis*, Cambridge University Press, Cambridge, 1994.

[41] J. Scott, *Social Network Analysis: A Handbook*, 2nd ed., Sage Publications, London, 2000.

[42] K.-I. Goh, B. Khang and D. Kim, Phys. Rev. E **64**, 051903 (2001).

[43] K.-I. Goh, B. Khang and D. Kim, Phys. Rev. Lett. **87**, 278701 (2001).

[44] U. Brandes, J. Math. Soc. **25** 163 (2001).

[45] M. E. J. Newman and M. Girvan, Phys. Rev. E **69**, 026113 (2004).

[46] M. E. J. Newman, Phys. Rev. Lett. **89**, 208701 (2002).

[47] M. E. J. Newman, Phys. Rev. E **67**, 026126 (2003).

[48] M. E. J. Newman, Proc. Natl. Acad. Sci. U.S.A. **98**, 404 (2001).

[49] H. Jeong, S. Mason, A.-L. Barabási, and Z. N. Oltvai, Nature **411**, 41 (2001).

[50] R. Albert, H. Jeong, and A.-L. Barabasi, Nature **401**, 130 (1999).

[51] M. E. J. Newman, Phys. Rev. E **70**, 056131 (2004).

[52] M. Marchiori and V. Latora, Physica A **285**, 539 (2000).

[53] V. Latora and M. Marchiori, Phys. Rev. Lett. **87**, 198701 (2001).

[54] M. E. J. Newman, Phys. Rev. E **64**, 016131 (2001).

[55] M. Granovetter, American J. Sociol. **78**, 1360 (1973).

[56] M. E. J. Newman, Proc. Natl. Acad. Sci. USA **98**, 404 (2001).

[57] W. Li and X. Cai, Phys. Rev. E **69**, 046106 (2004).

[58] R. Guimerá and L. A. N. Amaral, Eur. Phys. J. B **38**, 381 (2004).

[59] R. Guimerá, S. Mossa, A. Turtschi and L. A. N. Amaral, Proc. Natl. Acad. Sci. USA **102**, 7794 (2005).

[60] M. Barthélémy, A. Barrat, R. Pastor-Satorras and A. Vespignani, Physica A **346**, 34 (2005).

[61] S. H. Yook, H. Jeong, A.-L. Barabasi and Y. Tu, Phys. Rev. Lett. **86**, 5835 (2001).

[62] B. B. Mandelbrot, *Fractals: Form, Chance and Dimension* (W. H. Freeman and Company, New York).

[63] O. Peters, C. Hertlein and K. Christensen, Phys. Rev. Lett. **88**, 178501 (2002).

[64] R. Voss and J. Clarke, Phys. Rev. B. **13**, 556 (1976).

[65] W. H. Press, Comments Astrophys. **7**, 103 (1978).

[66] P. Bak, C. Tang and K. Wiesenfeld, Phy. Rev. Lett. **59**, 381 (1987).

[67] C. Tebaldi, M. De Menech, and A. L. Stella, Phys. Rev. Lett. **83**, 3952 (1999).

[68] S. Lübeck, Phys. Rev. E. **61**, 204 (2000).

[69] O. Biham, E. Milshtein, and O. Malcai, Phys. Rev. E **63**, 61309 (2001).

[70] D. Dhar, arxiv:cond-mat/9909099.

[71] G. Daniel and D. Sornette in *Encylopedia of Quantitative Finance* (1st section) ed. by P. Mehrling and M. Taqqu (Wiley, Chichester, England, 2009).

[72] M. F. M. Osborne, in *The Random Character of Stock Merket Prices*, ed. P. Cootner (Cambridge, MIT, 1964).

[73] B. Mandelbrot, J. Business **36**, 394 (1963).

[74] R. N. Mantegna and H. E. Stanley, Nature **376**, 46 (1995).

[75] J. McCauley, arxiv:physics/0606002.

[76] A. Johansen, O. Ledoit and D. Sornette, International Journal of Theoretical and Applied Finance **3**, 219 (2000).

[77] P. Bak, S.F. Nørrelykke, and M. Shubik, Phys. Rev. E **60**, 2528 (1999).

[78] A. Smith, *An Inquiry into the Nature and Causes of the Wealth of Nations* (Methuen and Co.,Ltd., ed. Edwin Cannan, London, 1904).

[79] W. Souma, Y. Fujiwara, H. Aoyama, Physica A **324**, 396 (2003).

[80] X. Li, Y. Y. Jin and G. Chen, Physica A **328**, 287 (2003).

[81] D. Garlaschelli and M. I. Loffredo, Phys. Rev. Lett. **93**, 188701 (2004).

[82] M. Á. Serrano, J. Stat. Mech. L01002 (2007).

[83] M. Á Serrano, M. Boguñá and A. Vespignani, Journal of Economic Interaction and Coordination **2**, 111 (2007).

[84] B. Cohen, The Edge of Chaos : Financial Booms, Bubbles, Crashes and Chaos (Wiley, Chichester, Engand 1997).

[85] B. Eichengreen, Globalizing Capital : A History of the International Monetary System (Princeton Univ. Press, 1998 ).

[86] Human Development Reports in `http://hdr.undp.org/`.

[87] K. Bhattacharya, G. Mukherjee, J. Saramäki, K Kaski and S. S. Manna, J Stat. Mech P02002 (2008).

[88] K. Bhattacharya, G. Mukherjee and S. S. Manna in *Econophysics of Markets and Business Networks*, ed. by A. Chatterjee *et al.*, Springer (2007).

[89] Version 4.1 of the data available in `http://privatewww.essex.ac.uk/~ksg/exptradegdp.html` has been used.

[90] Software Himmeli v3.0.1 is used `http://www.lce.hut.fi/~vmakine2/himmeli/`.

[91] K. S. Gleditsch, Journal of Conflict Resolution **46**, 712 (2002).

[92] D. Stauffer and A. Aharony, *Introduction to Percolation Theory* (CRC Press, 1994).

[93] D. A. Irwin, World Trade Review **1**, 89 (2002).

[94] S. Zhou and R. J. Mondragón, IEEE Commun. Lett. **8**, 180 (2004).

[95] M. Molloy and B. Reed, Random Struct. Algorithms **6**, 161 (1995).

[96] M. Molloy and B. Reed, Combinatorics, Probab. Comput. **7**, 295 (1998).

[97] V. Colizza, A. Flammini, M. Á. Serrano, and A. Vespignani, Nature Physics **2**, 110 (2006).

[98] S. Maslov and K. Sneppen, Science **296**, 910 (2002).

[99] S. Maslov, K. Sneppen and A. Zaliznyak, Physica A **333**, 529 (2004).

[100] M. Á Serrano, M. Boguñá and R. Pastor-Satorras, Phys. Rev. E **74**, 055101 (2006).

[101] D. S. Callaway, J. E. Hopcroft, J. M. Kleinberg, M. E. J. Newman and S. H. Strogatz, Phys. Rev. E **64**, 041902 (2001).

[102] Z. Burda and A. Krzywicki, Phys. Rev. E **67**, 046118 (2003).

[103] M. Boguñá, R. Pastor-Satorras and A. Vespignani, Eur. Phys. J. B **38**, 205 (2004).

[104] E. Almaas, B. Kovacs, T. Viscek, Z. N. Oltvai and A.-L. Barabási, Nature **427**, 839 (2004).

[105] M. Barthélemy, A. Barrat, R. Pastor-Satorras and A. Vespignani, Physica A **346**, 34 (2005).

[106] B. Derrida and H. Flyvbjerg, J. Phys. A **20**, 5273 (1987).

[107] M. Barthélémy, B. Gondran and E. Guichard, Physica A **319**, 633 (2003).

[108] M. Girvan and M. E. J. Newman, Proc. Natl. Acad. Sci. USA **99**, 7821 (2002).

[109] G. Palla, I. Derényi, I. Farkas and T. Vicsek, Nature **435**, 814 (2005).

[110] I. Derényi, G. Palla and T. Vicsek, Phys. Rev. Lett. **94**, 160202 (2005).

[111] S. Wuchty and E. Almaas, Proteomics **5**, 444 (2005).

[112] S. N. Dorogovtsev, A. V. Goltsev and J. F. F. Mendes, Phys. Rev. Lett. **96**, 040601 (2006).

[113] A. V. Goltsev, S. N. Dorogovtsev and J. F. F. Mendes, Phys. Rev. E **73**, 056101 (2006).

[114] J. Adler, Physica A **171**, 453 (1991).

[115] G. Bianconi and M. Marsili, Europhys. Lett. **74**(4), 740 (2006).

[116] I. M. Bomze, M. Budinich, P. M. Pardalos and M. Pelillo in *Handbook of Combinatorial Optimization* ed. by D.-Z. Du and P. M. Pardalos (Kluwer Academic, 1999).

[117] J. Tinbergen, 1962, "An Analysis of World Trade Flows", in *Shaping the World Economy*, Tinbergen, ed. New York: Twentieth Century Fund.

[118] K. Head, *Gravity for Beginners*, 2003, http://economics.ca/keith/gravity.pdf.

[119] A. A. Drăgulescu and V. M. Yakovenko, Eur. Phys. J. B **17**, 723 (2000).

[120] A. Chakraborti and B. K. Chakrabarti, Eur. Phys. J. B **17**, 167 (2000).

[121] A. Chatterjee, B. K. Chakrabarti and S. S. Manna, Physica Scripta T **106**, 36 (2003); A. Chatterjee, B. K. Chakrabarti and S. S. Manna, Physica A **335**, 155 (2004).

[122] G. Bianconi and M. Marsili, Phys. Rev. E **70**, 035105(R) (2004).

[123] P. Fronczak, A. Fronczak and J. A. Holyst, Phys. Rev. E **73**, 046117 (2006).

[124] D. Garlaschelli, A. Capocci and G. Caldarelli, Nature Physics **3**, 813 (2007).

[125] S. S. Manna and K. Bhattacharya, Eur. Phys. J. B **54**, 493 (2006).

[126] K. Bhattacharya and S. S. Manna, Physica A **384**, 15 (2007).

[127] J. M. Carlson, J. S. Langer, B. E. Shaw and C. Tang, Phys. Rev. A **44**, 884 (1991).

[128] K. E. Sieh, J. Geophys. Res. **83**, 3907 (1978).

[129] W. D. Stuart and G. M. Mavko, J. Geophys. Res. **84**, 2153 (1979).

[130] M. Y. Choi and B. A. Huberman, J. Phys. C **17**, L673 (1984).

[131] Y. Y. Kagan, Physica D **77**, 162 (1994).

[132] D. Marsan, C. J. Bean, S. Steacy and J. McCloskey, J. Geophys. Res. **105**, (B12) 28081 (2000).

[133] P. G. Okubo and K. J. Aki, J. Geophys. Res. **92**, 345 (1987).

[134] J. Davidsen and M. Paczuski, Phys. Rev. Lett. **94**, 048501 (2005).

[135] M. Baiesi and M. Paczuski, Phys. Rev. E **69**, 066106 (2004).

[136] F. Omori, J. Coll. Sci. Imp. Univ. Tokyo **7**, 111 (1894).

[137] T. Utsu, Geophys. Mag. **30**, 521 (1961).

[138] T. Utsu, Y. Ogata, and R. S. Matsu'ura, J. Phys. Earth **43**, 1 (1995).

[139] B. B. Gutenberg and C. F. Richter, Bull. Seismol. Soc. Am. **34**, 185 (1944).

[140] P. Bak, K. Christensen, L. Danon, T. Scanlon, Phys. Rev. Lett. **88**, 178501 (2002).

[141] K. Christensen, L. Danon, T. Scanlon and, P. Bak, Proc. Natl. Acad. Sci. **99**, 2509 (2002).

[142] Á. Corral, Phys. Rev. Lett. **92**, 108501 (2004).

[143] Á. Corral, Phys. Rev. E **68**, 035102(R) (2003).

[144] P. Bak and C. Tang, J. Geophys. Res. **94**, 15635 (1989)

[145] P. Bak and C. Tang in Fractals in *Fractals in the Earth Sciences*, ed. by Barton *et al.*, New York:Plenum (1994).

[146] R. Burridge and L. Knopoff, Bull. Seismol. Soc. Am. **57**, 341 (1967).

[147] T. Mikumo and T. Miyatake, Geophys. J. R. **54**, 417 (1978).

[148] T. Mikumo and T. Miyatake, Geophys. J. R. **59**, 497 (1979).

[149] J. M. Carlson and J. S. Langer, Phys. Rev. Lett. **62**, 2632 (1989).

[150] J. M. Carlson and J. S. Langer, Phys. Rev. A **40**, 6470 (1989).

[151] M. de Sousa Vieira, G. L. Vasconcelos and S. R. Nagel, Phys. Rev. E **47**, R2221 (1993).

[152] J. H. Dieterich, Pure Appl. Geophys. **116**, 790 (1978); J. Geophys. Res. **84**, 2161 (1979).

[153] J. Lomnitz-Adler, L. Knopoff and G. Martinez-Meckler, Phys. Rev. A, **45**, 2211 (1992).

[154] M. Ostuka, Phys. Earth Planet. Inter. **6**, 311 (1972).

[155] K. Ito and M. Matsuzaki, J. Geophys. Res. **95**, 6853 (1990).

[156] S. R. Brown, C. H. Scholz and J. B. Rundle, Geophys. Res. Lett. **18**, 215 (1991).

[157] H. Nakanishi, Phys. Rev. A **41**, 7086 (1990).

[158] H. Nakanishi, Phys. Rev. A **43**, 6613 (1991).

[159] V. Frette, K. Christensen, A. Malthe-Sørenssen, J. Feder, Torstein Jessang and Paul Meakin, Nature, **379**, 49 (1996).

[160] Z. Olami, H. J. S. Feder and K. Christensen, Phys. Rev. Lett. **68**, 1244 (1992).

[161] P. Grassberger, Phys. Rev. E **49**, 2436 (1994).

[162] J. X. de Carvalho and C. P. C. Prado, Phys. Rev. Lett. **84**, 4006 (2000).

[163] S. Lise and M. Paczuski, Phys. Rev. E **63**, 036111 (2001).

[164] B. Drossel, Phys. Rev. Lett. **89**, 238701 (2002).

[165] G. Molchan, Pure appl. geophys. **162**, 1135 (2005).

[166] A. Saichev and D. Sornette, arxiv:physics/0606001.

[167] K. Bhattacharya, G. Mukherjee and S. S. Manna in *Econophysics of Wealth Distributions*, ed. by A. Chatterjee *et al.* (Springer, 2005).

[168] M. Levy and S. Solomon, Physica A **242**, 90 (1997).

[169] A. A. Drăgulescu and V. M. Yakovenko, Physica A **299**, 213 (2001).

[170] W. J. Reed and B. D. Hughes, Phys. Rev. E **66**, 067103 (2002).

[171] H. Aoyama, W. Souma, and Y. Fujiwara, Physica A **324**, 352 (2003).

[172] S. Sinha, arxiv:cond-mat/0502166.

[173] E. W. Montroll and M. F. Shelesinger, J. Stat. Phys. **32**, 209 (1982).

[174] W. Souma, Fractals **9**, 463 (2001).

[175] W. souma, arxiv:cond-mat/0202388.

[176] T. Di Matteo, T. Aste and S. T. Hyde, arxiv:cond-mat/0310544.

[177] F. Clementi and M. Galegati, Physica A **350** 427 (2005).

[178] V. M. Yakovenko and A. C. Silva in *Econophysics of Wealth Distributions* ed. by A. Chatterjee, S. Yarlagadda and B. K. Chakrabarti (Springer, Italy, 2005).

[179] A. A. Drăgulescu and V. M. Yakovenko, Eur. Phys. J. B **20**, 585 (2001).

[180] F. Slanina, Phys. Rev. E **69**, 046102 (2004).

[181] P. A. Samuelson, *Economics*, 11th Edition, McGraw-Hill Inc., Auckland, 195 (1980).

[182] V. M. Yakovenko in *Enclyclopedia of Complexity and System Science* (Springer-Verlag, Heidelberg, 2008).

[183] S. Ispolatov, P. L. Krapivsky and S. Redner, Eur. Phys. J. B **2**, 267 (1998).

[184] J. Angle, Social Forces **65**, 293 (1986).

[185] J. Angle, Physica A **367**, 388 (2006).

[186] M. H. Ernst in *Fractals in Physics*, ed. by L. Piertronero and E. Tossatti (Elsevier, Amsterdam, 1986) p. 289.

[187] A. Das and S. Yarlagadda, Phys. Scripta T **106**, 39 (2003).

[188] M. Patriarca, A. Chakraborti and K. Kaski, Phys. Rev. E **70**, 016104 (2004).